Palladium Telluride Quantum Dots Biosensor for the Determination of Indinavir Drug

UNIVERSITY *of the*
WESTERN CAPE

By

Usisipho Feleni

(BSc Honours)

A thesis submitted in partial fulfilment of the requirements for the degree of

Magister Scientiae in Nanoscience

Faculty of Science

University of the Western Cape

Cape Town, South Africa

Supervisor: Prof Emmanuel I. Iwuoha

November 2013

Abstract

Indinavir is a potent and well tolerated protease inhibitor drug used as a component of the highly active antiretroviral therapy (HAART) of HIV/AIDS, which results in pharmacokinetics that may be favourable or adverse. These drugs work by maintaining a plasma concentration that is sufficient to inhibit viral replication and thereby suppressing a patient's viral load. A number of antiretroviral drugs, including indinavir, undergo metabolism that is catalysed by cytochrome P450-3A4 enzyme found in the human liver microsomes. The rate of drug metabolism influences a patient's response to treatment as well as drug interactions that may lead to life-threatening toxic conditions, such as haemolytic anaemia, kidney failure and liver problems. Therapeutic drug monitoring (TDM) during HIV/AIDS treatment has been suggested to have a potential to reduce drug toxicity and optimise individual therapy. A fast and reliable detection technique, such as biosensing, is therefore necessary for the determination of a patient's metabolic profile for indinavir and for appropriate dosing of the drugs. In this study biosensors developed for the determination of ARV drugs comprised of cysteamine self-assembled on a gold electrode, on which was attached 3-mercaptopropionic acid-capped palladium telluride (3-MPA-PdTe) or thioglycolic acid-capped palladium telluride (TGA-PdTe) quantum dots that are cross-linked to cytochrome P450-3A4 (CYP3A4) in the presence of 1-ethyl-3(3-dimethylaminopropyl) carbodiimide hydrochloride and N-hydroxysuccinimide. The quantum dots were synthesized in the presence of capping agents (3-MPA or TGA) to improve their stability, solubility and biocompatibility. The capping of PdTe quantum dots with TGA or 3-MPA was confirmed by FTIR, where the SH group absorption band disappeared from the spectra of 3-MPA-PdTe and TGA-PdTe. The particle size of the quantum dots (< 5 nm) was estimated from high resolution transmission electron microscopy (HRTEM) measurements. Optical properties of the materials were confirmed by UV-Vis spectrophotometry which produced absorption

bands at ~320 nm that corresponded to energy band gap values of 3 eV (3.87 eV) for TGA-PdTe (3-MPA-PdTe) quantum dots. The electrocatalytic properties of the quantum dots biosensor systems were studied by cyclic voltammetry (CV) for which the characteristic reduction peak at 0.75 V was used to detect the response of the biosensor to indinavir. Results for indinavir biosensor constructed with 3-MPA-SnSe quantum dots are also reported in this thesis. The three biosensors systems were very sensitive towards indinavir; and gave low limits of detection (LOD) values of 3.22, 4.3 and 6.2 ng/mL for 3-MPA-SnSe, 3-MPA-PdTe and TGA-PdTe quantum dots biosensors, respectively. The LOD values are within the 'maximum plasma concentration' (C_{max}) value of indinavir (5 - 15 ng/mL) normally observed 8 h after drug intake.

Key words

Indinavir drug

Cytochrome P450-3A4 (CYP3A4)

Quantum dots

Self-assembled monolayers

Biosensors

Cyclic voltammetry

Limit of detection (LOD)

Therapeutic drug monitoring (TDM)

Declaration

I declare that ‘‘*Palladium telluride quantum dot biosensor for the determination of indinavir drug’’* is my own work, that it has not been submitted before for any degree or examination in any other university, and that all the sources I have used or quoted have been indicated or acknowledged as complete references.

Usisipho Feleni November 2013

Signed ……

Acknowledgement

I would like to thank God for giving me the strength to complete my work.

A special thanks to my supervisor, Prof Emmanuel Iwuoha, for guidance, support and for believing in me throughout the study.

To my family and friends, I say a big thank you for your love, motivation and support throughout the period of the study.

To Chemistry Department staff and SensorLab researchers, thank you for your friendship and support.

Dedication

This work is dedicated to: my late grandfather Swaphi John Feleni, uncle Mbonisi Feleni and aunt Nomgqibelo Sindisiwe Feleni; my grandmother Nonkuthalo Beauty Feleni and mother Sindiswa Ngoza Feleni, and my siblings Lwandisolomntu Feleni, Ofentse Feleni and Uligwiba Abena Feleni.

Table of contents

Title page……*i*

Abstract.....*ii*

Key words.....*iv*

Declaration.....*v*

Acknowledgement.....*vi*

Dedication.....*vii*

Table of contents.....*viii*

List of abbreviations..... *xiii*

List of figures.....*xv*

Chapter one.....*1*

1.0 Summary.....2

1.1 Background.....2

1.2 Problem statement and motivation.....4

1.3 Aims and objectives.....6

1.4 Thesis lay-out.....11

Chapter two.....*12*

Literature review.....*13*

2.0 Summary.....13

2.1 Indinavir drug.....13

2.2 Self-assembled monolayers (SAMs) **14**

2.3 Quantum dots **15**

2.3.1 Types of quantum dots 16

2.3.1.1 Tin selenide quantum dots 16

2.3.1.2 Palladium telluride quantum dots 16

2.3.1.3 Surface capping agents 17

2.3.1.4 Immobilization of quantum dots on surfaces 18

2.4 Biosensors **19**

2.4.1 Enzyme based electrochemical biosensors 20

2.5 Enzymes **21**

2.5 1 Cytochrome P450 21

Chapter three ***24***

Experimental ***25***

3 1 Summary **25**

3.2 Reagents **25**

3.3 Instrumentation **26**

3.3.1 Spectroscopic techniques 27

3.3.1.1 UV-Vis spectroscopy 27

3.3.1.2 Fourier transforms infra-red spectroscopy (FTIR) 28

3.3.2 Microscopic techniques 28

3.3.2.1 High resolution scanning electron microscopy (HRSEM) 28

3.3.2.2 High resolution transmission electron microscopy (HRTEM) 29

3.3.3 Electrochemical techniques 29

3.3.3.1 Cyclic voltammetry 29

3.4 Methodology 31

3.4.1 Synthesis of selenide and telluride quantum dots 31

3.4.11 Mercaptopropionic acid-capped tin selenide quantum dots (3-MPA-SnSeQDs) 31

3.4.1.2 Thioglycolic acid- capped palladium telluride quantum dots (TGA-PdTeQDs) 31

3.4.1.3 Mercaptopropionic acid-capped palladium telluride quantum dots (3-MPA-PdTeQDs) 32

3.4.2 Fabrication of CYP 3A4 biosensors 33

3.4.2.1 Fabrication of CYP3A4 biosensor: *3-MPA-SnSeQDs/L-cyst/Au* biosensor system for indinavir 33

3.4.2.2a Fabrication of CYP3A4 biosensor: *TGA-PdTeQDs/Cyst/Au* biosensor system for indinavir 34

3.4.2.2b Fabrication of CYP3A4 biosensor: *3-MPA-PdTeQDs/Cyst/Au* biosensor system for indinavir 34

3.4.2.3 Preparation of indinavir stock solution 34

Chapter four* *36

Results and discussion* *37

4.0 Summary 37

4.1 Characterisation of 3-MPA-SnSe quantum dots 37

4.1.1 UV-Vis spectrophotometry of 3-MPA-SnSeQDs 37

4.2 Electrochemical characterisation of 3-MPA-SnSeQDs and L-cyteine 38

4.2.1 Electrochemistry of Au/3-MPA-SnSe quantum dots 38

4.2.2 Electrochemistry of Au/L-cysteine 40

4.2.3 Electrochemistry of Au/L-cyst/3-MPA-SnSeQDs/CYP3A4 biosensor modification 41

4.2.4 Electrochemistry of L-cyst, 3-MPA-SnSeQDs and biosensor 43

4.3 Biosensor measurements 44

4.4. Microscopy of L-cyst, 3-MPA-SnSe quantum dots and the biosensor 46

4.5 Electrochemical characterisation of biosensor responses for indinavir drug. 48

4.5.1 Calibration curve for Au/L-Cyst/3-MPA-SnSeQDs/CYP3A4 biosensor. 49

Chapter five *.....50*

5.1 Characterisation of TGA-PdTe QDs 52

5.1.1 UV-Vis spectrophotometry of TGA-PdTeQDs 52

5.2 Spectroscopic studies of TGA-PdTeQDs.....56

5.2.1 Fourier transformed infrared of TGA-PdTeQDs.....56

5.3 Microscopic characterisation of TGA-PdTeQDs 57

5.3.1 High resolution transmission electron microscopy 57

5.4 Electrochemical characterisation of TGA-PdTeQDs 58

5.4.1 Electrochemistry of TGA-PdTeQDs 58

5.5 Biosensor measurements. 64

5.5.1 Electrochemistry of biosensor 64

5.5.2 Stability measurements of biosensor 70

5.6 Microscopic studies of biosensor.....74

5.6.1 High resolution scanning electron microscopy (HRSEM).....74

5.7 UV-vis spectrophotometry of biosensor 75

Chapter six**.....*77***

6.1 Characterisation of 3-MPA-PdTeQDs 78

6.1.1 UV-Vis spectrophotometry of 3-MPA-PdTeQDs 78

6.2 Electrochemical characterisation of 3-MPA-PdTeQDs 81

6.2.1 Electrochemistry of 3-MPA-PdTeQDs 81

6.3 Microscopic studies of 3-MPA-PdTeQDs 84

6.3.1 High resolution transmission electron microscopy (HRTEM) 84

6.4 Biosensor measurements 85

6.4.1 Electrochemistry of biosensor 85

6.4.2 Stability of biosensor 88

6.5 Microscopic studies of biosensor 90

6.5.1 High resolution transmission electron microscopy 90

Chapter seven 92

7.0 Conclusion 93

References 95

List of abbreviations

HIV	Human immunodeficiency virus
AIDS	Acquired immunodeficiency syndrome
SAM	Self assembled monolayer
CYP3A4	Cytochrome P450-3A4 enzyme
3-MPA	3-mercaptopropionic acid
TGA	Thioglycolic acid
PdTeQDs	Palladium telluride quantum dots
L-cyst	L-cysteine
Cyst	Cysteamine
HAART	Highly active antiretroviral therapy
TDM	Therapeutic drug monitoring
ART	Antiretroviral therapy
IDV	Indinavir drug
WHO	World Health Organisation
CISN	Cancer Information Support Network
C_{max}	Highest observed plasma concentration
T_{max}	Time to highest observed plasma concentration
AUC	Area under plasma concentration-time curve
AuE	Gold electrode
PBS	Phosphate buffer solution
UV-Vis	Ultraviolet-visible spectrophotometry
FT-IR	Fourier Transformation Infrared spectroscopy
CV	Cyclic voltammetry

EDS	Energy dispersive spectrometry
HRSEM	High resolution scanning electron microscopy
HRTEM	High resolution transmission electron microscopy
RDE	Rotating disc electrode
EDC	1-ethyl-3(3-dimethylaminopropyl) carbodiimide hydrochloride
NHS	N-Hydroxysuccinimide
E_{pc}	Cathodic peak potential
E_{pa}	Anodic peak potential

List of figures

Figure 1: Schematic representation of HIV protease enzyme and protease inhibitor (indinavir complex). 4

Figure 2.1: Schematic representations for development of CYP3A4/3-MPA-SnSeQDs/L-cyst/Au biosensor. 8

Figure 2.2: Schematic representation for development of CYP3A4/TGA-PdTeQDs/Cyst/Au biosensor……..... 10

Figure 3: Indinavir drug 13

Figure 4: The scheme of thioglycolic acid capped PdTe quantum dots. 18

Figure 5: Immobilization of quantum dots on a substrate via covalent bonding 19

Figure 6: Schematic for electrocatalytic oxygenation reaction of indinavir-bound CYP3A4 23

Figure 7: UV-Vis spectra of 3-MPA-SnSe quantum dots..... 38

Figure 8: Cyclic voltammograms of bare Au and Au/3-MPA-SnSe quantum dots in 0.1 M PBS pH 7.4 at 50 mV/s. 40

Figure 9: Cyclic voltammograms of bare Au and Au/L-Cysteine in 0.1 M PBS pH 7.4 at 50 mV/s..... 41

Figure 10: Cyclic voltammograms of bare Au and Au/L-Cyst/3-MPA-SnSeQDs/CYP3A4 in 0.1 M PBS pH 7.4 at 50 mV/s 43

Figure 11: Cyclic voltammograms illustrated different films deposited onto gold electrode 0.1 M PBS pH 7.4 at 50 mV/s. (black line) Bare gold, (red line), (green line) Au/3-MPA-SnSeQDs and (blue line) Au/L-Cyst/3-MPA-SnSeQDs/CYP3A4. 44

Figure 12: Cyclic voltammograms of Au/L-Cyst/3-MPA-SnSeQDs/CYP3A4 biosensor responses to successive additions of indinavir in 0.1 M PBS pH 7.4 at 20 mV/s. 45

Figure 13: Scanning electron micrographs of (a) bare Au electrode, (b) Au/L-cyst, (c) Au/L-cyst/3-MPA-SnSe quantum dots, (d) Au/L-cyst/3-MPA-SnSeQDs/CYP3A4.....47

Figure 14: Cyclic voltammograms of CYP3A4/3-MPA-SnSeQDs/L-cyst/Au biosensor response to successive additions of indinavir in 0.1 M PBS pH 7.4 at 20 mV/s. 48

Figure 15: Calibration curve drawn from the linear region of biosensor responses in Fig.14. 50

Figure 16: UV-Vis of (a) TGA capping agent, (b) $PdCl_2$, (c) TGA-$PdCl_2$, and (d) NaHTe 52

Figure 17: UV-Vis of TGA-PdTeQDs 53

Figure 18: Fluorescence spectra of TGA-PdTeQDs excited at 320 nm where (a) 30 min, (b) 40 min, (c) 50 min and (d) 60 min.....55

Figure 19: FT-IR spectra for TGA-PdTeQDs.....56

Figure 20: HRTEM of TGA-PdTeQDs.....57

Figure 21: Energy dispersive X-ray (EDX) spectrum of TGA-PdTeQDs 58

Figure 22: Cyclic voltammograms of metal precursors where (a) Au electrode, (b) Te and (c) NaHTe performed in 0.1 M PBS at 13 mV/s. 59

Figure 23: Cyclic voltammogram of Au/$PdCl_2$ in 0.1 M phosphate buffer solution.....60

Figure 24: CV of Au and Au/TGA-PdTeQDs in 0.1 M phosphate buffer solution 61

Figure 25: Cyclic voltammogram of Au/Cyst modified electrode in 0.1 M PBS.....62

Figure 26: Cyclic voltammograms of (a) Au/Cyst and (b) Au/Cyst/TGA-PdTeQDs in 0.1 M PBS 63

Figure 27: Cyclic voltammograms of (a) Au/CYP3A4 (b) Au/TGA-PdTeQDs/CYP3A4 in aerobic conditions in 0.1 M PBS at 500 mV/s 64

Figure 28: Cyclic voltammograms of (a)Au, (b) Au/Cyst, (c) Au/TGA-PdTeQDs and (d) Au/CYP3A4 with 0.05 M of IDV and without in 0.1 M PBS at 500 mV/s. 65

Figure 29: Cyclic voltammograms of CYP3A4/TGA-PdTeQDs/Cyst/Au biosensor responses to successive addition of IDV in phosphate buffer on pH 7.4 at 500 mV/s. 66

Figure 30: Calibration curve drawn from linear region of biosensor responses in Fig.29. 67

Figure 31: Cyclic voltammograms of CYP3A4/TGA-PdTeQDs/Cyst/Au biosensor with successive additions of IDV and acetaminophen 68

Figure 32: Schematic representation of acetaminophen 69

Figure 33: Cyclic voltammograms of CYP3A4/TGA-PdTeQDs/Cyst/RDE in 0.1 M PBS at 500 mV/s. 70

Figure 34: Cyclic voltammograms of CYP3A4/TGA-PdTeQDs/Cyst/RDE with and without rotating the electrode in 0.1 M PBS at 500 mV/s. 72

Figure 35: UV-Vis of (a) indinavir drug (b) CYP3A4/IDV at 0.05 nM 73

Figure 36: (A)-(D) Represents the HRSEM of Cyst,TGA-PdTeQDs, Cyst/TGA-PdTeQDs and Cyst/TGA-PdTeQDs/CYP3A4 done on aluminium stub 74

Figure 37: UV-Vis of (a) Cyst, (b) Cyst/TGA-PdTeQDs and (c) Cyst/TGA-PdTeQDs/CYP3A4 biosensor in 0.1 PBS pH 7.4. 75

Figure 38: UV-Vis spectrum of 3-MPA-PdTeQDs 78

Figure 39: Fluorescence spectra of 3-MPA-PdTeQDs 79

Figure 40: FT-IR spectra of 3-MPA-PdTeQDs.....80

Figure 41: A multi-scan rate studies of 3-MPA-PdTeQDs using cyclic voltammetry in 0.1 M phosphate buffer solution. 81

Figure 42: Cyclic voltammograms of Au/Cyst/3-MPA-PdTeQDs in 0.1 M phosphate buffer solution at different scan rates. 83

Figure 43: HRTEM of 3-MPA-PdTeQDs.....84

Figure 44: Cyclic voltammograms of CYP3A4/3-MPA-PdTeQDs/Cyst/Au in 0.1 M phosphate buffer solution at 500 mV/s.....86

Figure 45: Calibration curve drawn from linear region of biosensor responses in Fig.44 87

Figure 46: Cyclic voltammograms of CYP3A4/3-MPA-PdTeQDs/Cyst/RDE biosensor stability in 0.1 M PBS. 88

Figure 47: Cyclic voltammograms of CYP3A4/3-MPA-PdTe QDs/Cyst/RDE biosensor stability in 0.1 M PBS 89

Figure 48: (A)-(D) Represents the HRSEM of Cyst, TGA-PdTeQDs, Cyst/TGA-PdTeQDs and Cyst/TGA-PdTe QDs/CYP3A4 performed on aluminium stub. 90

Chapter one

1.0 Summary

This chapter describes the aspects involved in the study namely; quantum dots, sensors, the cytochrome P450-3A4, linking agents such as L-cysteine, human immunodeficiency virus (HIV) infection, antiretroviral (ARV) drugs in general and model drug used in the study (indinavir drug) which belongs to a class called protease inhibitors. The main focus in this chapter is the relationship between these aspects and their contribution towards a useful and successful study. The chapter also included the problem statement and motivation, aim and objectives of the study as well as thesis outline.

1.1 Background

Human immunodeficiency virus (HIV) belongs to the class called retrovirus, which carries genetic information in the form of RNA. The virus destroy a type of defense cells in the body called a CD4 helper lymphocyte (Host cells), which plays an important role in controlling HIV replication (Norris and Rosenberg, 2002; Zhong and Yeh, 1999). Thus when a virus is attached to the CD4 cells it causes damage in the process leading to fewer functioning CD4 cells and weakening the ability of different cells within the immune system that join forces together and fight off future infections. Therefore an infected patient becomes more susceptible to contract opportunistic infections which can be caused by whole host of microorganisms leading to a development of symptoms when there is no immune system for prevention (Weiss, 2008). There are significant impacts which the disease have on society based on cultural, social and economic effect to a country with large number of victims. According to World Health Organisation (WHO), there are an estimated number of more than

33.3 million people infected with HIV worldwide and nearly virus resulted in deaths of more than 25 million people in the past three decade (Michaud *et al*, 2012).

The most critical component of replicative cycle is HIV-1 protease enzyme which is responsible for the generation of mature, functional viral enzymes and structural proteins through cleavage of viral Gag and Gag-Pol precursor polyproteins (Wensing *et al*., 2010; Kohl *et al*, 1988). An investigation on HIV protease structure and its substrate has led into a development of antiretroviral (ARV) drugs in a goal of deducing and maintaining maximum suppression of HIV replication and foster maximum $CD4^+$ cell counts to improve the quality of life for people who have HIV infection (Lin, 1997). The earliest drugs developed to fight against HIV/AIDS were nucleosides which comprises of the following drugs: zidovudine or didanosine and stavudine but their therapy is limited by high toxicity levels and a rapid development of viral resistance (Moyle, 1995; Tomasselli and Heinrikson, 2000). Thus there was an urgent need for development of new class of ARV drugs that can inhibit the viral replication by delaying emergence of viral resistance and less toxic. These new developed drugs are called protease inhibitors, which were designed to mimic the transition state of peptide substrate and compete with them for binding the active site of the protease enzyme i.e.an enzyme that breaks a long chainlike molecule of proteins into shorter fragments (Foisy and Sommadossi, 1999). An important role played by these ARV drugs in HIV replication cycle is the inhibition of active site of viral enzyme to prevent the breaking by forming non-infectious viral particles (Clavel and Hance, 2004) and they are used as a component of highly active antiretroviral therapy (HAART) which results in dramatic reduction changes in the viral load and increase the amount of CD4 count. Several other studies linking the decline of morbidity and mortality to (HAART) have been reported (Wlodawer and Vondrasek, 1998) and current literature suggests that these drugs are metabolised by CYP3A4 isoform and being abundant forms in the liver responsible for formation of metabolites that can be

excreted in urine (Chiba, 1997; Zuber *et al*., 2002). Hence all its substrates may be able to compete and leads to risk of drug interactions (Dresser *et al*., 2000). The following figure shows the structure of HIV protease enzyme and protease inhibitor, Indinavir complex.

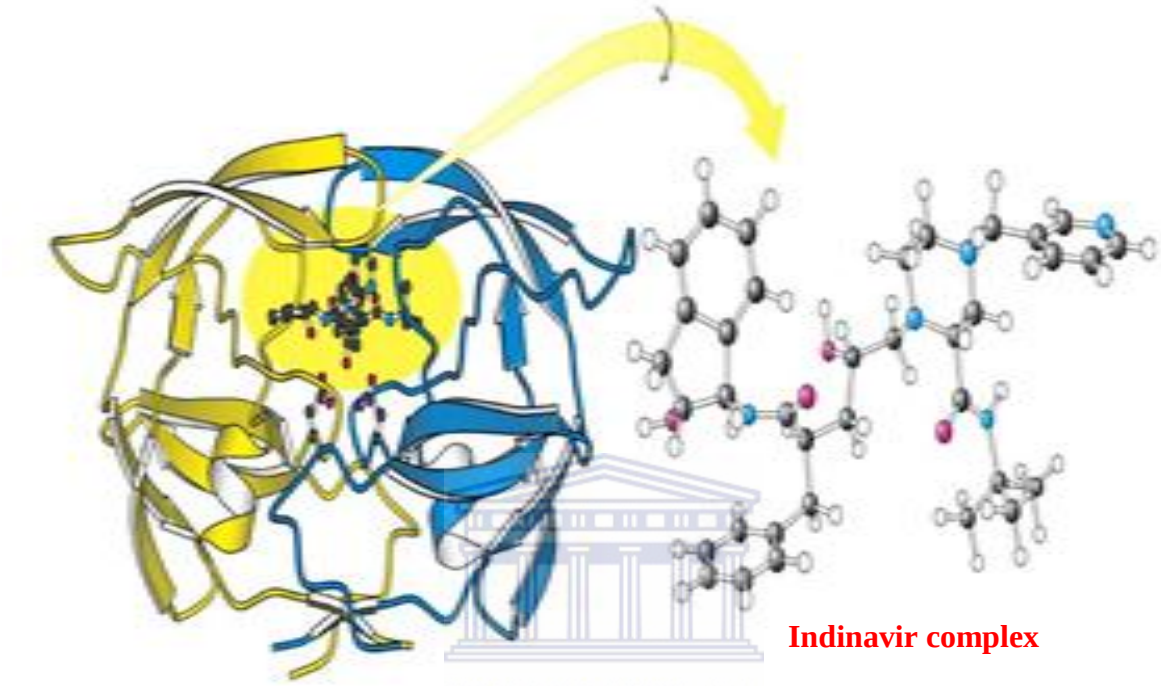

Figure 1: Schematic representation of HIV protease enzyme and protease inhibitor (indinavir complex).

1.2 Problem statement and motivation.

Protease inhibitors have played a major role in decreasing the mortality and morbidity among people with HIV infection (Arts and Hazuda, 2012), however it has been shown that the variability in drug metabolism have substantial effect on clinical outcomes in patients due to impact of inter-individual responsiveness to same dose of given drug (Pokorna *et al*., 2009.; Michaud *et al*,2012), such effects may be caused by poor adherence, virological resistance and pharmacological issues (Ford *et al*.,2004; Cressy and Lallemant, 2007; de Requena *et al*.,

2003). According to Cancer Information Support Network (CISN) metabolism of drug is affected by numerous factors of environment and genetic origin i.e. slow metabolizers and normal metabolizers. Slow metabolizer individuals tend to accumulate substantially higher drug concentration which increase the risk for drug related adverse events (life threatening toxicity such as vomiting and kidney stones) such patients may require smaller dose while normal metabolizers breaks down drug too quickly and require high dose. The effect of such factors complicates the life of diagnosed patients and need a therapy to monitor them. There have been several reports in relation with protease inhibitor exposure, their activity and toxicity in combination with wide inter-individual variability in pharmacokinetics which resulted in growing interest in therapeutic drug monitoring (TDM) of antiretroviral drugs as a tool in management of HIV infected people (van Heeswijk *et al*., 2002). The process of drug monitoring can be done by optimization of antiretroviral therapy potent to reduce toxicity and adequate viral suppression. Several relative simple techniques which can be used in hospital for measurements of protease inhibitors have been described (Frappier *et al*., 1998; Sarasa-Nacenta *et al*., 2001). Such techniques includes highly performance liquid chromatography with ultra-violet detection (HPLC) and also Liquid chromatography or mass spectrometry (LC/MS) but the problem with these techniques is the requirement of large volume of samples, expensive application and maintenance and not giving results in real time. Several works has been reported on assays for determination of concentration of HIV protease inhibitor, indinavir in serum/plasma (Burger, *et al*., 1997). Current literature suggested that an assay by (Marzolini *et al*.,2000) can measure protease inhibitors and non-nucleoside reverse transcriptase that may not be sensitive enough for quantification of trough concentration in patients on a single protease inhibitor containing regimes, the problem has led into development of a device that will be fast, portable, cheap, easy to monitor and use small volume of analyte in order to address the issues of patients falling ill as a result of

inappropriate dosing and treatment. The device can be achieved by placing a sensor material with nanomaterial for fast responses in electrochemical biosensors. In our study a combination of CYP3A4 and electron mediator (quantum dots) has been used for electrochemical study and modelling of ARV drug metabolism therefore the status of metabolism of ARV drugs in patients would be evaluated by the use of biosensor consisting of cysteamine modified 3-MPA-PdTeQDs and TGA-PdTeQDs and samples of plasma and urine.

1.3 Aims and objectives

The aim of this study was to develop quantum dot modified biosensors for determination of indinavir drug. The biosensors developed on gold electrode using capped palladium telluride quantum dots, capped tin selenide quantum dots, L-cysteine or cysteamine and CYP3A4 enzyme. Fabrication of CYP3A4 biosensor: *3-MPA-SnSeQDs/L-cyst/Au* biosensor system for indinavir involved:

I. Immobilisation of a gold electrode with L-cysteine, the binding formed a self-assembled monolayers modified electrode (L-cyst/Au SAMs) by taking advantage of strong sulphur-gold interaction.
II. The synthesis of aqueous route SnSe capped with 3-mercaptopropionic acid and immobilisation of 3-MPA-SnSeQDs onto self-assembled monolayer of L-cyst/Au for 2 h, which then reacted chemically with free amino group from the L-cysteine in the presence of cross-linking agents (EDC/NHS) via formation of a strong ester amide bond.
III. Characterisation of 3-MPA-SnSeQDs/L-cyst/Au using CV, UV and SEM

IV. The construction of biosensor by binding the amino groups of enzyme CYP3A4 with 3-MPA-SnSeQDs/L-cyst/Au quantum dots (carboxylic acid) to form biocompatible surfaces.

V. Testing of CYP3A4/3-MPA-SnSeQDs/L-cyst/Au biosensor in the presence and absence of indinavir using CV, UV and SEM respectively.

The following scheme representations the development of CYP3A4/3-MPA-SnSeQDs/L-cyst/Au biosensor.

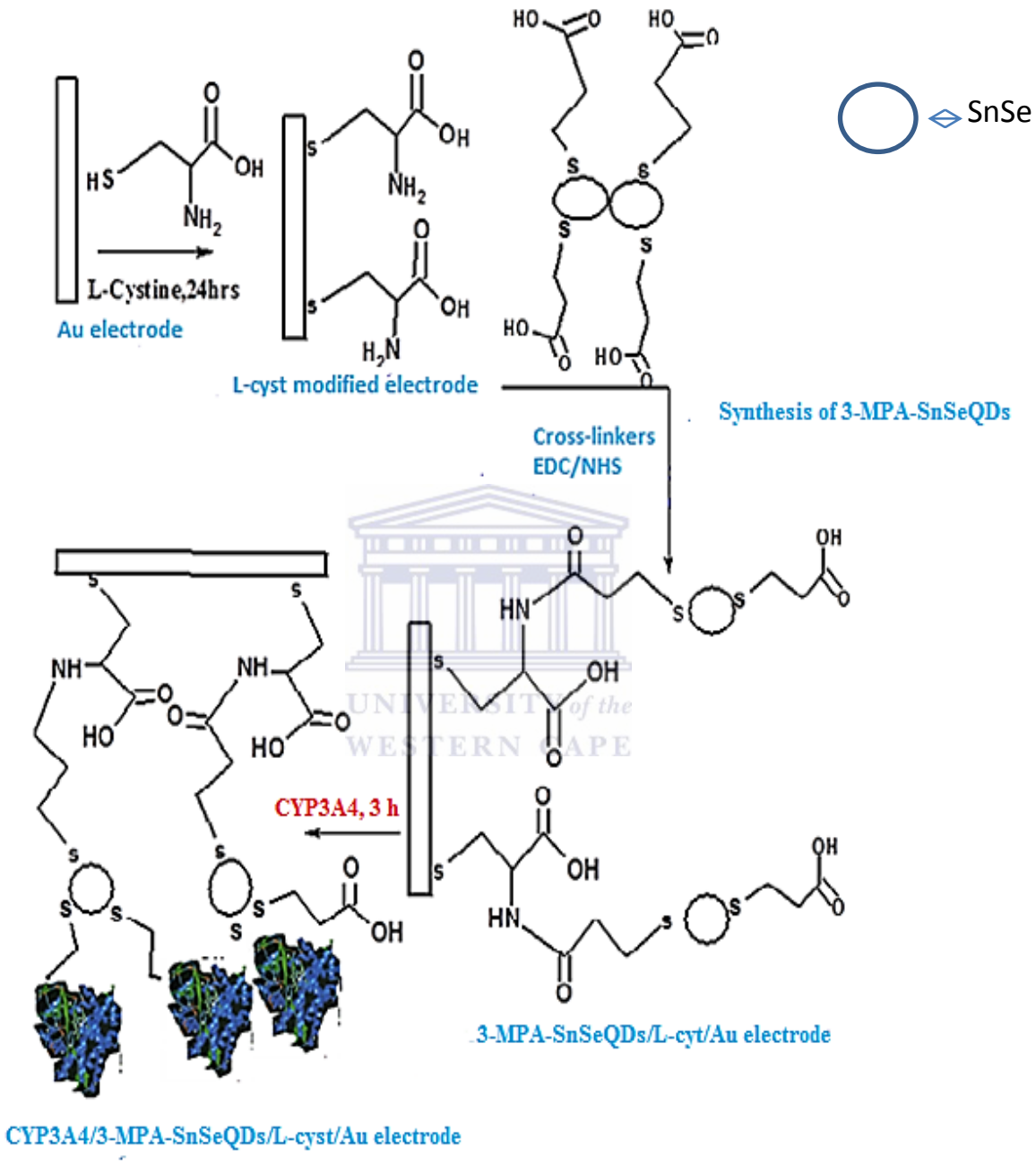

Figure 2.1: Schematic representations for development of CYP3A4/3-MPA-SnSeQDs/L-cyst/Au biosensor

Fabrication of CYP3A4 biosensor: *TGA-PdTeQDs/Cyst/Au* biosensor system for indinavir involved:

I. Surface modification of gold electrode with cysteamine, resulting in the formation of self-assembled monolayer (SAM) on a gold electrode by taking advantage of strong sulphur-gold interaction.

II. Further modification of cysteamine modified geld electrode with 3-mercaptopropionic acid capped PdTe or thioglycolic acid capped PdTe quantum dots in the presence of carbodiimide and succinimide cross linking agents.

III. Incorporation of CYP3A4 onto cysteamine and 3-mercaptopropionic acid or thioglycolic acid capped PdTe quantum dots modified gold electrode resulting in CYP3A4/TGA-PdTeQDs/Cyst/Au biosensor

IV. Testing of CYP3A4/TGA-PdTeQDs/Cyst/Au biosensor in the presence and absence of indinavir using CV, UV and SEM respectively.

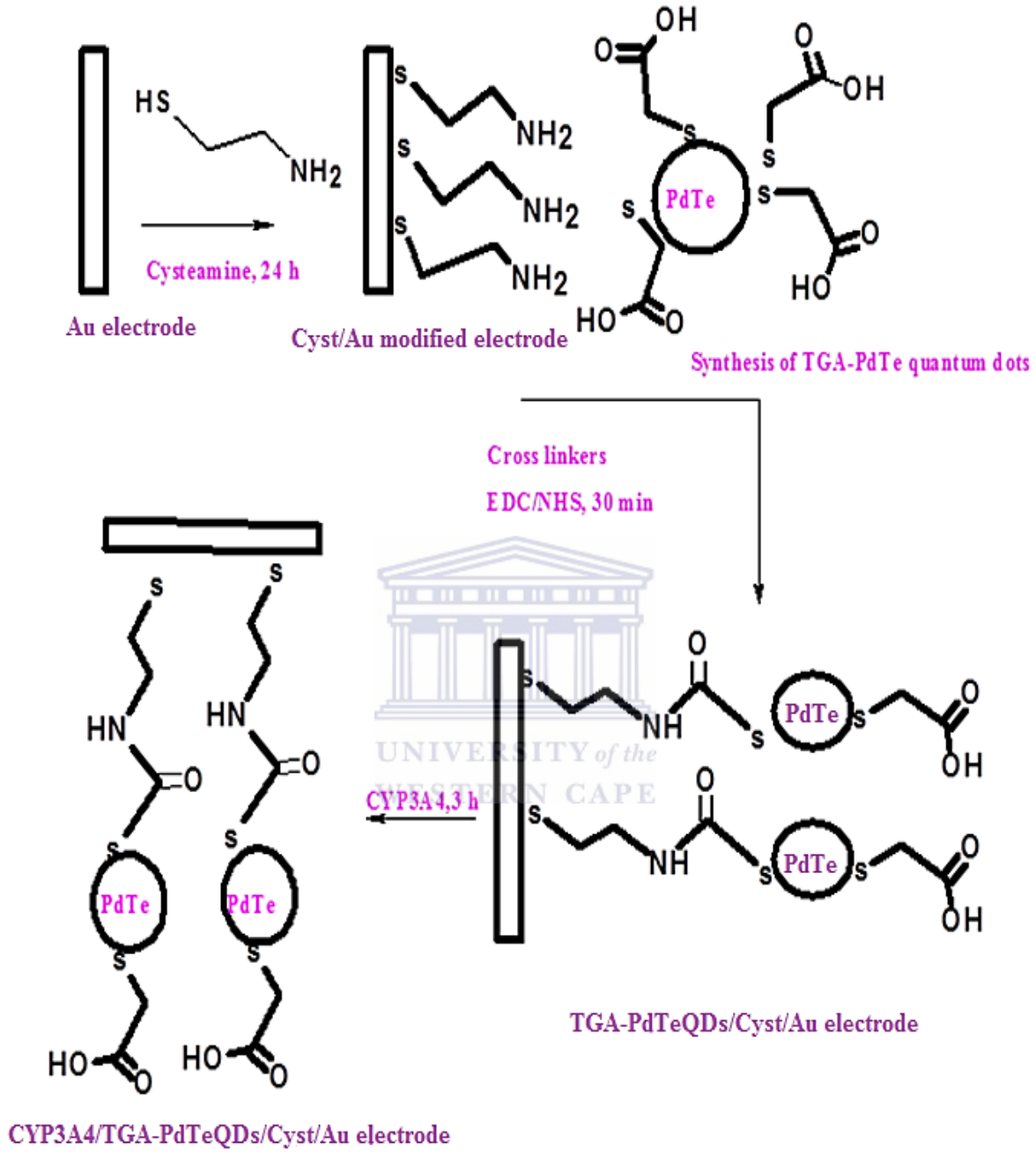

Figure 2.2: Schematic representations for the development of CYP3A4/TGA-PdTeQDs/Cyst/Au

1.4 Thesis lay-out

This thesis is presented in seven chapters

Chapter 1: Gives brief background information on the project, problem statement and motivation as well as aims and objectives.

Chapter 2: Provides a detailed literature review

Chapter 3: Consists of reagents, procedures and instrumentations used for the success of this study.

Chapter 4: Illustrates morphological, spectroscopic, electrochemical results obtained from L-cyst, nanomaterial (3-MPA-SnSeQDs) and developed biosensor CYP3A4/3-MPA-SnSeQDs/L-cyst/Au

Chapter 5: Provides spectroscopic, morphological and electrochemical results obtained from linker, Cyst: nanomaterial, TGA-PdTeQDs and developed biosensor and detection.

Chapter 6: Provides spectroscopic, morphological and electrochemical results obtained from linker, Cyst: nanomaterial, 3-MPA-PdTeQDs and developed biosensor and detection.

Chapter 7: Represents conclusion and recommendations

Chapter two

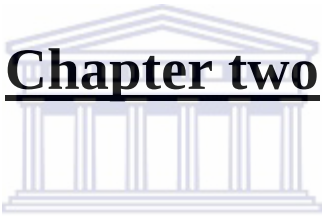

2.0 Summary

This chapter covers the role of self-assembled monolayers and their applications in the field of sensors. Also this chapter gives an introduction of quantum dots detailing their composition and properties. Types of quantum dots, their functionalization and immobilization process applied in field of sensors are also described in this chapter. The family of enzyme (Cytochrome P450) and its isoform used for successful study (CYP3A4), electrode immobilization and brief description of indinavir drug and pharmacokinetic use.

2.1 Indinavir drug

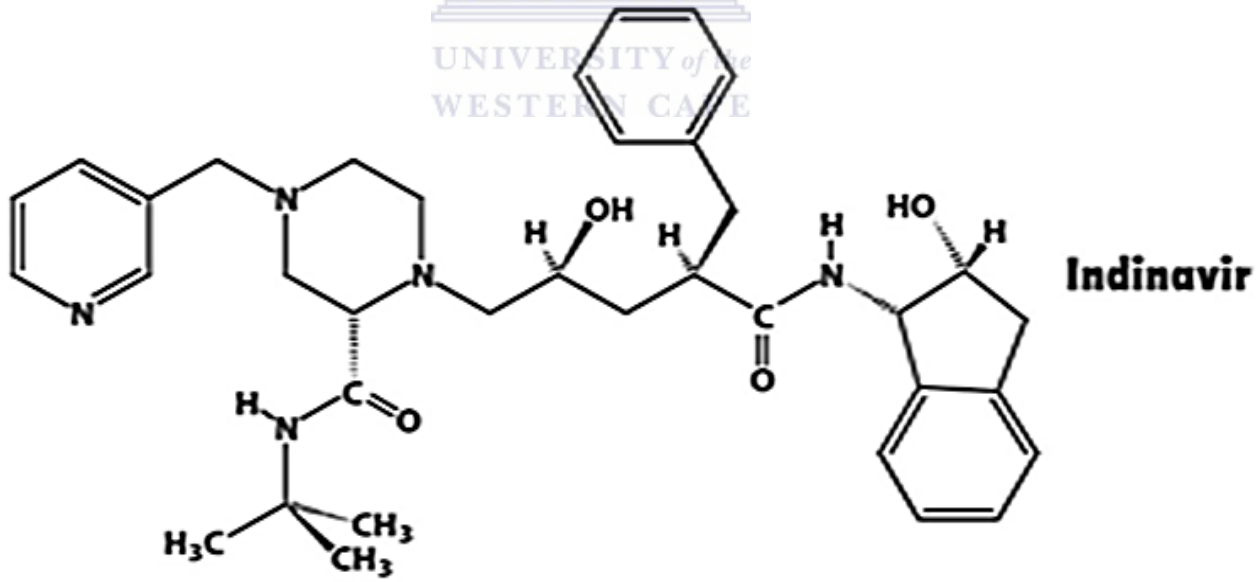

Figure 3: Indinavir drug

Indinavir drug is a protease inhibitor manufactured by Merck in 1996, where the strategy began on transition-state mimetic concept (Rich *et al*., 1991). Amongst any other drug, indinavir blocks the activity of the protease enzyme, which HIV uses to break up large polyproteins into the smaller pieces required for assembly of new viral particles. In pharmacokinetic, the drug is 60% protein bound in circulation and has been investigated by (Steigbigel *et al*, 1996; Lewis II and Terriff, 1997) by using high dose of indinavir monotherapy for comparing the amount of increase in CD4 lymphocyte with respect to decrease in viral load. This investigation has led into pharmacokinetic studies which indicated that indinavir drug is well absorbed in healthy volunteers and patients with AIDS, after a single dose of 800 mg indinavir drug in fasted state where the C_{max}, T_{max} and *AUC* values were 10.9 μM, 12 h and 21 μM.h respectively (Lin, 1997) but showed a decrease in C_{max} and *AUC* values when administered with meal high in calories fat and protein. These studies have been compared with combined drug administration i.e. indinavir drug (800 mg) with non-nucleoside reverse transcriptase (NNRTs) stavudine (40 mg) which resulted in a change in both indinavir *AUC* and stavudine *AUC* as compared to sole administration.

2.2 Self-assembled monolayers (SAMs)

A scientific discovery on alkanethiols performed on noble metal was done in 1980's; such noble metals including gold have largely been employed in different methodologies and techniques for investigation of molecule, catalyst and electron transfer (Caevalhal, 2004). The methodologies involves the modification of electrodes via functionalization of thiol group which has been attractive and of prime importance in sensor technology since their adsorption onto gold surface can result in formation of well-organised self-assembled monolayers (Wirde and Gelius, 1999; Mozaffari and Shervedani, 2005; Brett *et al*., 2003) and

offers a starting place in the construction of electron transfer models (Campuzano *et al*., 2006; Weng and Du, 2002). Alkanethiols such as cysteamine and L-cysteine have been broadly applied as linker molecules to immobilize functional organic, inorganic materials as well as proteins (Zhang *et al*., 2005) and have played a crucial role in biosensor fabrication and promoter in bioelectrochemistry (Karlsson *et al*., 1997). An investigation on application of self-assembled monolayers for the design of modified electrodes and biosensors was reviewed by Mandler. In this work cysteamine and L-cysteine have been used to form self-assembled thiol layer on gold electrode surface for promotion of electron transfer.

2.3 Quantum dots

Quantum dot term was operated by Mark Reed at Texas Instrument and known as semiconductors ranging from 2-10 nm, due to their small sizes they display unique optical and electrical properties that differ in character to those corresponding to bulk materials (Khatei *et al.,* 2011). Quantum dots were discovered and prepared at the beginning of 1980s by Alexei Ekimov in a glass (Bawendi *et al*., 1990) and by Louis E. Brus, 1984 in colloidal solutions. The effect of their small size causes energy levels of different bands to be quantized in relation to the size of the dot (Michalet *et al*., 2005). As the size of quantum dots becomes smaller, the energy bag gap becomes larger which results in more energy needed to excite electrons from valence band to conduction band or the band gap becomes blue shifted (Hambrock *et al*., 2001). They have wide range of applications in diverse fields ranging from drug delivery (Vicent *et al*., 2006), biosensing (Chan and Nei, 1998), materials for solar cells and photovoltaics (Hunch *et al*., 2003) and in light emitting diodes (Coe *et al*., 2002).

2.3.1 Types of quantum dots

2.3.1.1 Tin selenide quantum dots

Tin selenide quantum dot belongs to (IV-VI) in periodic table. These (IV-VI) chalcogens present electronic and transport properties such as high dielectric constants, narrow band gaps and high carrier mobilities (Nimtiz *et al*., 1983). Fabrication of IV-VI semiconductors for solid state device began in 1874 with Ferdinand Braun's report on electrical rectification (McCann, 2006). At present, most attention is centred on IV-VI used primarily in optoelectronic devices designed for detection and emission of mild-infrared electrochemical radiation (Pearson and llegems, 1975), laser diodes and photovoltaic cells which are used in different applications such as industrial process monitoring, medical diagnostics and atmospheric pollution control.

2.3.1.2 Palladium telluride quantum dots

Platinum group metal chalcogenides are platinum group metal containing sulphur, selenium, tellurium and oxygen and have attracted attention in recent years due to catalysis and material science relevance (Dey and Vimal, 2004) which pose extensive applications in electrochemical industry in multilayer ceramic capacitor (MLCCs). Due to their semiconductor properties they are used in low-voltage and low-energy contacts, thick-and thin-film circuits, thermocouples and furnace components, and electrodes (Raybaud *et al*., 1997). An investigation of modified sensors based on the chemical modification of electrode with immobilized nanoparticles of transition metal palladium was done by (Miao *et al*., 2000).

Several synthetic methods have been reported since the first synthesis of monodispersed CdTe nanocrystal (Murray *et al*., 1993). The development of colloidal synthesis provides the ability to precisely tailor the structural characteristics (e.g., size, shape, composition of nanoparticles) thus this method is applicable for biological application of quantum dots to give rise to their solubility, stability, non-toxic to biomolecules, non-agglomerate and biocompatibility. Publication by (Ndangili *et al*., 2011), the author used zinc selenide quantum dots functionalized with 3-mercaptopropionic acid to give rise to water soluble and biocompatible nanocrystals.

2.3.1.3 Surface capping agents

Surface capping agents are used to functionalize quantum dots in colloidal synthesis to inhibit nanoparticle overgrowth, aggregation and control the structural characteristics of formed nanoparticles (Niu *et al*., 2013) and the choices of choosing a good capping agent depends on solvent type, size of quantum dot and its surface chemistry (Colvin *et al*., 1994). The process of capping is utilized to promote catalytic performance of nanoparticles and interactions such as hydrophobic, electrostatic or chemisorption which provides a strong binding of capping agent to nanoparticle surface. In this study 3-mercaptopropionic acid and thioglycolic acid have been used in the synthesis to bind quantum dots from thiol group (-SH) and free carboxylic group used for attachment of biomolecules (Xing and Rao, 2008).

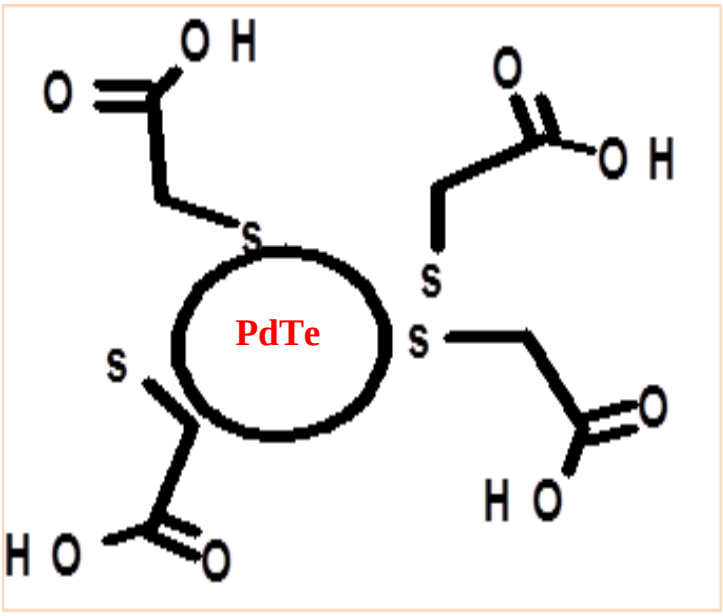

Figure 4: Schematic representation of thioglycolic acid capped PdTe quantum dots

2.3.1.4 Immobilization of quantum dots on surfaces

Quantum dots have been immobilized onto planar surfaces in the fabrication of photonic devices and design of various sensing platform (Gaponik *et al*., 2002). A famous method used involves covalent coupling between chemical groups present on the substrate and functional groups located at quantum dot surface. This method is achieved by using cross linking agents such as EDC which is used to couple carboxylic group to primary amines and have been used in wide applications such as forming amide bonds in peptide synthesis (Panchaud *et al*., 2008) and NHS, a water-soluble analog (Sulfo-NHS) often included in EDC coupling protocols to improve efficiency or create dry-stable (amine-reactive) intermediates (Sam *et al*., 2009). This approach involves the coupling of carboxylate functionalized quantum dots to terminal amine group resulting in a dense quantum dot film (Shavel et al., 2005).

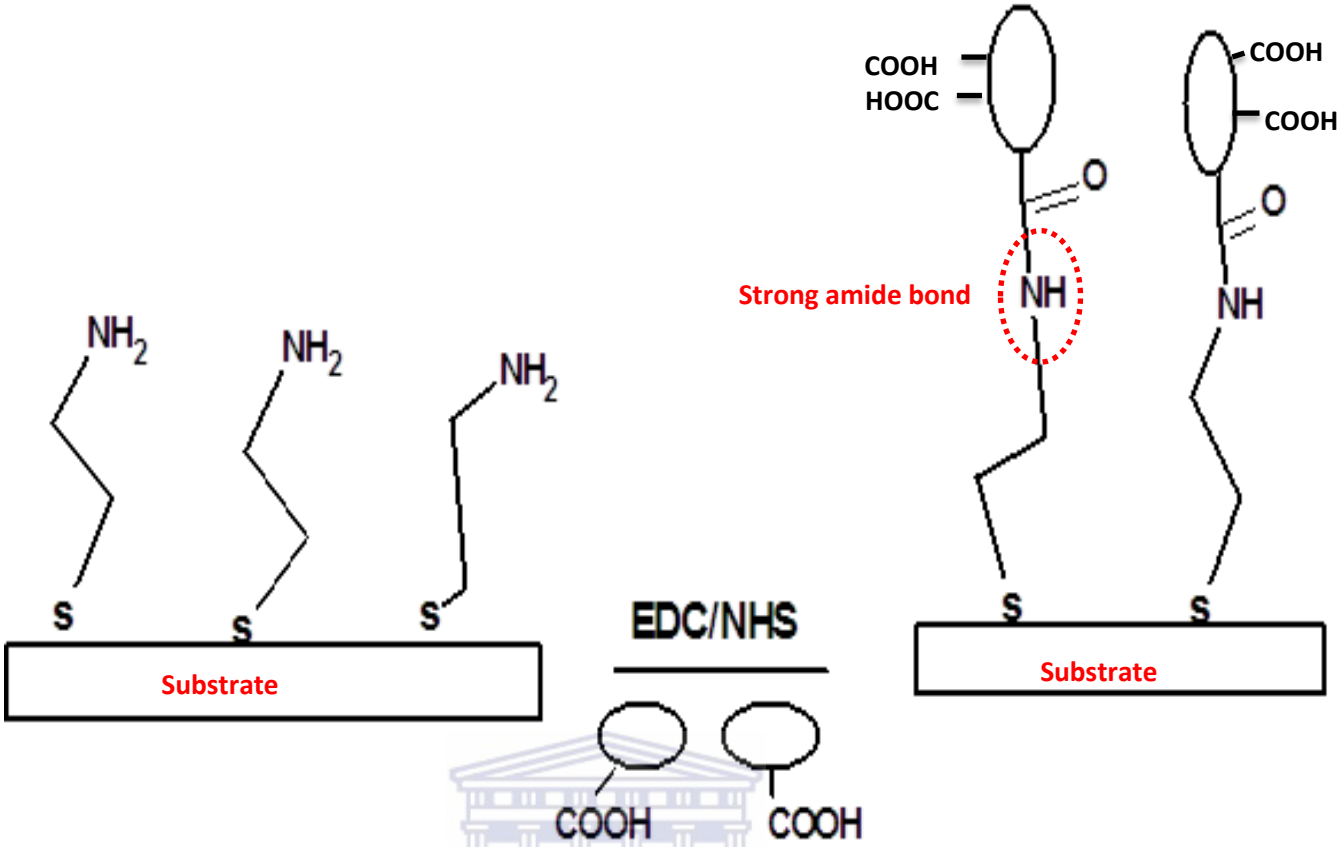

Figure 5: Immobilization of quantum dots on a substrate via covalent bonding

2.4 Biosensors

Biosensors are of interest within the field of modern analytical chemistry and pharmaceutics due to major demands and opportunities that appearing in clinical diagnostics, environmental analysis, food analysis and production monitoring (Ngoepe *et al*., 2013). Biosensors are devices that utilises biological components such as enzyme, antibody and nucleic acid to indicate the amount of material. The major part of biosensor is biological recognition system which translates information from the analyte concentration into a chemical or physical output signal with a defined sensitivity and its purpose is to provide the sensor with a high degree of selectivity for the analyte to be measured while the transducer part of the sensor serves to transfer the signal from the output domain of the recognition system, mostly to the

electrical domain because it provides bidirectional signal transfer (Thevenot *et al*., 2001). Concept of biosensor was introduced by Professor Leland C.Clark in 1962 whereby he described how to make electrochemical sensors more intelligent by adding enzyme transducer as membrane enclosed sandwich.

Biosensors are divided into basic groups depending on their methods of signal transductions: these groups are optical, mass, electrochemical, magnetic, micromechanical and thermal sensors (Sethi, 1994).

2.4.1 Enzyme based electrochemical biosensors

Enzymes are proteins with high catalytic activity and selectivity towards substrates and have been used for decades to assay the concentration of diverse analytes. Their commercial availability at high purity levels makes them very attractive for mass production of enzyme sensors since they have unique properties (Corcuera and Cavelieri, 2003). Biosensors constituting enzymes employ a class of enzymes known as oxidoreductases since they are heavily involved in metabolism and catalyses reduction or oxidation reactions with direct electron transfer which makes them highly suitable for electrochemical sensors providing real time monitorization of the target biomolecules (Trojanowicz *et al*., 1995). Enzyme based electrochemical biosensors can be produced by immobilizing enzyme onto working electrode surface to take the advantage of redox recycling effect and faradaic currents generated by redox cycle is due to increased mass transport of redox active species of the enzyme thus enhancing sensitivity and improves the signal to noise ratio and detection limit of the biosensor (Chen *et al*., 1999; Mena *et al*., 2005). Electrochemical measurements of CYPs immobilized on bare electrode had been investigation by (Bistolas *et al*., 2005) and found that electron transfer between electrode and enzyme's active site was poorly accomplished,

therefore mediators such as nanomaterials and conducting polymers were introduced to promote electron transfer to and from the enzyme to produce better signal (Sadik *et al.*, 2010). Since 1970's attempts have concentrated on the construction and development of electrochemical sensors Publication by (Nxisani,2012), the author used 3-mercaptopropionic acid capped gallium selenide (3-MPA-Ga_2Se_3) quantum dots as a mediator incorporated with CYP3A4 enzyme to promote electron transfer to and from the enzyme. In this study thioglycolic acid capped palladium telluride quantum dots (TGA-PdTe), 3-mercapopropionic acid palladium telluride quantum dots (3-MPA-PdTe) and 3-mercaptopropionci acid capped tin selenide quantum dots (3-MPA-SnSe) have been used as mediators for the promotion of electron transfer in the system.

2.5 Enzymes

2.5.1 Cytochrome P450

Cytochrome P450s were first discovered in 1955 in rat liver microsomes and characterized by an intense absorption band at 450 nm in the presence of carbon monoxide (Degtyarenko, 1995) and being a large family of heme-enzymes used to catalyse diversity of chemicals and involved in metabolism of many drugs, xenobiotic which holds biactivation responsibility (Estabrook *et al*., 1996; Shumyantseva *et al*., 2005). CYPs and other mixed function monooxygenases are located on the smooth endoplasmic reticulum of cells throughout the body with the highest concentrations in the liver and intestines. This CYP family comprises of many isoforms such as (CYP1A1, 2C9, 2C19, 2D6) which are responsible for drug metabolism in the body (Williams *et al*., 2004; Schneider and Clark, 2013) with CYP3A4 known as a major form of cytochrome P450 in the adult liver which metabolizes the greatest proportions of drugs thus its characteristics attracted the field of pharmacology and virology for study of newly developed drugs and their monitorisation (Gunaratna, 2000). Publication

by (Hendricks *et al*., 2009), the author used this type of enzyme in nanobiosensor fabrication for 2, 4-dichlorophenol. In this study CYP3A4 enzyme was used as a bio-component in developed electrochemical sensor for indinavir drug.

Figure 6 below describes the binding of indinavir drug onto the active site of the enzyme followed by reduction of an electron and shift spin state from low spin to high spin. Mono-oxygen onto the active site may lead to another electron reduction and formation of by-product

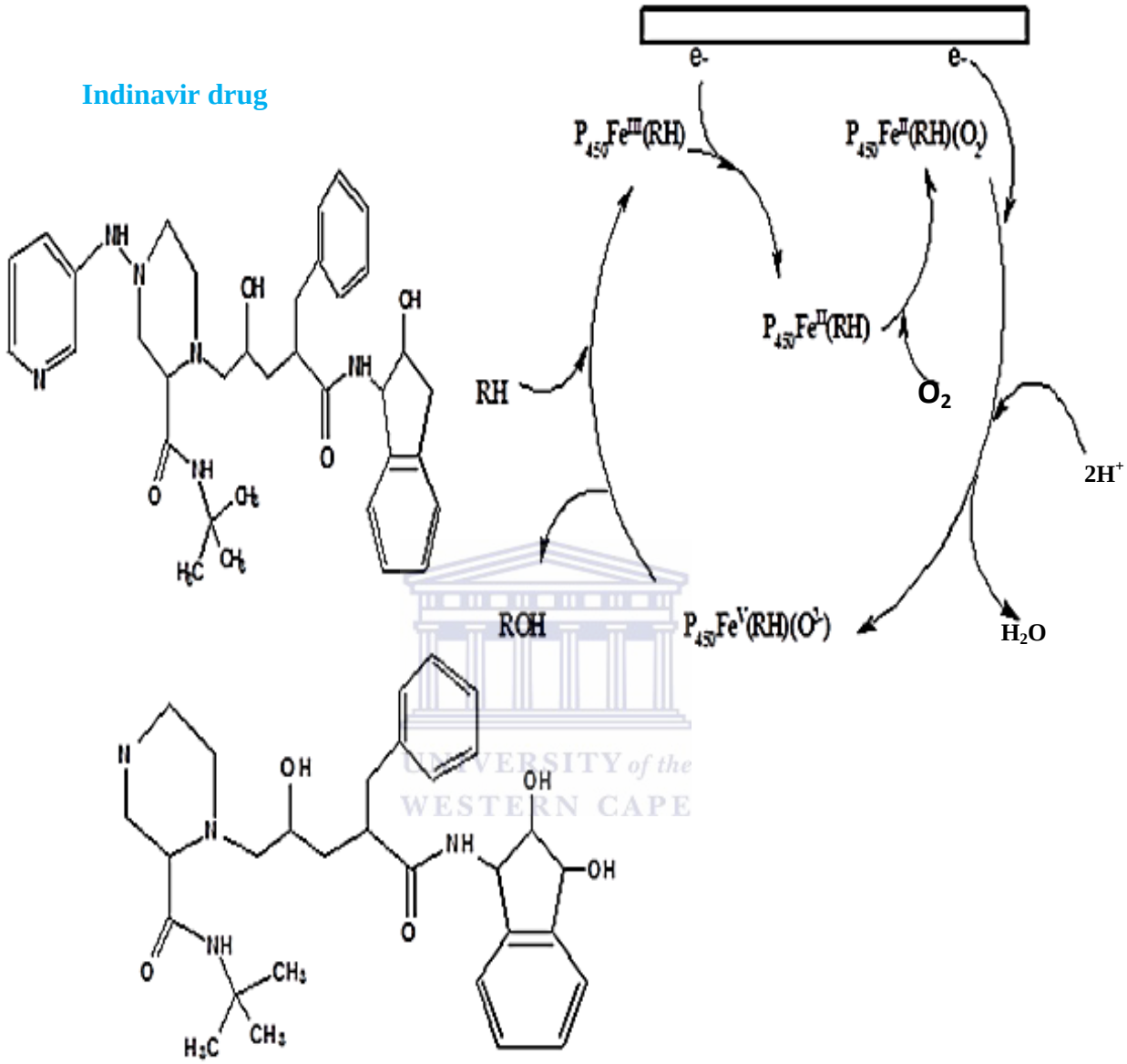

Figure 6: Schematic for electrocatalytic oxygenation reaction of indinavir-bound CYP3A4

Chapter three

Experimental

3 1 Summary

This chapter describes the procedures for the synthesis of 3-MPA-SnSeQDs, 3-MPA-PdTeQDs and TGA-PdTeQDs using appropriate reagents and different routes. This chapter also includes the immobilization procedure used to attach the enzyme for the development of biosensor. Included here are the characterization procedures for the biosensors as well as other materials used towards the fabrication of the biosensors using various techniques; spectroscopic (UV, FTIR and PL), microscopic (HRSEM, HRTEM) and electrochemical (CV).

3.2 Reagents

Analytical reagent grade Tin chloride (98%), palladium chloride (99.9%) 3-mercaptopropionic acid (MPA) (≥ 99%), thioglycolic acid (TGA) (≥ 99%), sodium hydroxide (≥ 99%), selenium powder (99.99%), sodium borohydrate (98%),hydrogen chloride (HCl) (37%), sodium dihydrogen phosphate monobasic anhydrous (H_2NaPO_4) (>99%) , disodium hydrogen phosphate dibasic (HNa_2PO_4) (>98%)**,** sodium phosphate monobasic dehydrate ($NaH_2PO_4.H_2O$), disodium hydrogen phosphate dibasic ($Na_2HPO_4.H_2O$) 1-ethyl-3-(3-dimethylaminopropyl) carbodiimide hydrochloride (EDC) and N-hydroxysuccinimide (NHS) (98%), L-cysteine (≥ 98%), cysteamine (≥ 98%) and Cytochrome P450-3A4 (CYP3A4) human expressed in *Saccharomyces cerevisiae* were purchased from Sigma Aldrich. Indinavir drug (Crixivan) and engineered Cytochrome P450-3A4 enzyme, purified from a full length human CYP3A4 cDNA clone and over expressed in *Escherichia coli* cells were purchased from Merck while the Alumina micro polishing pads were obtained from Buehler,

LL, USA. 0.1 M phosphate buffer solution, pH 7.4 was prepared from disodium hydrogen phosphate dibasic and sodium dihydrogen phosphate monobasic using Milli Q water purification. The indinavir drug was used without any purification and dissolved in 0.1 M PBS pH 7.4 whereby the active ingredient was removed and undissolved components were removed using filtering through a Whatman polytetrafluoroethylene syringe filter (pore size 0.3 µm).

3.3 Instrumentation

All electrochemical measurements were done using BAS100W integrated automated electrochemical work station from Bio Analytical Systems (BAS), Lafayette, USA and Princeton Applied Research Potentiostat model 273A. Ultraviolet-visible (UV-Vis) measurements were made using a Nicolet Evolution 100 UV-Visible spectrometer (Thermo Electron, UK) where the samples were placed in quartz cuvettes before analyses. All cyclic voltammograms were recorded with computer interfaced to BAS 100W and Princeton 273A electrochemical work station using a 10 mL electrochemical cell with three electrodes set up was used. The electrodes used in the study were (1) gold working electrode (A = 0.0201 cm^2) from BAS, (2) platinum wire from Sigma Aldrich acted as counter electrode and (3) Ag/AgCl from BAS kept in (3 M NaCl) was the reference electrode and alumina micro polishing pads were obtained from Buehler, LL, USA and were used for polishing the gold electrode before modification. HRTEM images were taken using Tecnai G2 F20X-Twin MAT 200kV Field Emission Transmission Microscopy from FEI (Eindhoven, Netherlands).All FTIR spectra were recorded on spectrum 100 FTIR spectrometer (PerkinElmer, USA) in a region of 400 to 4000 cm^{-1}.

3.3.1 Spectroscopic techniques

3.3.1.1 UV-Vis spectroscopy

Ultraviolet-visible spectroscopy (UV-Vis) is a technique used to study molecules and their electronic transitions, molar absorptivity (ε) which ranges from 0 to 10^5 and transition with molar absorptivity less than 10^3 (Chen,2013). The technique is used to confirm the identity of the substance through measured spectrum with reference spectrum (Tony, 1996) and for semiconductors this technique is used to offer convenient method to estimate optical band gaps due to electronic transitions between the valence band and conduction band. The transition metals arise from 3d and are quite broad and affected by ligands, solvents and charge transfer which occurs between the metal and ligand undergo jump from one orbital centred on ligand to an orbital centred on a metal. UV-Vis is a complementary technique to fluorescence since the transition of a molecule releases photons from excited state to ground state, and uses the absorption band (excitation) wavelength to detect emission of light from molecule. UV-Vis spectroscopy has limitations compared to other techniques because it shows only few broad absorbance bands and provides limited qualitative information and also pH, temperature may have an influence on changing the intensity and absorption maxima.

In the study by (Priyam *et al*., 2005) , the author used cysteine-capped cadmium selenide quantum dots synthesised in aqueous solution which exhibited absorption bands at 320 nm and shifted to 380 nm at different refluxing time to monitor the growth of quantum dots. Similar results had been found in the study for 3-MPA-SnSeQDs, 3-MPA-PdTeQDs and TGA-PdTeQDs.

3.3.1.2 Fourier transforms infra-red spectroscopy (FTIR)

Fourier transforms infra-red spectroscopy (FTIR) is a powerful tool that has strength to identify functional groups of molecules and (IR) portion of spectrum gives information regarding vibrational and rotational motion of atoms in molecules is widely used for qualitative analysis (Pegram, 2007). This technique allows molecules to excite to higher energy by absorbance of infrared radiation and the energy of absorbed IR radiation increases with amplitude of the vibrational motion of bonds in molecules (Griffiths *et al*., 2007). In this study FTIR had been used to study the presence of 3-mercaptopropionic acid, thioglycolic acid in the synthesized quantum dots. The study by (Khene *et al*., 2011) used TGA-CdTeQDs which exhibited C ═O stretch at 1542cm^{-1} due to carboxylic acid functional group of CdTeQDs and the absence of SH stretch from the CdTeQDs spectra which showed an interaction between the CdTeQDs and the TGA capping agent .Similar results were found in our study.

3.3.2. Microscopic techniques

3.3.2.1 High resolution scanning electron microscopy (HRSEM)

High resolution scanning electron microscopy (HRSEM) is one of most powerful technique fort studying surface morphology of material (Joy, 2009). This technique has been developed for the observation of surface fine structures through the introduction of an electron beam deceleration method and HRSEM image has been used to show not only the arrangement of mesopores but also fluctuations of the pore size and shape without damage or contamination during cross-sectioning and the ability to filter collected signals and high-resolution low voltage backscatter imaging which allows observation of compositional differences as well as

precise location of nanoparticles within the individual pores. The study by (Poznyak *et al*., 2005), indicates the use of HRSEM to determine surface morphology of TGA or 3-MPA capped CdTeQDs. The results obtained from study showed that the nanoparticles were spherical in shape and similar results were observed in our study.

3.3.2.2 High resolution transmission electron microscopy (HRTEM)

High resolution transmission microscopy is the technique that provides structural and distribution information at better than 0.2 nm, and the crystallographic information of particle of atom in materials (Smith, 1997). The technique uses phase contrast resulting from an interference of several beams and determines whether the particle that makes the specimen are dispersed or agglomerated. The technique is limited in high magnification imaging which requires high electron dose where by the specimen needs to be relatively insensitive (Howe *et al*., 2003). Quantum dots tend to agglomerate if no stabilizing agents are used to prevent this. In this study HRTEM was used to confirm the size and shape, distribution and morphology of synthesized quantum dots. In a study by (Hui, 2013), carboxylic-capped CdS quantum dots showed individual particle sizes of 2-5 nm. Similar results were observed in our study for 3-MPA-PdTeQDs and TGA-PdTeQDs.

3.3.3 Electrochemical techniques

3.3.3.1 Cyclic voltammetry

Cyclic voltammetry (CV) has become an important and widely used electroanalytical technique in many areas of chemistry. This technique is widely used for the study of redox processes, for understanding reaction intermediates, and for obtaining stability of reaction products (Mathson and Nicholas, 1938). It is also used in the measurement of kinetic rates

and constants, determination adsorption processes on surfaces electron transfer and reaction mechanisms (Bard and Faulkner, 1980). This technique is based on varying the applied potential (E) at a working electrode in both forward and reverse directions (at different scan rates) while monitoring the current (i). In many cases the applied potential is varied or the current is monitored over a period of time (t). Thus, all voltammetric techniques can be described as some function of E, i, and t. They are considered active techniques (as opposed to passive techniques such as potentiometry) because the applied potential forces a change in the concentration of an electroactive species at the electrode surface by electrochemically reducing or oxidizing it. The limitation of this technique is based on substance which is only oxidizable or reducible in a range where the solvent and the electrode are electrochemically inert. The most important parameters in a cyclic voltammogram are the peak potentials (E_{pc}, E_{pa}) and peak currents (i_{pc}, i_{pa}) of the cathodic and anodic peaks, respectively. If the electron transfer process is fast compared with other processes (such as diffusion), the reaction is said to be electrochemically reversible, and the peak separation is given by:

$$\Delta E_p = \left| E_{pc} - E_{pa} \right| = 2.303 \, RT/nF \qquad (1)$$

Thus, for a reversible redox reaction at 25 °C with *n* electrons ΔE_p should be $0.0592/nV$.

The formal reduction potential (E^o) for a reversible couple is given by:

$$E^\circ = \frac{E_{pa} + E_{pc}}{2} \qquad (2)$$

In a study by (Khene *et al*., 2011), the characterisation of TGA-CdTeQDs has been done to determine the electrochemical properties of CdTeQDs on a gold electrode surfaces whereby

two peaks located at -0.6 V and -0.9 V were attributed to reduction of Te^{IV} to Te^{0} and Te^{0} to Te^{2-} with one peak observed for CdTeQDs which was also observed in our study.

3.4 Methodology

3.4.1 Synthesis of selenide and telluride quantum dots

3.4.1.1 Mercaptopropionic acid-capped tin selenide quantum dots (3-MPA-SnSeQDs)

$SnCl_2.2H_2O$ (0.06 g) and 3-mercaptopropionic acid (132.9 µL) were dissolved in 10 mL of deionised water in a three neck round bottomed flask, followed by adjustment of the pH to 12 by the addition of 2 M NaOH solution and the colour changed to green. The mixture was stirred and bubbled with N_2 gas for 30 min. Separately, another solution of NaHSe was prepared by mixing selenium powder 0.254 g and equamolar grams of $NaBH_4$ in 10 mL deionised water. This solution was stirred continuously at room temperature for 30 min until the solution attained a dark yellow colour. Then 5 mL of the NaHSe solution was injected into the ($SnCl_2$ and 3-MPA) solution and the colour changed to pale yellow. After that the reaction quenched immediately when placed in the freezer at 20 ºC.

3.4.1.2 Thioglycolic acid- capped palladium telluride quantum dots (TGA-PdTeQDs)

$PdCl_2$ (0.332 g, 1.875 mmol) and thioglycolic acid (TGA) (392 µL, 5.625 mmol) were dissolved in 10 mL of deionised water in a three neck round bottomed flask, followed by adjustment of the pH to 11.8 by addition of 5 M NaOH solution. The mixture was stirred and bubbled with N_2 gas for 30 min. In another container, a fresh solution of NaHTe was prepared by mixing tellurium powder (0.254 g, 1.25 mmol) and $NaBH_4$ (0.151 g, 2.5 mmol) in 10 mL deionised water and heated to 80^0C for 30 min until the solution attained a light

purple colour. The molar ratio of Pd^{2+}/TGA/Te was 1.5:3:1. Thereafter, 5 mL of NaHTe solution was injected into the ($PdCl_2$ and TGA) solution and a colour changed was observed from reddish to orange then greenish colour after some time. After injection, the solution was heated to 100 $^{\circ}$C and the aliquots of the resultant product were collected at different time intervals in order to monitor the growth of TGA capped-PdTeQDs.

3.4.1.3 Mercaptopropionic acid-capped palladium telluride quantum dots (3-MPA-PdTeQDs)

$PdCl_2$ (0.332 g, 1.875 mmol) and 3-mercaptopropionic acid (3-MPA) (490 µL, 5.625 mmol) were dissolved in 10 mL of deionised water in a three neck round bottomed flask, followed by adjustment of the pH to 11.8 by addition of 5 M NaOH solution. The mixture was stirred and bubbled with N_2 gas for 30 min. In a clean flask, a solution of NaHTe was prepared by mixing tellurium powder (0.319 g, 1.25 mmol) and $NaBH_4$ (0.189 g, 2.5 mmol) in 10 mL deionised water and covered by aluminium foil at room temperature for 30 min until the solution attained a light purple colour. The molar ratio of Pd^{2+}/TGA/Te was 1.5:3:1. Then 5 mL of NaHTe solution was injected into the ($PdCl_2$ and 3-MPA) solution and a colour changed was observed from reddish to dark orange after some time. After injection, the solution was heated to 100 $^{\circ}$C and the aliquots of resultant product were collected at different time intervals in order to monitor the growth of 3-MPA capped-PdTeQDs.

3.4.2 Fabrication of CYP 3A4 biosensors

3.4.2.1 Fabrication of CYP3A4 biosensor: *3-MPA-SnSeQDs/L-cyst/Au* biosensor system for indinavir

In the fabrication process of biosensor, a gold electrode was first polished with 1 µm, 5 min, 0.3 µm, 10 min and 0.05 µm, 20 min alumina slurries in glassy polishing pads respectively, followed by ultrasonication in absolute ethanol and distilled water for 5 min each. The clean Au electrode was then immersed in a solution containing 0.02 M L-cysteine solution at room temperature for 24 h and kept in the dark in order to form a well characterised, self-assembled monolayer on metal electrodes (Au). This was used as a strategy to immobilise and organise biomolecules at the interface and also give stability and provide electron transfer (Goncolves et al., 2007). After that the L-cyst/Au modified electrode was rinsed carefully with distilled water to remove unbound L-cysteine molecules. The L-cyst/Au modified electrode was then activated by dipping into a solution containing 1:1 of (EDC/NHS) for 30 min followed by drop coating of SnSe nanocrystals functionalized with 3-mercaptopropionic acid solution for 2 h to form 3-MPA-SnSeQDs/L-cyst/Au modified gold electrode. A volume of 3 µL of a 4 µM CYP3A4 enzyme solution was then drop coated onto 3-MPA-SnSeQDs/L-cyst/Au modified electrode surface and allowed to dry for 3 h at -4 ºC. The resulting electrode was rinsed gently with distilled water to remove any physical adsorbed enzyme. This fabrication process resulted into CYP3A4/3-MPA-SnSeQDs/L-cyst/Au (biosensor) and was kept at -4 ºC in 0.1 M PBS when not in use.

3.4.2.2a Fabrication of CYP3A4 biosensor: *TGA-PdTeQDs/Cyst/Au* biosensor system for indinavir

The developed biosensor used cysteamine as a linking material whereby a monolayer was formed on gold electrode surface due to gold-sulphur interaction. The Cyst/Au modified electrode was then activated by dipping into a solution containing 1:1 of (EDC/NHS) for 30 min followed by drop coating of PdTe nanocrystals functionalized with thioglycolic acid solution for 2 h to form TGA-PdTeQDs/Cyst/Au modified electrode. A volume of 3 µL of concentrated CYP3A4 enzyme solution was then drop coated onto TGA-PdTeQDs/Cyst/Au modified gold electrode surface and allowed to dry for 3 h at -4 ºC. The resulting electrode was rinsed gently with distilled water to remove any physical adsorbed enzyme. This fabrication process resulted into CYP3A4/TGA-PdTeQDs/Cyst/Au (biosensor) and was kept at -4 ºC in 0.1 M PBS when not in use.

3.4.2.2b Fabrication of CYP3A4 biosensor*: 3-MPA-PdTeQDs/Cyst/Au* biosensor system

The biosensor fabrication process was similar to the description given in Section 3.4.2.2a except that a different capping agent (3-mercaptopropionic acid**)** was used. The resultant biosensor system, CYP3A4/3-MPA-PdTeQDs/Cyst/Au, was kept at -4 ºC in 0.1 M PBS when not in use.

3.4.2.3 Preparation of indinavir stock solution

A capsule of indinavir drug was placed in a 25 mL volumetric flask which was filled up to the mark with 0.1 M sodium phosphate buffer solution, pH 7.4. Un-dissolved components were removed by filtering the formed suspension through a Whatman polytetrafluoroethylene

syringe filter (pore size 0.3 µm) into a clean storage bottle and the concentration of prepared indinavir was found to be 28.08 µM. The solution was used as stock indinavir solution from which all the other working solutions were prepared using appropriate dilutions with 0.1 M sodium phosphate buffer.

Chapter four

Results and discussion

4.0 Summary

This chapter deals with characterisation of the L-cysteine, 3-MPA-SnSeQDs and CYP3A4 used as a proof of concept for the development of the biosensor of interest. Their properties were investigated using techniques such as CV, SEM and UV-vis.

4.1 Characterisation of 3-MPA-SnSe quantum dots

4.1.1 UV-Vis spectrophotometry of 3-MPA-SnSeQDs

The UV-Vis absorption spectrum of the 3-MPA-SnSe is shown in **Fig 7** Herein the optical properties of the quantum dots are exhibited by a weak broad absorption band at 350 nm associated with energy band gap of 3.5 eV value (Menade *et al*., 2013). The broad absorption peak indicates inhomogeneity of the particle size distribution be due to interferences from carrier matrix, i.e. different reagents used during the synthesis.

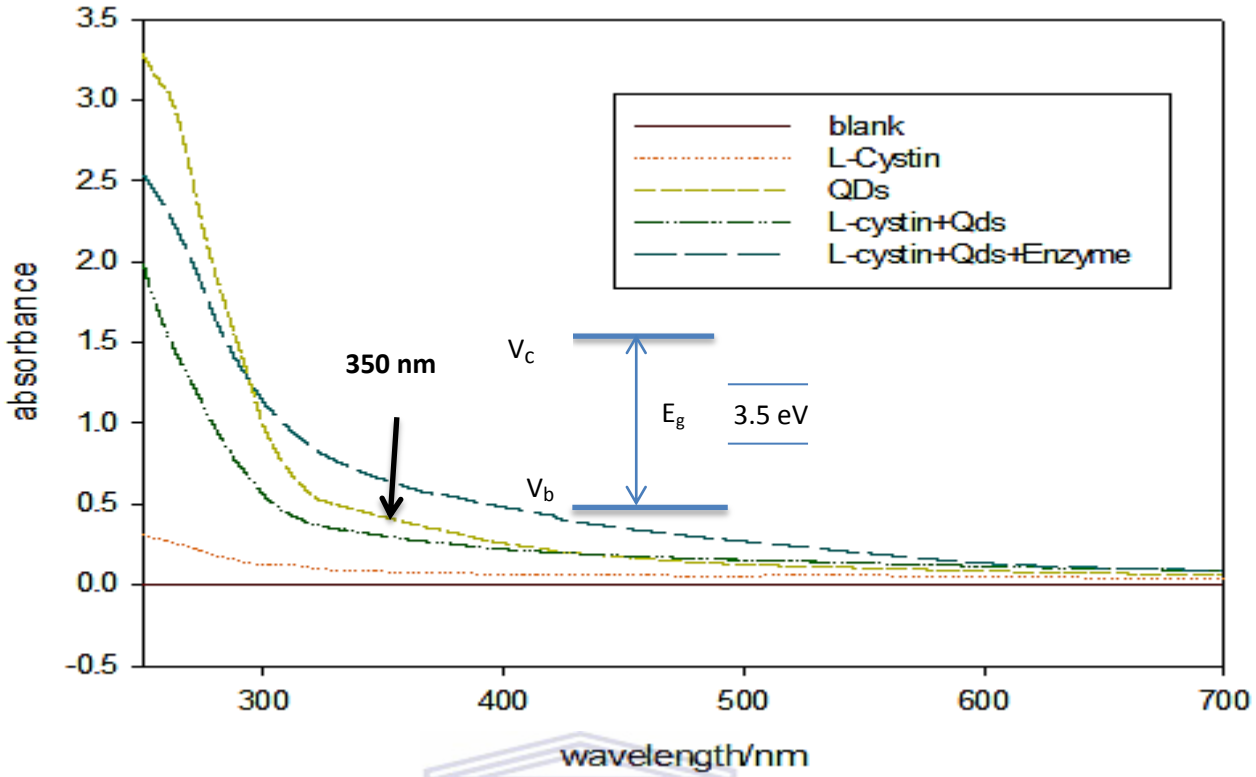

Figure 7: UV-Vis spectra of 3-MPA-SnSe quantum dots

4.2 Electrochemical characterisation of 3-MPA-SnSeQDs and L-cysteine

4.2.1 Electrochemistry of Au/3-MPA-SnSe quantum dots

Figure 8 depicts cyclic voltammograms of bare Au electrode and 3-MPA-SnSe quantum dots immobilized onto the Au electrode in 0.1 M PBS solution. For the bare electrode, three reduction peaks where observed attributed to gold oxide E_{pc} = (400 mV, -200 mV and -500 mV) and one oxidation peak attributed to the formation of gold oxide E_{pa} = (1100 mV), CV showed a decrease in peak separation E_{pc} = 405 mV that was due to electrode oxygen reduction. The peak at -50mV corresponded to the reduction of O_2 to H_2O_2 while the peak at -500 mV is responsible for a further reduction of H_2O_2. As compared to bare Au electrode, the Au/3-MPA-SnSe quantum dots also exhibited three reduction peaks at 405 mV, -20 mV and -380 mV but two oxidation peaks at 400 mV and 990 mV. The reduction peak at (405 mV)

showed an increase in peak current than that of bare gold electrode at approximately the same region. Observed here is also a shift to more negative potentials as a result of the capping agent 3-MPA donating negative charges to the SnSe quantum dots. When the bare gold electrode was scanned using redox potentials in cyclic voltammetry, the formation of a monolayer of electrosorbed oxygen at gold electrode was shown in the following mechanism (Bruckensten and Shay, 1985).

(a) $Au\text{-}(H_2O)_{ads} \rightarrow Au\text{-}OH + H^+ + e^-$ (3)

(b) $Au\text{-}OH \rightarrow Au{=}O + H^+ + e^-$ (4)

and finally the placed reaction

(c) $Au{=}O + H_2O \rightarrow O{=}Au\text{-}(H_2O)_{ads}$ (5)

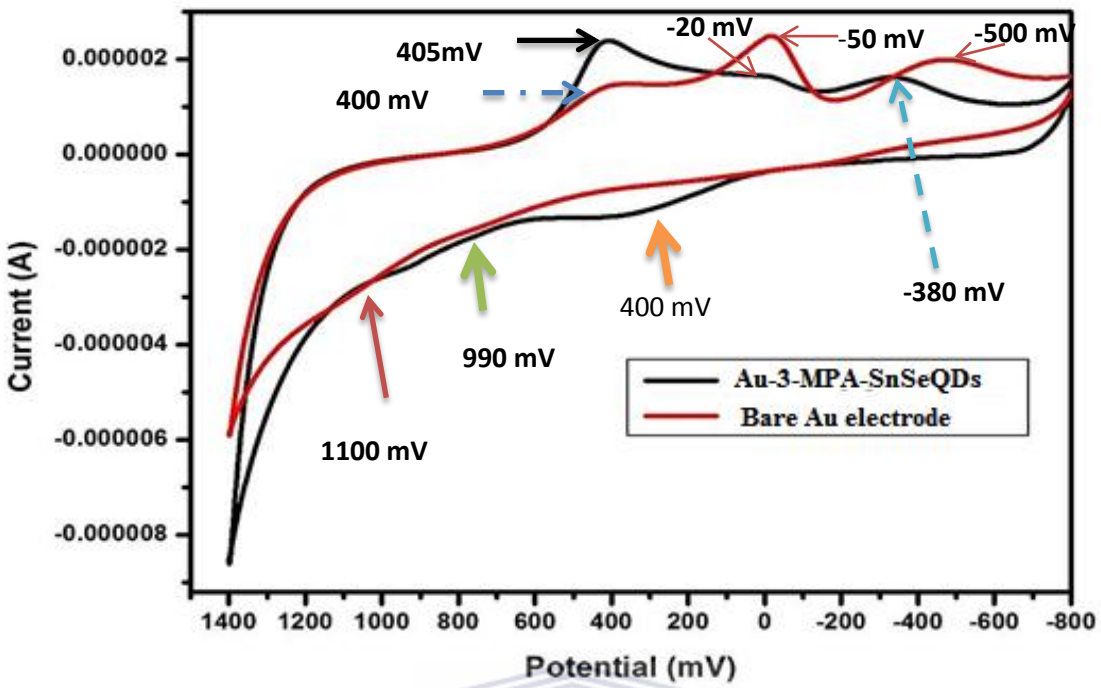

Figure 8: Cyclic voltammograms of bare Au and Au/3-MPA-SnSeQDs in 0.1 M PBS pH 7.4 at 50 mV/s

4.2.2 Electrochemistry of Au/L-cysteine

Figure 9 shows the cyclic voltammogram of Au/L-cysteine where two reduction peaks were exhibited at (476 mV and -6 mV) attributed to desorption of thiol (Hager and Brolo, 2002). A high peak current separation compared to the bare electrode was observed. One oxidation peak at (800 mV) due to adsorption of the thiol group was observed and found to be more enhanced that what was seem from the bare electrode. A shift to more negative potentials was seen meaning that the reduction process was favoured with an indication of an electron transfer resulting from the thiol group acting as a promoter due to its high affinity for gold hence their redox peaks potentials occurred at same potential (Zhao *et al.*, 2006).

The adsorption process of sulphur onto gold is described by the following equation (Wierse *et al*., 1978).

$$Au\text{-}H_2O + S^{2-} \leftrightarrow Au\text{-}S_{ads} + H_2O + 2e^- \quad (6)$$

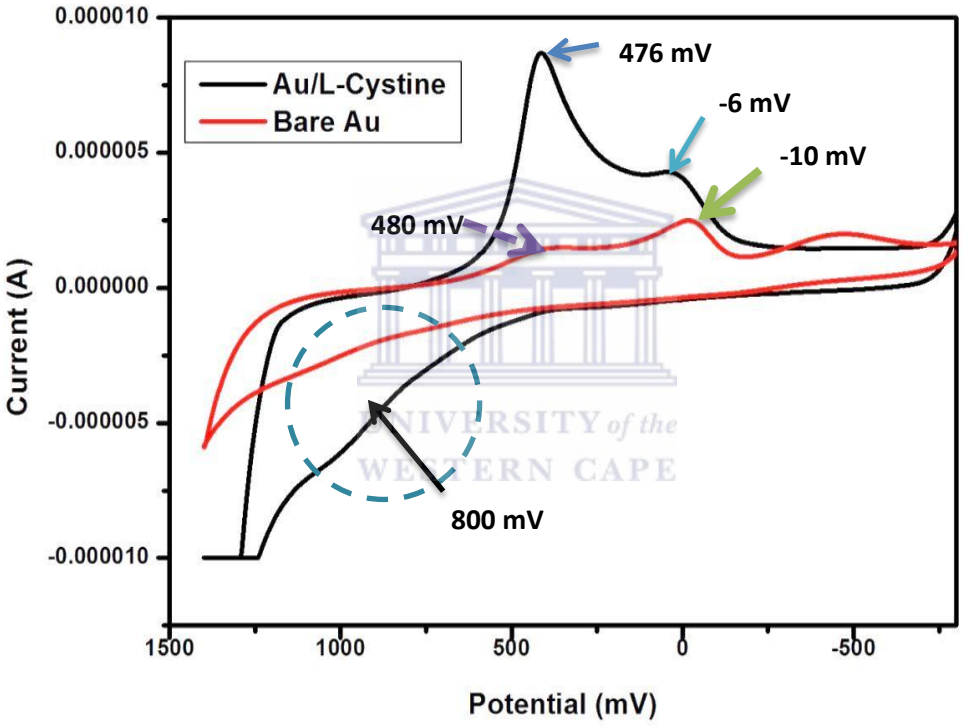

Figure 9: Cyclic voltammograms of bare Au and Au/L-cysteine in 0.1 M PBS pH 7.4 at 50 mV/s

4.2.3 Electrochemistry of Au/L-cyst/3-MPA-SnSeQDs/CYP3A4 biosensor modification

Figure 10 shows a cyclic voltammogram of Au/L-cyst/3-MPA-SnSeQDs/CYP3A4 (biosensor) without the analyte additions, the biosensor exhibited a good current response indicating a quasi-reversible process characterised by the presence of redox potentials with

reduction peaks (E_{pc} = 600 mV and -250 mV) and an oxidation peak (E_{pa} =750 mV) which shifted towards negative potential. this huge shift was due to the coupling between (NH_2) of building block material (L-cysteine) and (COOH) of 3-MPA-SnSe quantum dots since 3-MPA-SnSe acted as a mediator by shuttling electrons to and from the enzyme to speed up the reaction. The layer- by- layer fabrication step was necessary for speeding up the reaction. An investigation regarding the direct electrochemistry of CYP3A4 using layer-by-layer films in order to improve the direct electron transfer between the heme proteins was done (Joseph *et al*., 2003). In this study a layer-by-layer improved the electron transfer of redox couples in CYP3A4/3-MPA-SnSeQDs/L-cyst/Au whereby the oxidation peak shifted to 750 mV and reduction peak to -250 mV as compared to bare electrode.

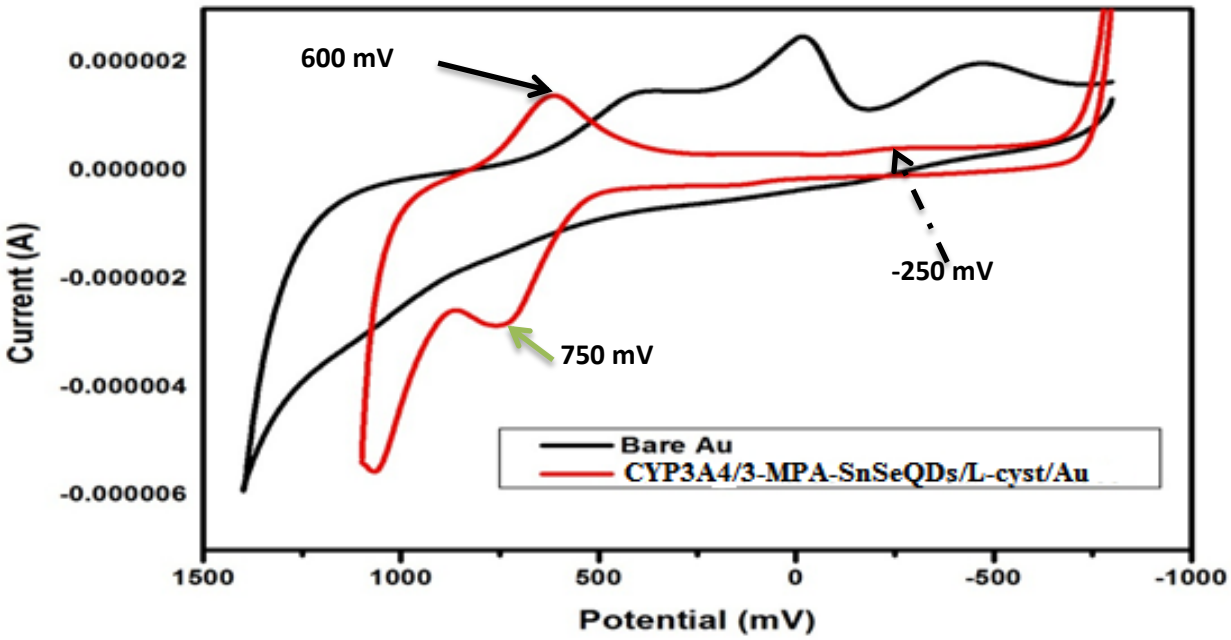

Figure 10: Cyclic voltammograms of bare Au and Au/L-Cyst/MPA-SnSeQDs/CYP3A4 in 0.1 M PBS pH 7.4 at 50 mV/s

4.2.4 Electrochemistry of L-cyst, 3-MPA-SnSeQDs and biosensor

Figure 11 shows a cyclic voltammograms of L-cyst, 3-MPA-SnSeQDs and CYP3A4/3-MPA-SnSeQDs/L-cyst/Au modified onto gold electrode in the absence of the analyte. The redox potential peaks of each layer showed an increase in peak current as compared to the bare gold electrode. The reduction peaks are seen to be shifting towards more positive potentials while the oxidation peaks are seen to be shifting to more negative potentials indicating an electron transfer and irreversible process.

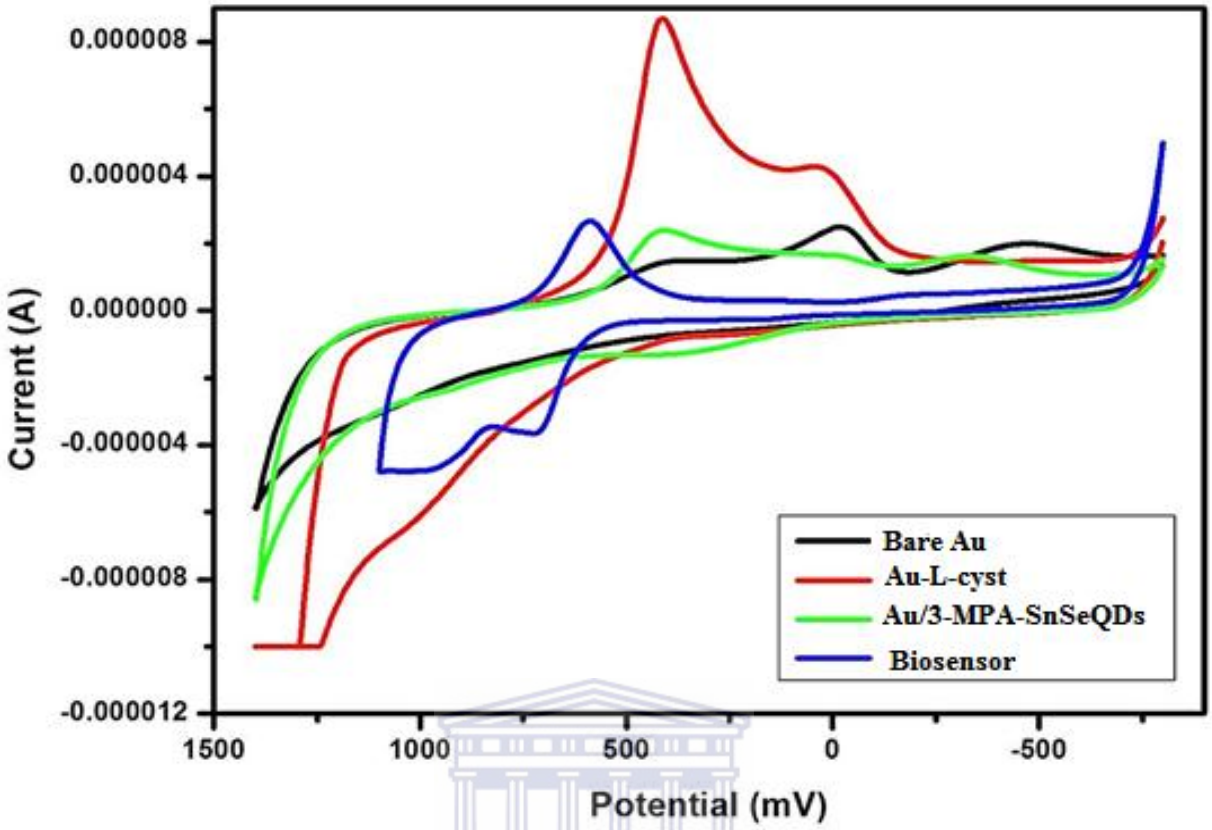

Figure 11: Cyclic voltammograms illustrated different films deposited onto gold electrode 0.1 M PBS pH 7.4 at 50 mV/s. (black line) Bare gold, (red line) , (green line) Au/3-MPA-SnSeQDs and (blue line) Au/L-cyst/3-MPA-SnSeQDs/CYP3A4

4.3 Biosensor measurements

The cyclic voltammetry was used to study the catalytic behaviour to successive additions of indinavir drug under aerobic conditions as shown in **Fig 12**, the aerobic conditions in the reaction was necessary for binding the monooxygenation and (HEME) of CYP3A4 (Fe^{2+}) in order to form Fe-O centre (Ignaszak *et al*., 2009). At 0 nM there was no catalytic signal observed for the CYP3A4/3-MPA-SnSeQDs/L-cyst/Au but when the analyte (indinavir) was added, a catalytic response was observed with a reduction peak (E_{pc} = -400 mV) which showed an increase at different additional concentrations of the analyte. Exhibited here is a

shift from -450 mV to -400 mV due to the presence of oxygen binding to the active site of the (HEME) until 0.098 nM concentration (saturation point) was reached. The electrochemical properties of L-cysteine and 3-MPA-SnSe quantum dots showed a decrease in peak currents as the analyte concentrations were added therefore an interaction only occurred between the active site of the enzyme and the analyte. The biosensor gave a very good response up to maximum concentration of 0.093 nM.

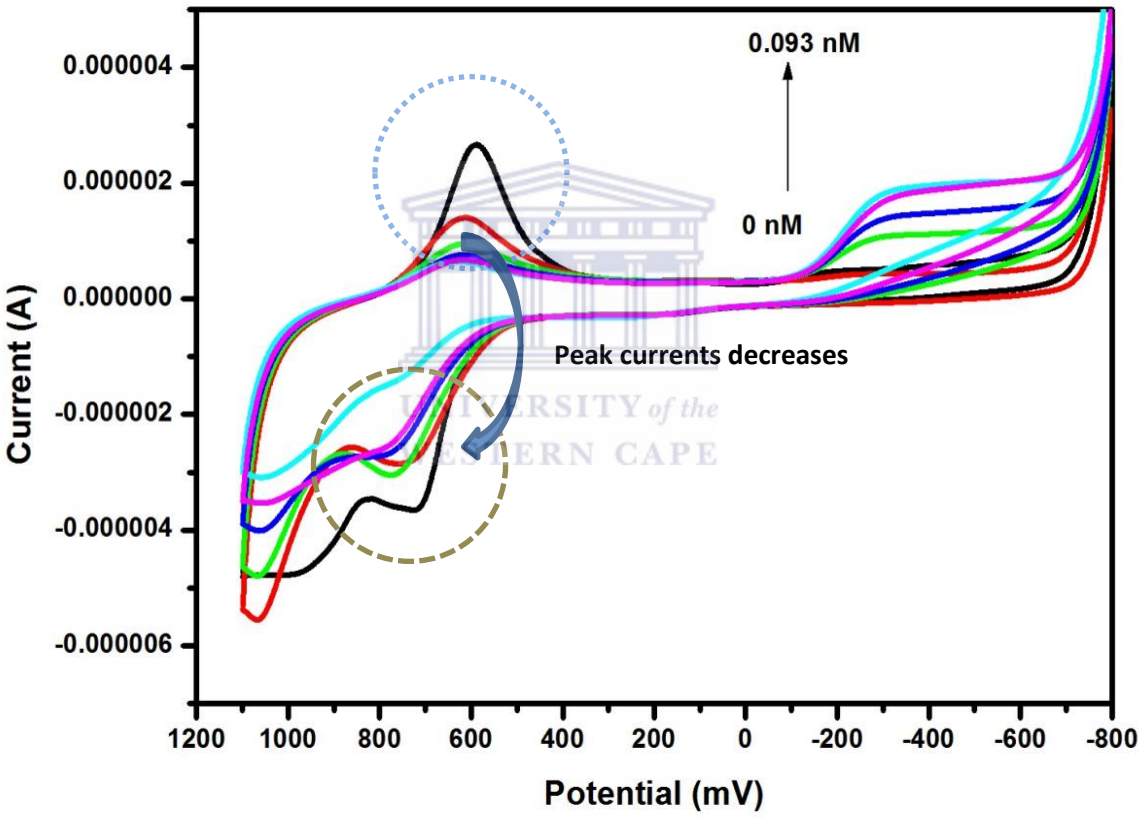

Figure 12: Cyclic voltammograms of Au/L-cyst/3-MPA-SnSeQDs/CYP3A4 biosensor responses to successive additions of indinavir in 0.1 M PBS pH 7.4 at 20 mV/s

4.4. Microscopy of L-cyst, 3-MPA-SnSe quantum dots and the biosensor

In **Fig 13**, the scanning electron micrographs of the various stages of electrode modification are shown. The SEM micrograph in **Fig 13(b)** shows the morphology after the immobilisation of L-cyst on a screen printed electrode. The morphology resembles a (smooth) flat flower onto the electrode surface which was due to chemisorbed L-cyst. **Fig 13(c)** shows a star shaped surface whereby the flat flower shaped L-cyst disappeared due to the binding or the interaction of the amino group of L-cysteine and the carboxylic group of the quantum dots which were cross-linked using (EDC/NHS). The quantum dots exhibited a charging effect due to their fluorescent properties while **Fig 13(d)** shows small bubbles of different sizes and very tiny bright dots which are caused by the enzyme immobilised onto the Au/L-cyst/3-MPA-SnSeQDs.

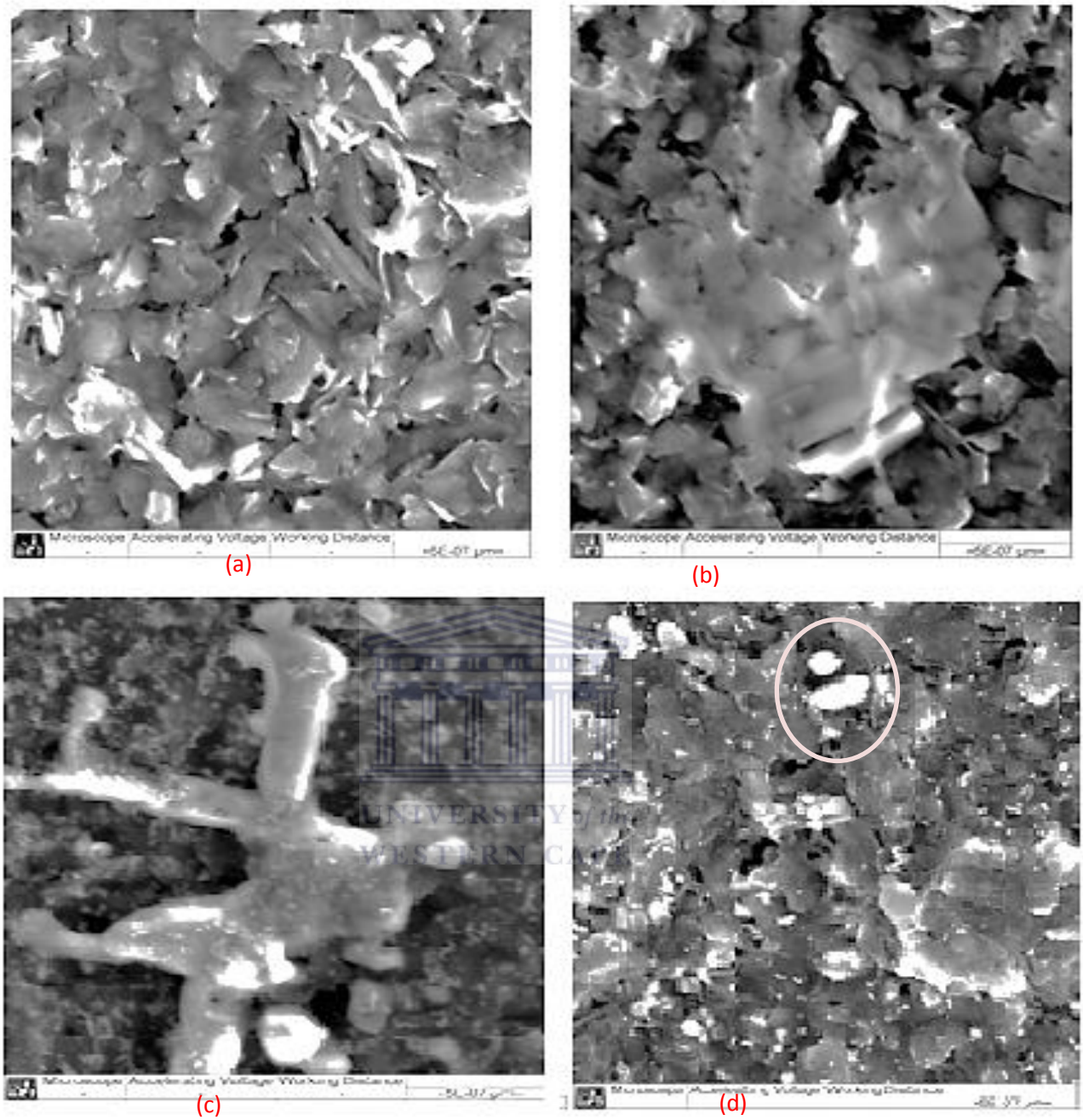

Figure 13: Scanning electron micrographs of (a) bare Au electrode, (b) Au/L-cyst, (c) Au/L-cyst/3-MPA-SnSeQDs, (d) Au/L-cyst/3-MPA-SnSeQDs/CYP3A4

4.5 Electrochemical characterisation of biosensor responses for indinavir drug

In order to ascertain the correct reduction currents for the biosensor responses, a short potential window (200 mV to -800 mV) was used for this evaluation. The increase in reduction potential and the shift in peak currents were observed for each indinavir addition. This CV response pattern was a characteristic of an electrocatalytic reaction of CYP biosensor in the presence of a substrate and an oxygen saturated solutions (Iwuoha *et al*., 1998).

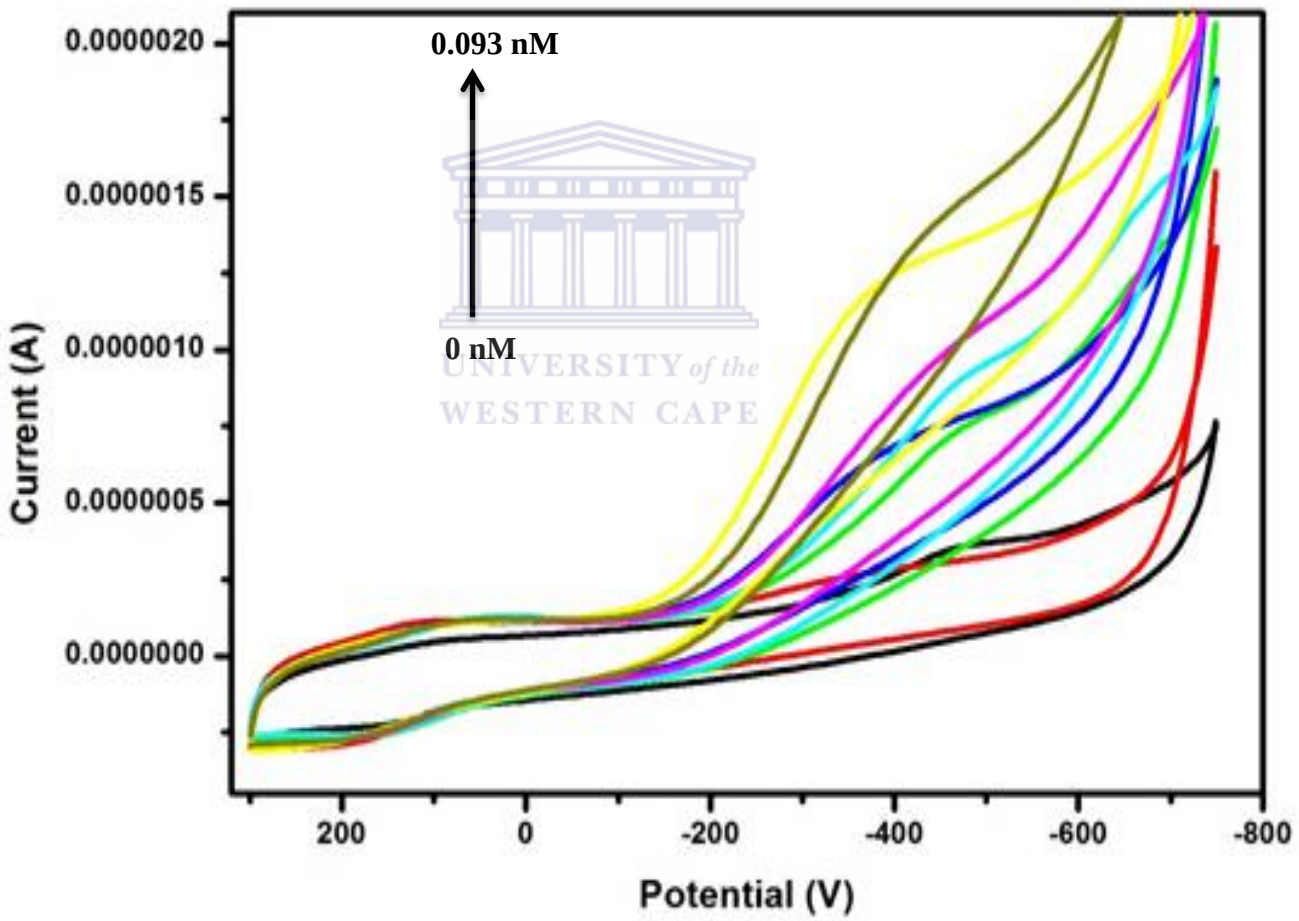

Figure 14: Cyclic voltammograms of CYP3A4/3-MPA-SnSeQDs/L-cyst/Au biosensor response to successive additions of indinavir in 0.1 M PBS pH 7.4 at 20 mV/s

4.5.1 Calibration curve for Au/L-cyst/3MPA-SnSeQDs/CYP3A4 biosensor

The interpretation of hyperbolic calibration curve obtained for the biosensor was explained using the Michaels-Menten kinetics for enzyme to substrate.

$$i = \frac{i_{max}[\text{indinavir}]}{K_M^{app} + [\text{indinavir}]} \quad (7)$$

The value of K_M^{app} obtained was 0.007.93 mM and the value of i_{max} was 1.29 μA. The low value for K_M^{ap} obtained for biosensor confirmed the CYP3A4 was immobilized in a biocompatible environment and retained its catalytic properties and high enzymatic activity towards indinavir. The biosensor sensitivity was determined to be 0.221 μA/nM with a response time of 11 s and limit of detection (LOD) of 3.22 ng/mL. Therefore the biosensor was suitable for low measuring the low concentrations of indinavir.

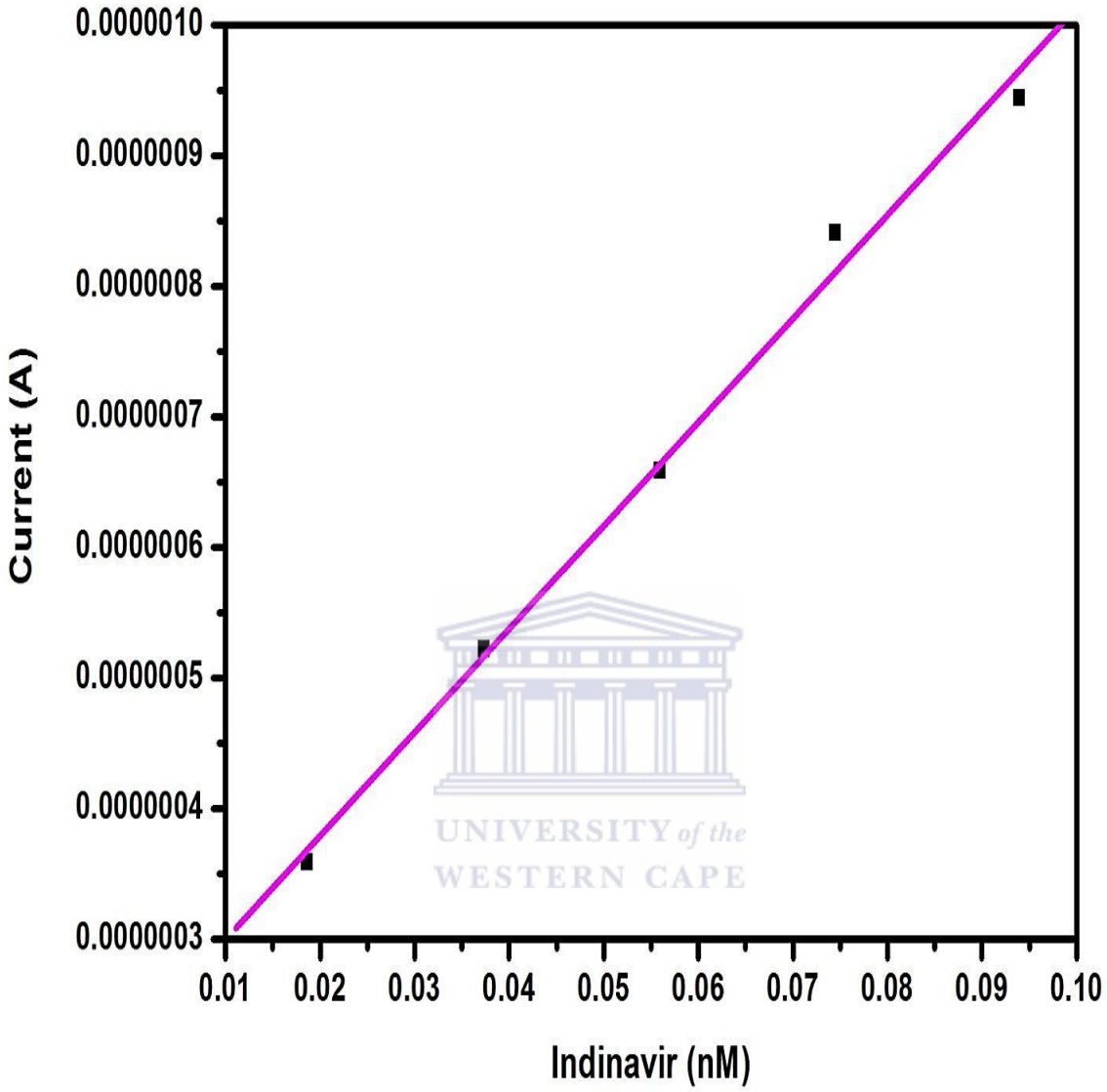

Figure 15: Calibration curve drawn from the linear region of the biosensor responses in Fig 14

Chapter five

5.1. Characterisation of TGA-PdTeQDs

5.1.1 UV-Vis spectrophotometry of TGA-PdTeQDs

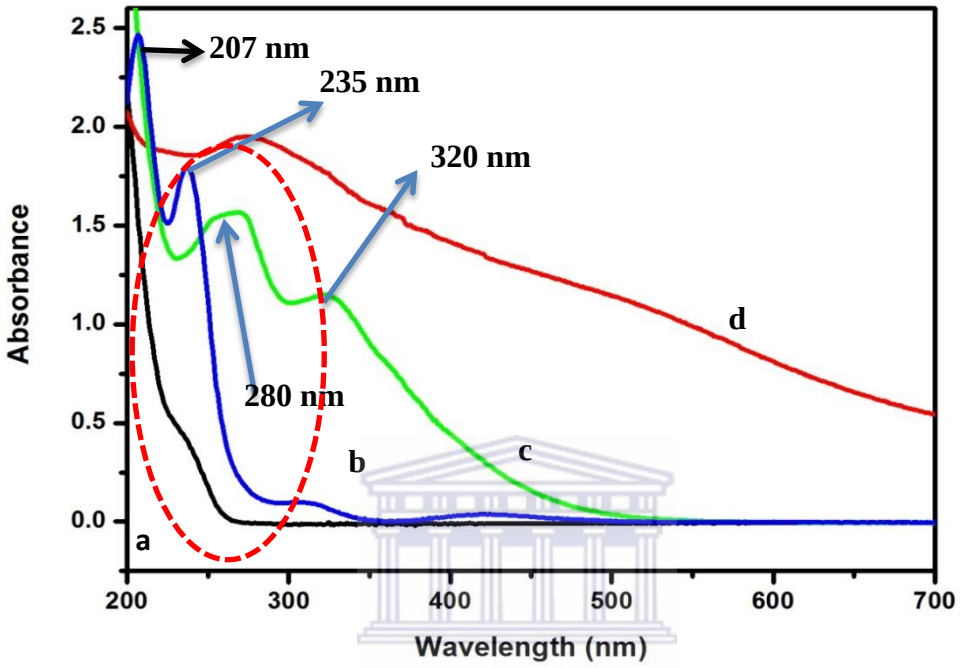

Figure 16: UV-Vis of (a) TGA capping agent, (b) $PdCl_2$, (c) TGA-$PdCl_2$, and (d) NaHTe

The absorbance band spectra of the precursors used in this study are shown in **Fig 15**(b) shows the absorbance bands of Palladium chloride ($PdCl_2$) appearing at 207 nm, 235 nm, 310 nm and 420 nm. **Fig 15**(c) shows the absorbance bands of palladium chloride mixed with thioglycolic acid during the synthesis exhibiting two absorbance bands one at 280 attributed to the interaction between ligand-to metal charge and the second absorbance band at 320 nm attributed to PdTeQDs. The absorbance band indicated in **Fig 15**(d) is due to NaHTe exhibiting a very broad peak in the range 250-320 nm.

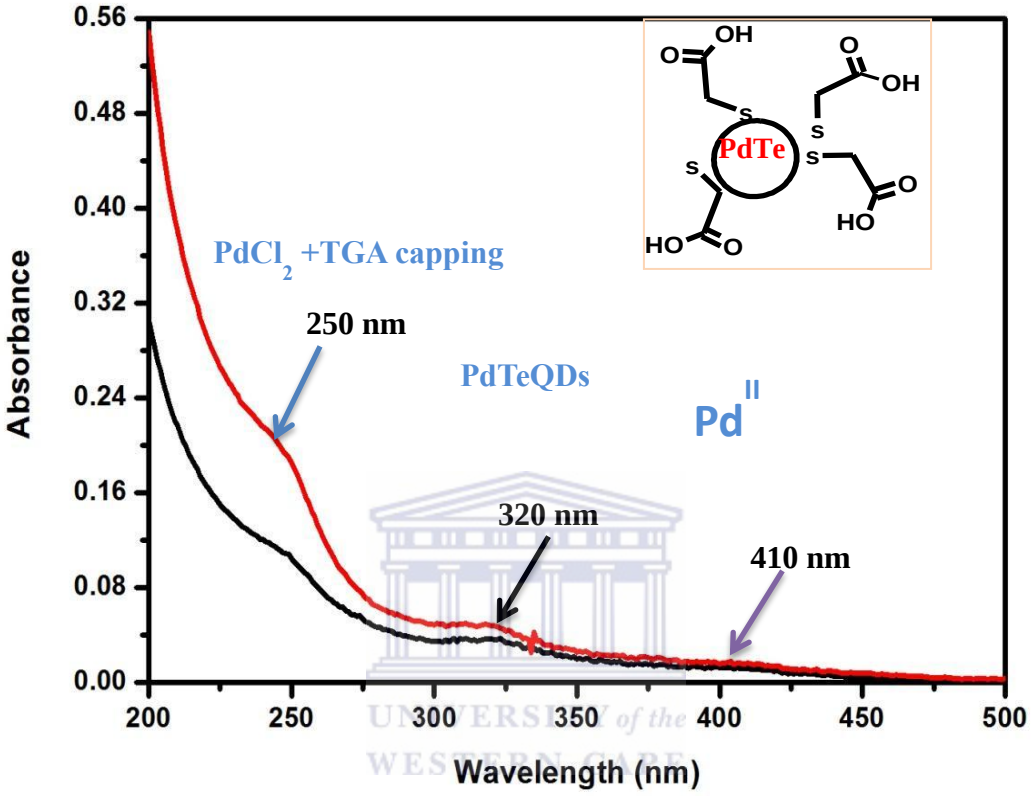

Figure 17: UV-Vis of TGA-PdTeQDs

The nature of interaction between the valence band and conduction band as well as the band gap size determines the optical properties of semiconducting materials. The absorption spectrum of TGA-PdTeQDs is shown in **Fig 17** exhibiting a broad absorption band at 320 nm associated with energy band gap of 3eV. The broad absorbance band is due to PdTeQDs however, the absorption band appearing at 250 nm is attributed to ligand-to-metal charge transition of Pd(II) ions (Yonezawa *et al*., 2001; Nemamcha *et al*., 2006). The observed

absorption band at 420 nm appearing at lower energy indicates the presence of Pd^{2+} ions in the reaction mixture (Petla *et al*., 2011; Namini *et al*., 2007).

Fluorescence spectroscopy is a powerful tool in biological research which relies greatly on the availability of sensitive fluorescent probes (Frasco and Chaniotakis, 2009). Fluorescence spectrum uses the excited band obtained from the UV-Vis in order to determine whether the material emits light. The spectra below presented the exhibition of emission peaks from 411-421 nm which shifted to larger wavelegths because of further particle growth (Zhang *et al*., 2002). The emission peak at 30 min was narrower than 40 min -60 min, indicating different sizes of quantum dots and also no further shift occurred between 50 min and 60 min indicating that the quantum dots had fully grown

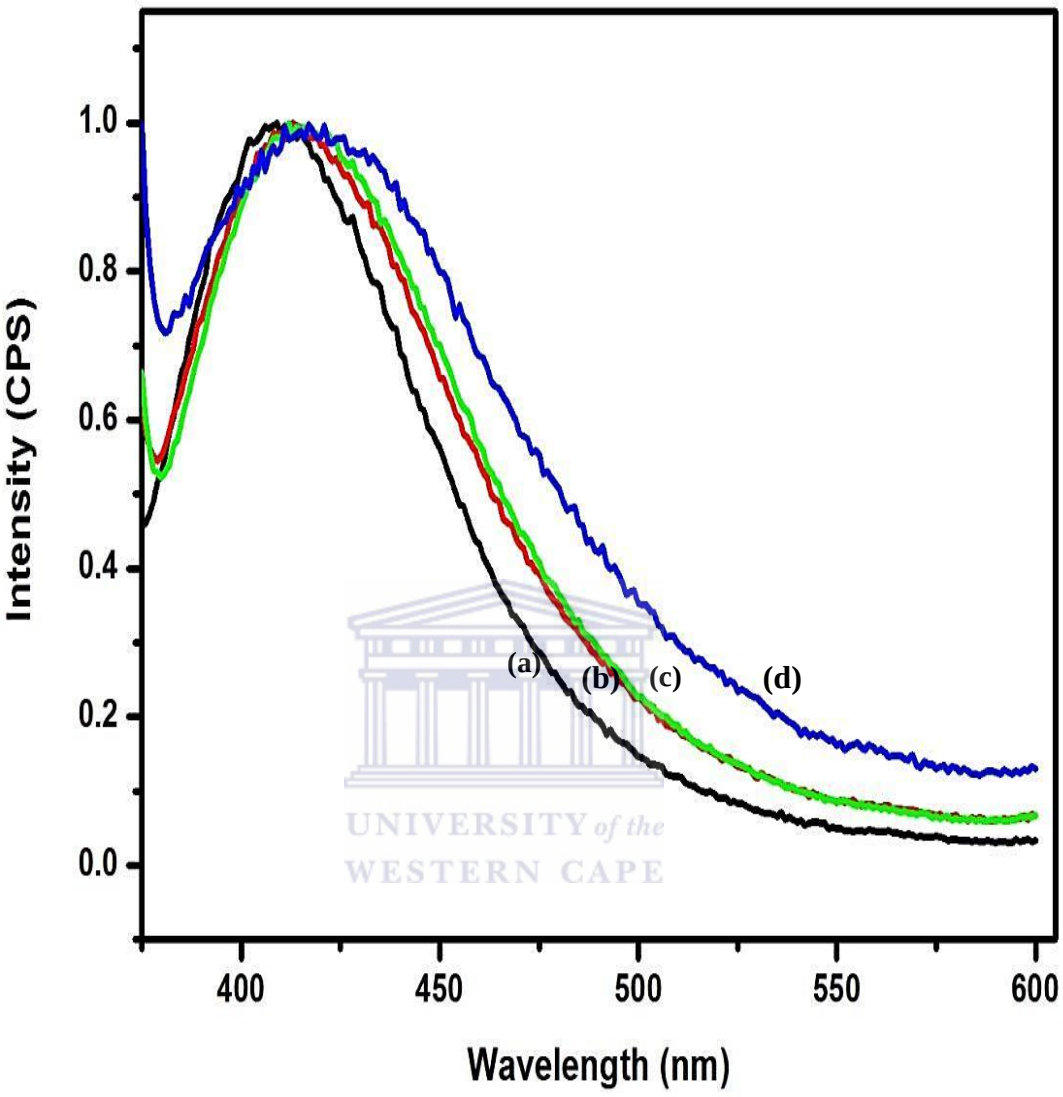

Figure 18: Fluorescence spectra of TGA-PdTeQDs excited at 320 nm where (a) 30 min, (b) 40 min, (c) 50 min and (d) 60 min

5.2. Spectroscopic studies of TGA-PdTeQDs

5.2.1 Fourier transformed infrared of TGA-PdTeQDs

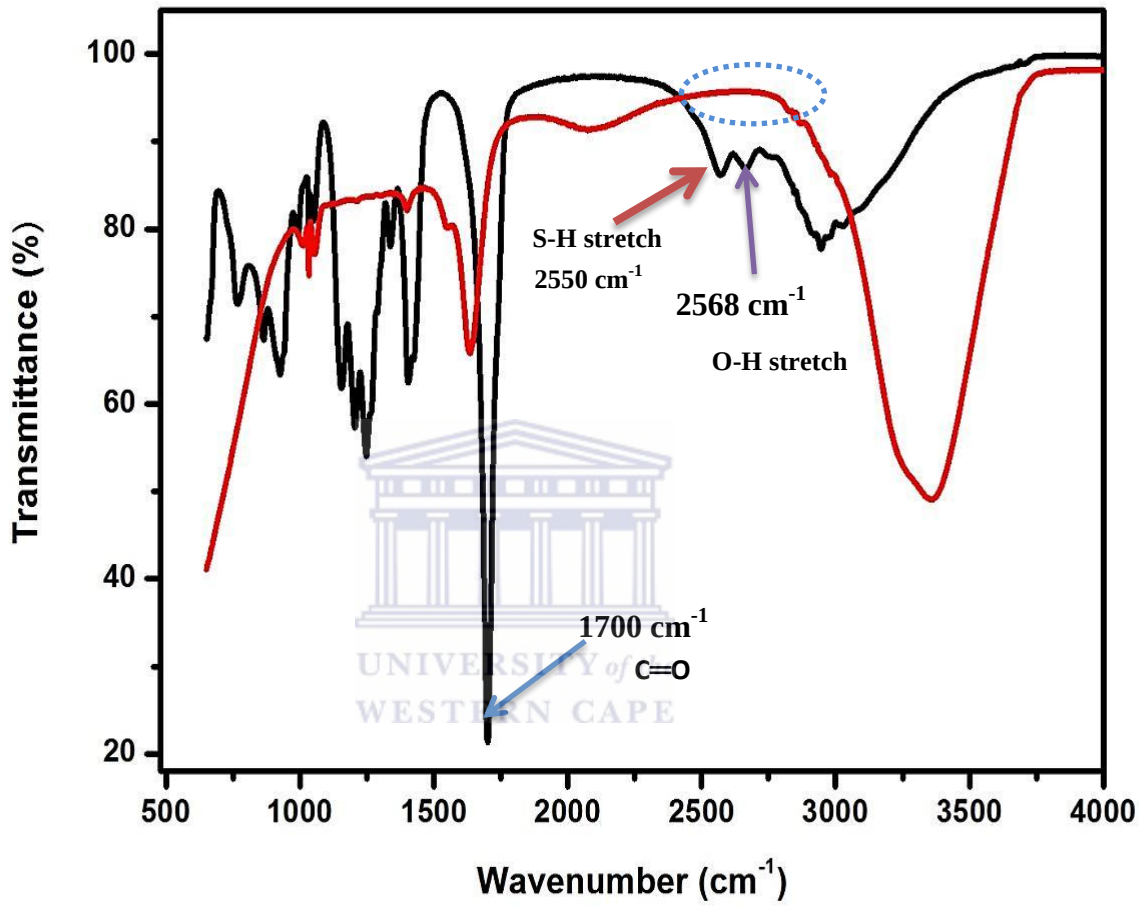

Figure 19: FT-IR spectra for TGA-PdTeQDs

The characteristic peaks belonging to TGA are shown in **Fig 19**. The peak at 2550 cm^{-1} is attributed to the stretching vibration of the S-H bond and the peak at 1700 cm^{-1} is attributed to vibration of the carboxylic group (Song *et al*., 2007). In addition, the S-H broad band stretching diminished at approximately 2550 cm^{-1} indicated the formation of S-Pd bonds between the TGA molecule and PdTe core. The vibration of the carboxylic group shifted

from 1700 cm-1 to 1660 cm^{-1} implying that COOH in TGA changed its anionic form into neutral aqueous solution (Liu *et al*., 2007).

5.3. Microscopic characterisation of TGA-PdTeQDs

5.3.1. High resolution transmission electron microscopy (HRTEM)

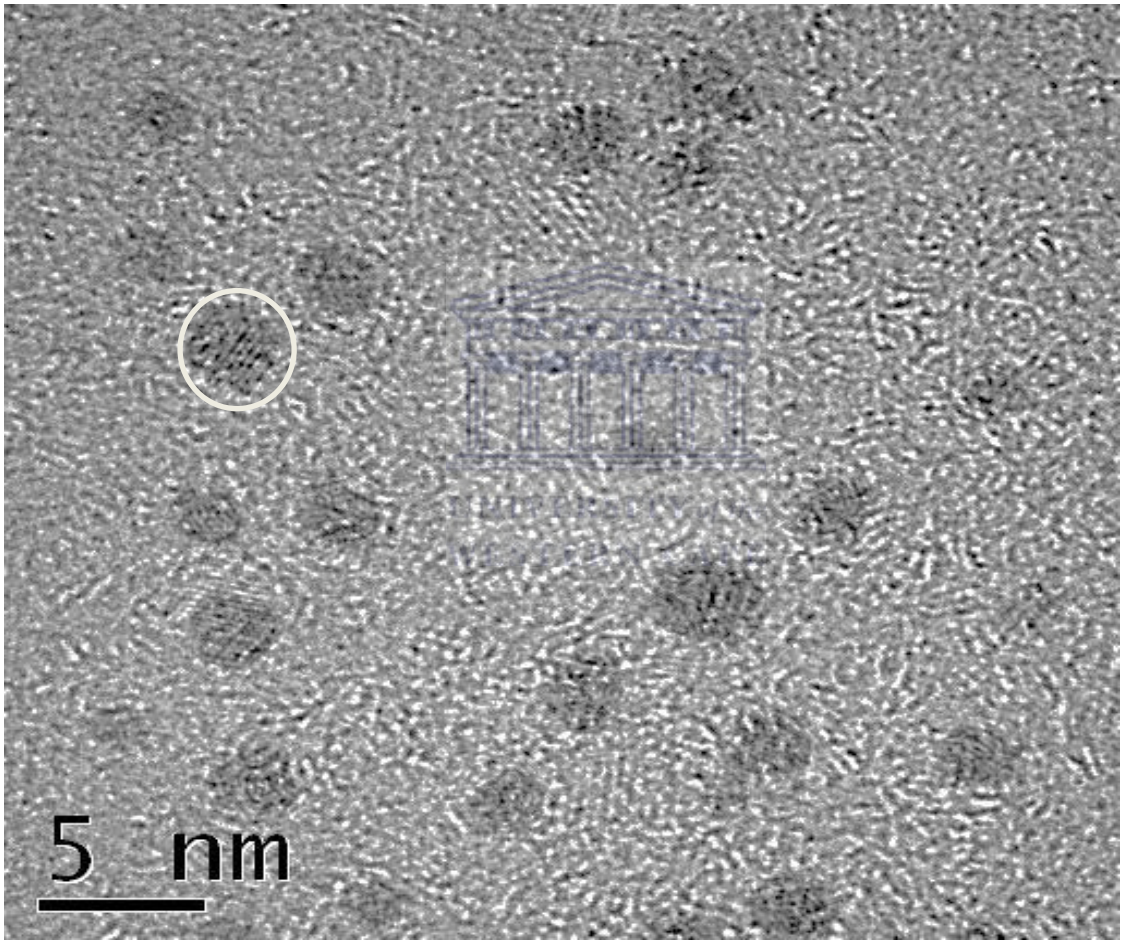

Figure 20: HRTEM of TGA-PdTeQDs

HRTEM determines the shape and size of nanoparticles. In **Fig 20**, the nanoparticles observed are uniformly distributed spherical structure (Hamizi *et al*., 2012) with size less than 5 nm. This confirmed the optical properties derived from UV-Vis where the particle

formed were very small. Energy dispersive X-ray spectrum shown in **Fig 21** revealed the chemical composition of as-prepared PdTeQDs interacting with thioglycolic acid.

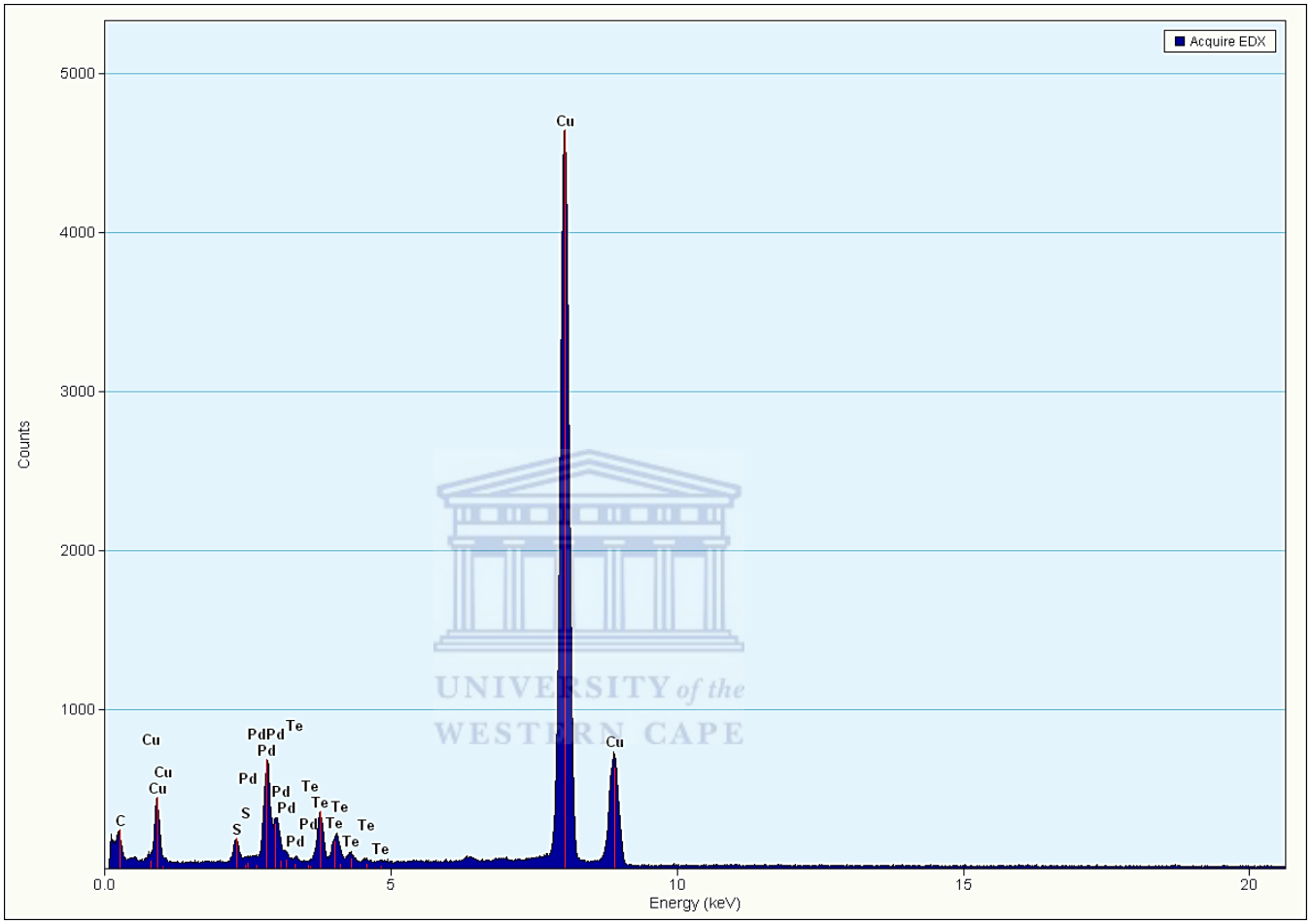

Figure 21: Energy dispersive X-ray (EDX) spectrum of TGA-PdTeQDs

5.4. Electrochemical characterisation of TGA-PdTeQDs

5.4.1. Electrochemistry of TGA-PdTeQDs

The cyclic voltammogram in **Fig 22**(b) revealed that the tellurium precursor had an oxidation peak at 0.4V which was absent in the bare Au. This curve indicates the highest peak current separation while a reduction peak at approximately -0.1V attributed to reduction of Te. For

Fig 22(c) a hump was observed at 0.1 V and an oxidation peak was observed at 0.2 V which was associated with the interaction of sodium hydrogen and tellurium.

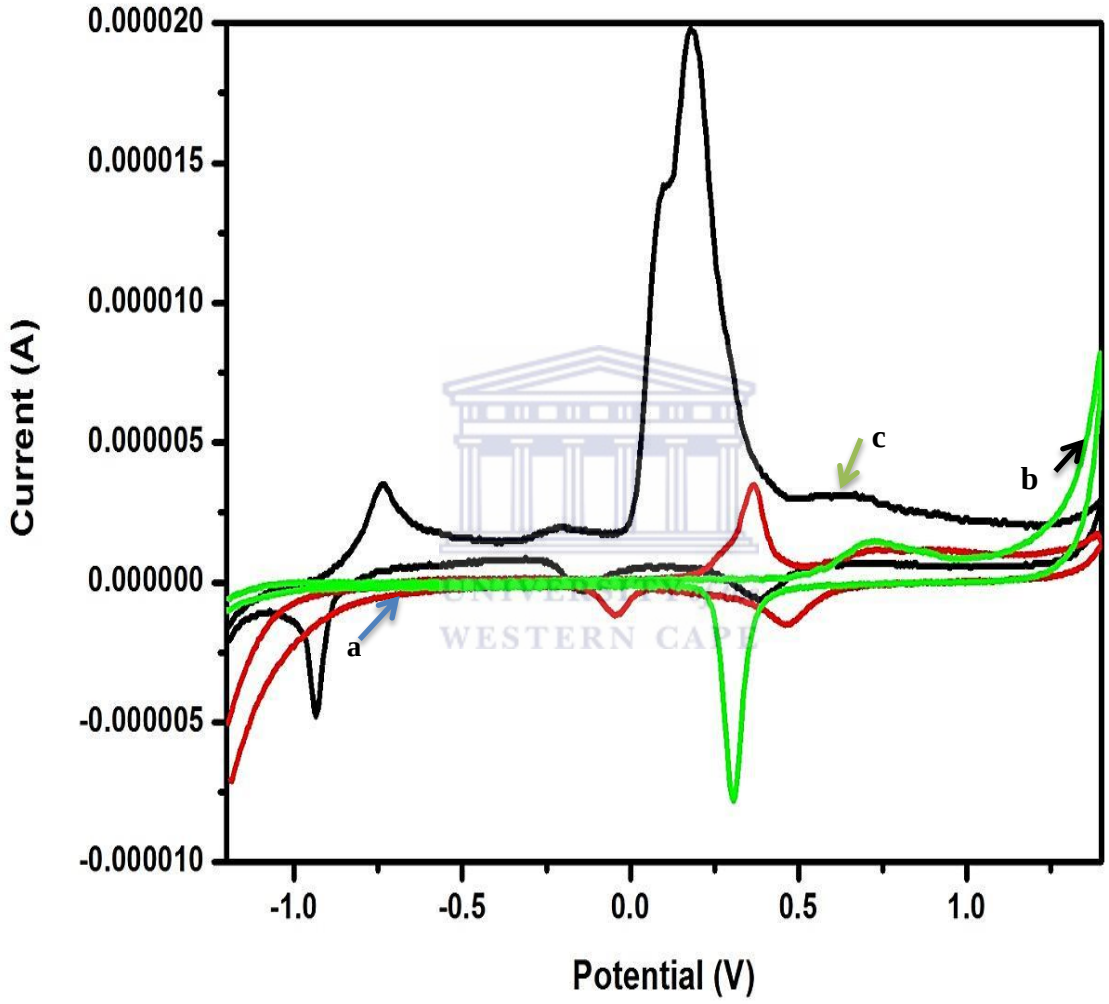

Figure 22: Cyclic voltammograms of metal precursors where (a) Au electrode, (b) Te and (c) NaHTe performed in 0.1 M PBS at 13 mV/s

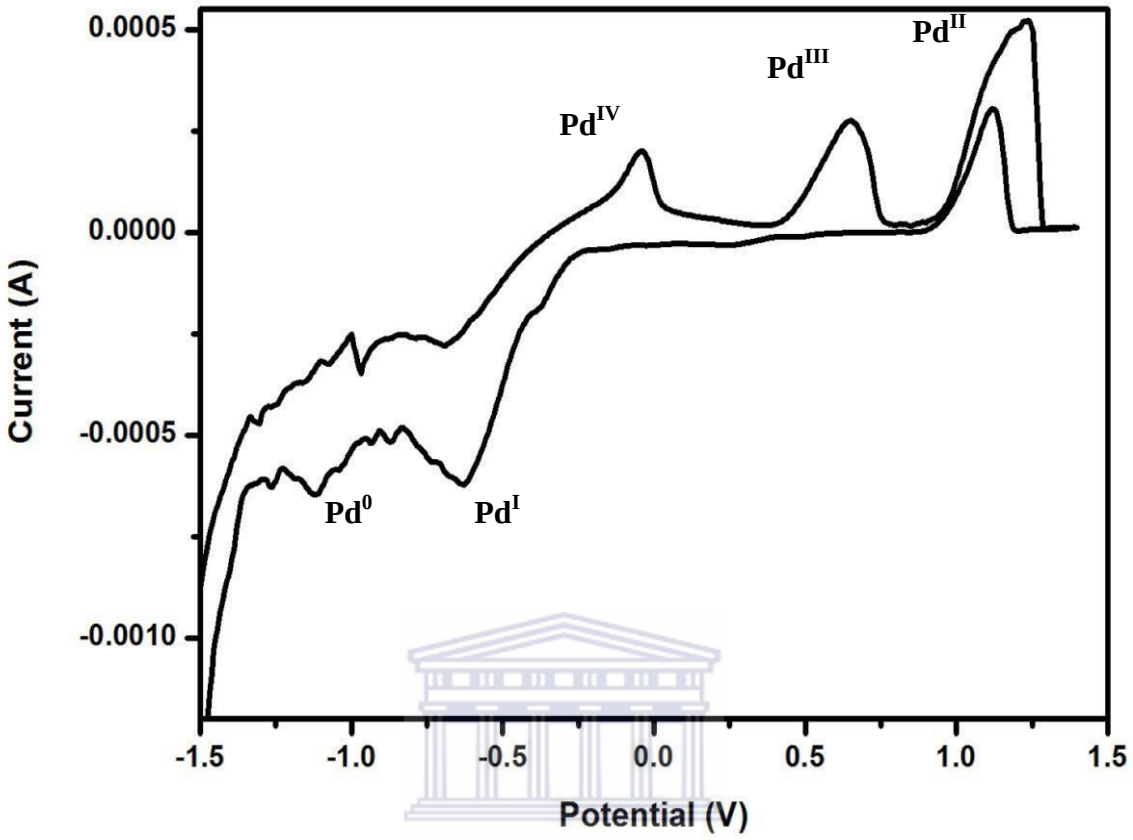

Figure 23: Cyclic voltammogram of Au/$PdCl_2$ in 0.1 M PBS pH 7.4

Most common oxidation states of palladium are 0, +1, +2, and +4 whereas the oxidation state +3 is rare. Three oxidation peaks were observed for (Pd^{IV}) which appeared at -0.15 V, (Pd^{III}) at 0.7 V and Pd^{II} at 1.25 V while two reduction peaks appeared at -0.6 V attributed to the reduction of Pd^{II} to (Pd^{I}) and further reduction to (Pd^{0}) at -1.1 V. The cyclic voltammogram of TGA- PdTeQDs shown in **Fig 24** indicated two oxidation peaks for (Pd^{IV}) and (Pd^{III}) and the reduction peak donated as (Pd^{I}). These findings indicate that these oxidation states were not stable enough and disappeared.

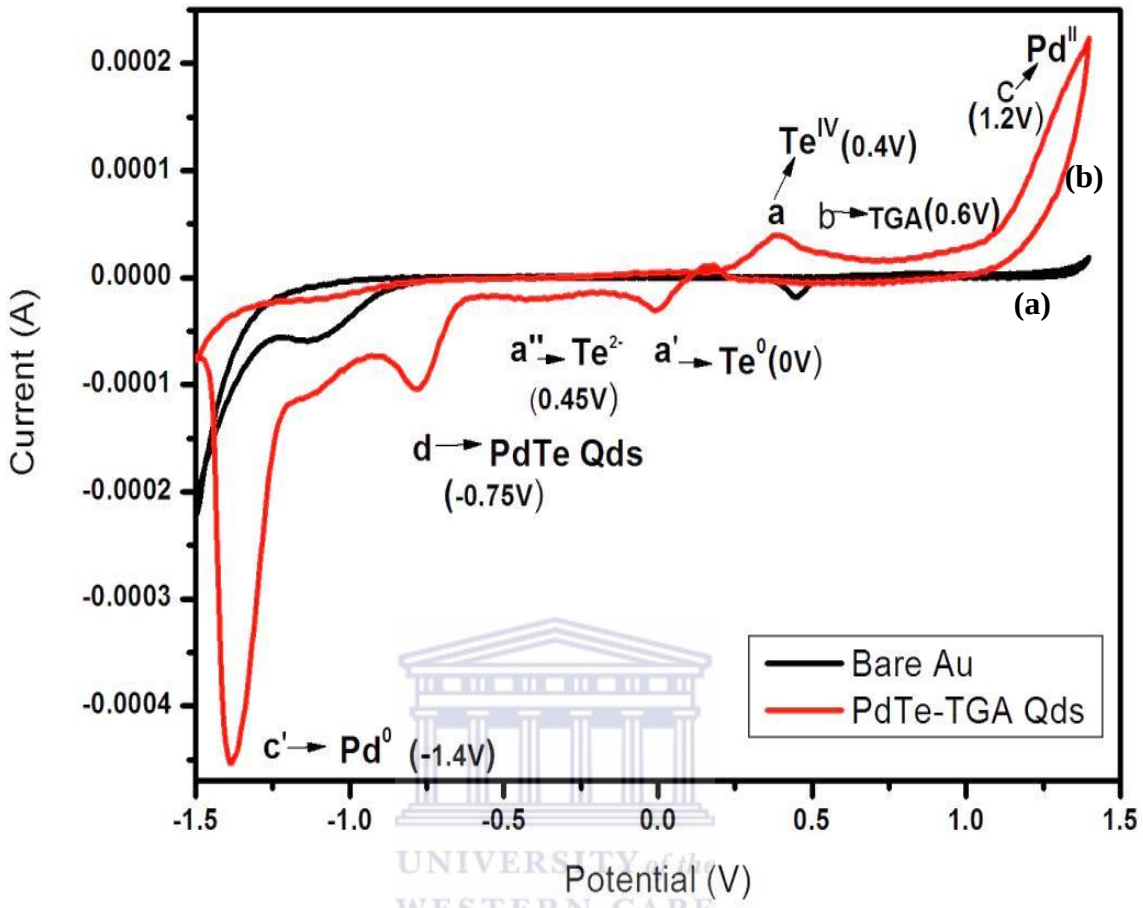

Figure 24: CV of Au and Au/TGA-PdTeQDs in 0.1 M phosphate buffer solution

Figure 24(a) shows the CV of Au electrode in buffer solution scanned at wide window potential region -1.5 to 1.5 V while the **Fig 24**(b) shows TGA-PdTeQDs into buffer solution which gave rise to a number of additional peaks. The oxidation peak at 0.4 V is attributed to tellurium (Te^{IV}) and the reduction peaks associated with reduction of Te^{IV} to Te^{0} appeared at 0V and further reduced to Te^{2-} at -0.45 V (Khene *et al.*, 2011). **Fig 24**(b) showed redox peak potentials for TGA capping agent which appeared at (E_{pa} = 0.6 V) and at (E_{pc} = 0.5 V) which was also observed by Poznyak and co-workers. **Fig 24**(c) shows an oxidation peak of (Pd^{II}) at 1.2 V with **c**′, presenting the reduction of Pd^{II} to Pd^{0} which appearing at more negative

potential because transition metals are more electronegative while the **Fig 24**(d) at -0.75 V is attributed to PdTeQDs Similar findings were obtained for 3-MPA-PdTeQDs as shown in the next chapter.

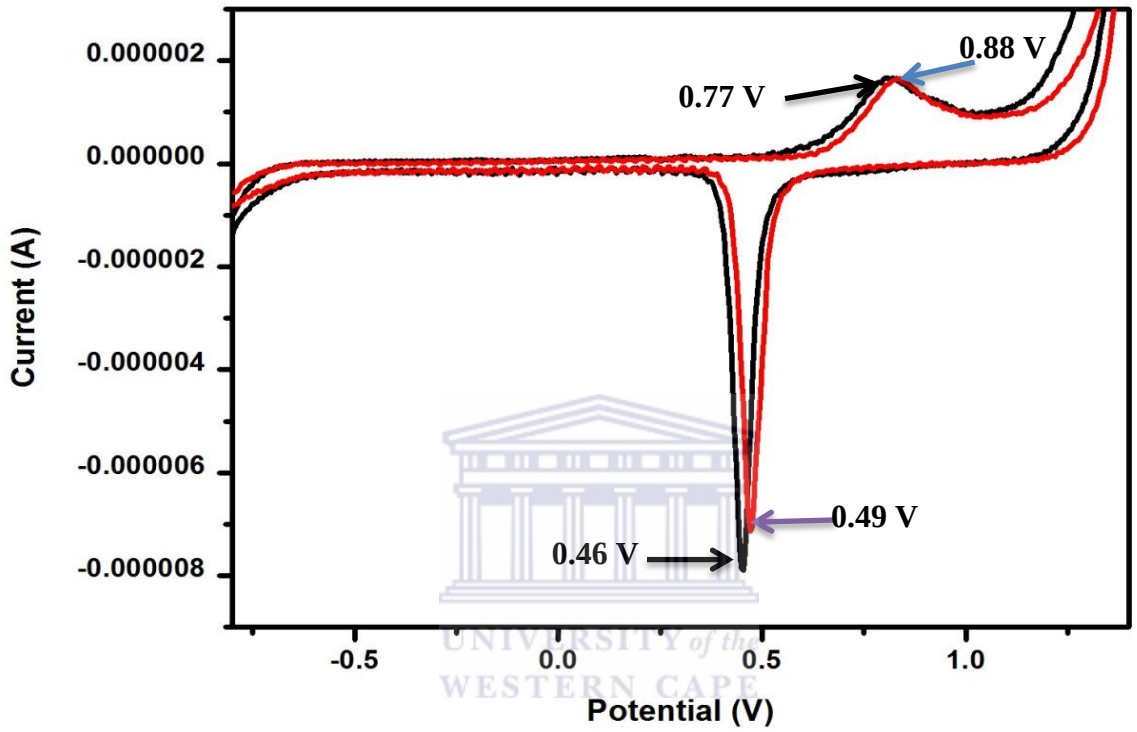

Figure 25: Cyclic voltammogram of Au/Cyst modified electrode in 0.1 M PBS

The heterogeneous electron transfer from gold electrode to the redox couple in buffer solution was influenced by the presence of activation and functionalization of cysteamine monolayer (Shabani et al., 2009), which resulted in a small peak potential separation and a slightly shifted to negative potential (Shervedani and Mozaffari, 2005). The observed cathodic peak (black line) at (E_{pc} = 0.46 V) and anodic peak (E_{pa} = 0.77 V) of cysteamine shifted to negative potential. When cysteamine was chemisorbed onto TGA-PdTe quantum dots as shown in **Fig 26**(b) the quantum dots on the thiol film had an influence on the interface property of the modified electrode and improve the electron transfer and self-

assembly of cysteamine monolayer on TGA-PdTe quantum dots. The quantum dots replaced negative charges and diminished the repulses of the electrode interface to the redox probe which resulted in the improvement of electron transfer of the modified electrode (Zhang *et al*., 2005). The CV obtained from Au/Cyst/TGA-PdTeQDs showed a reduction peak with high peak current separation at (-0.8 V) which was attributed to TGA-PdTeQDs and an oxidation peak at 0.2 V which was not present in Au/Cyst.

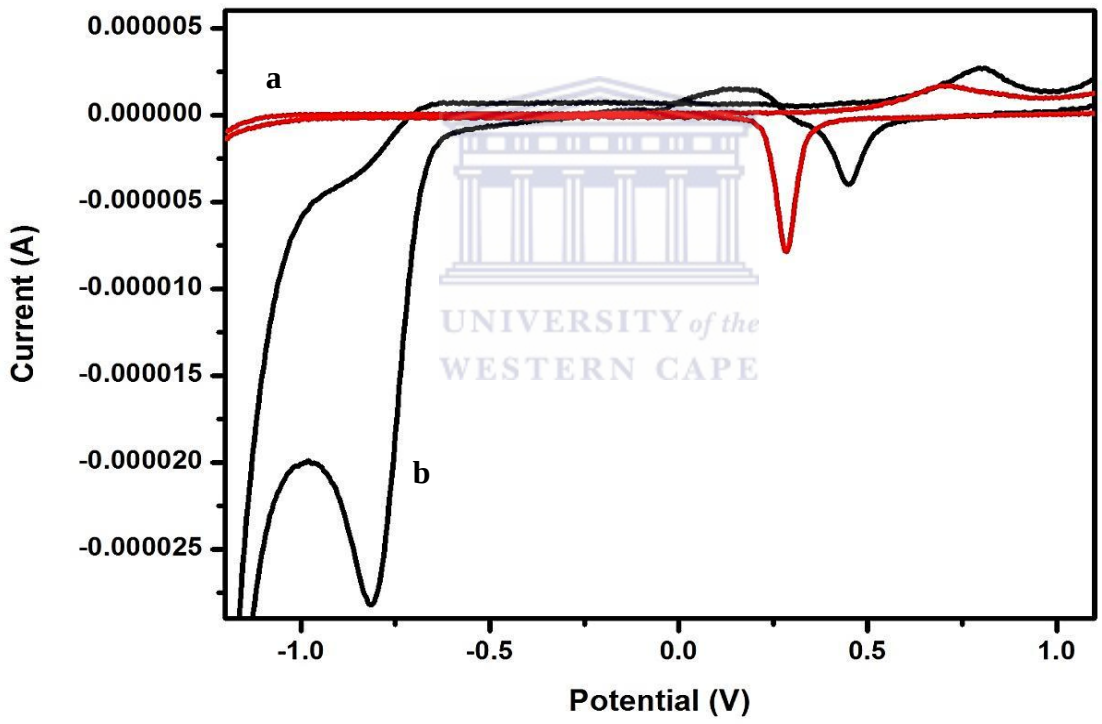

Figure 26: Cyclic voltammograms of (a) Au/Cyst and (b) Au/Cyst/TGA-PdTeQDs in 0.1 M PBS pH 7.4

5.5. Biosensor measurements

5.5.1. Electrochemistry of biosensor

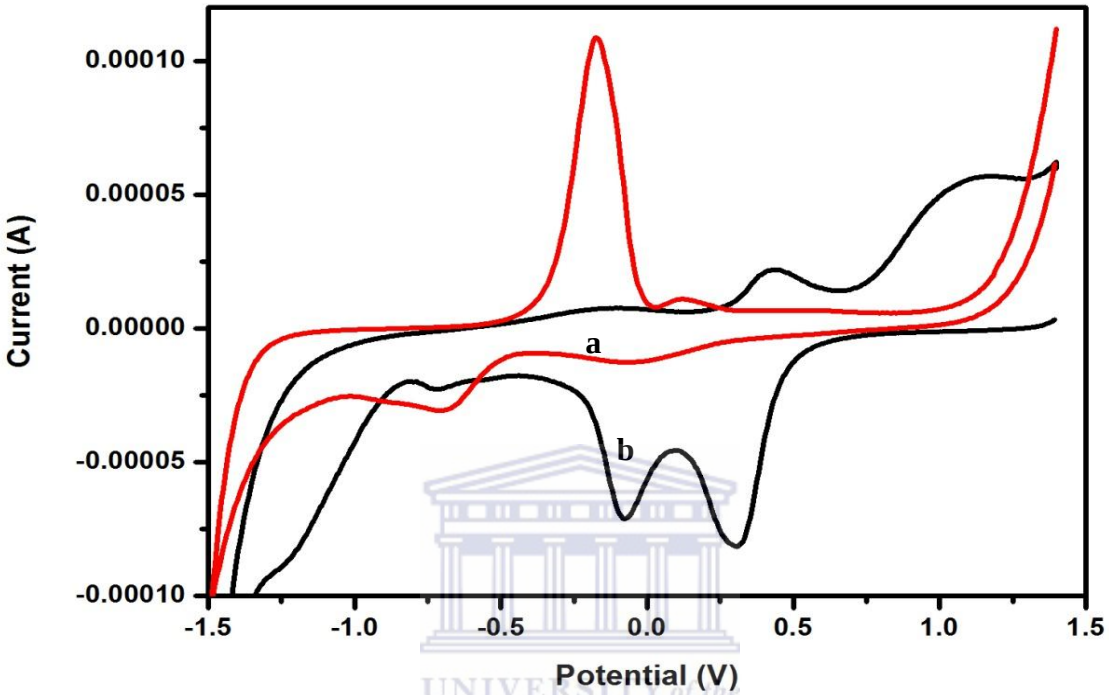

Figure 27: Cyclic voltammograms of (a) Au/CYP3A4 (b) Au/TGA-PdTeQDs/CYP3A4 in aerobic conditions in 0.1 M PBS at 500 mV/s

Quantum dots have been used in biochemistry to provide efficient electron transport and are suitable and stable matrix for enzyme incorporated onto gold electrode. In aerobic conditions the reduction peak at (E_{pc} =-0.15 V) of Au/TGA-PdTeQDs /CYP3A4 increased due to the quantum dots acting as mediator and promoting electron transfer to and from the enzyme (Shumyantseva *et al*., 2007). The oxidation peak at (E_{pa} = 0.48 V) shifted to more positive potential than Au/CYP3A4 which exhibited oxidation peak at (E_{pa} = 0.1 V) in the absence of the mediator. The electron transfer reaction as indicated in **Fig 28**(a) occurred successfully between the enzyme and electrode but at a distance from the electrode surface meaning that

the stability of the enzyme onto gold electrode surface was not good enough to hold enzyme thus the direct electron transfer was very slow.

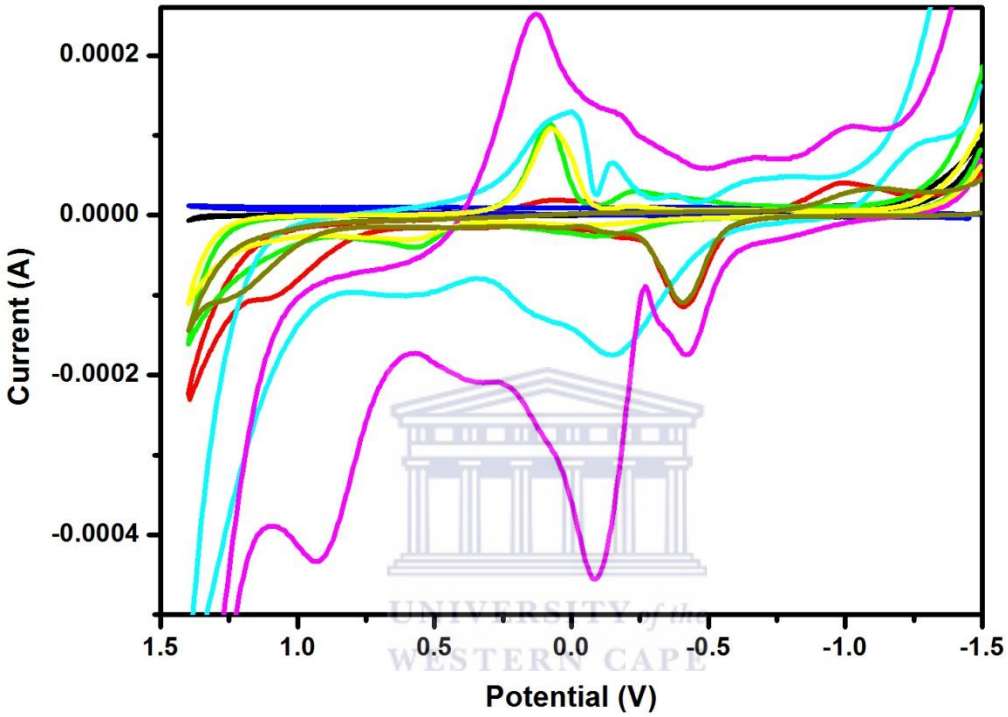

Figure 28: Cyclic voltammograms of (a)Au, (b) Au/Cyst, (c) Au/TGA-PdTeQDs and (d) Au/CYP3A4 with 0.05 M of IDV and without in 0.1 M PBS at 500 mV/s

A set of controlled experiments were performed to evaluate the response of platform to pin-point the exact modifier that was responsible for biosensor response in detecting indinavir drug. As shown in **Fig 28**(a) (red line) when IDV was added on bare Au electrode there was no response also in (b) (blue line) Au/Cyst no reduction peak was observed thus no notable response. **Fig 28**(c) Au/TGA-PdTeQDs (pink line) showed a huge reduction peak than Fig 28(d) Au/CYP3A4 which gave small response indicating that the response of biosensor was due to TGA-PdTeQDs and CYP3A4.

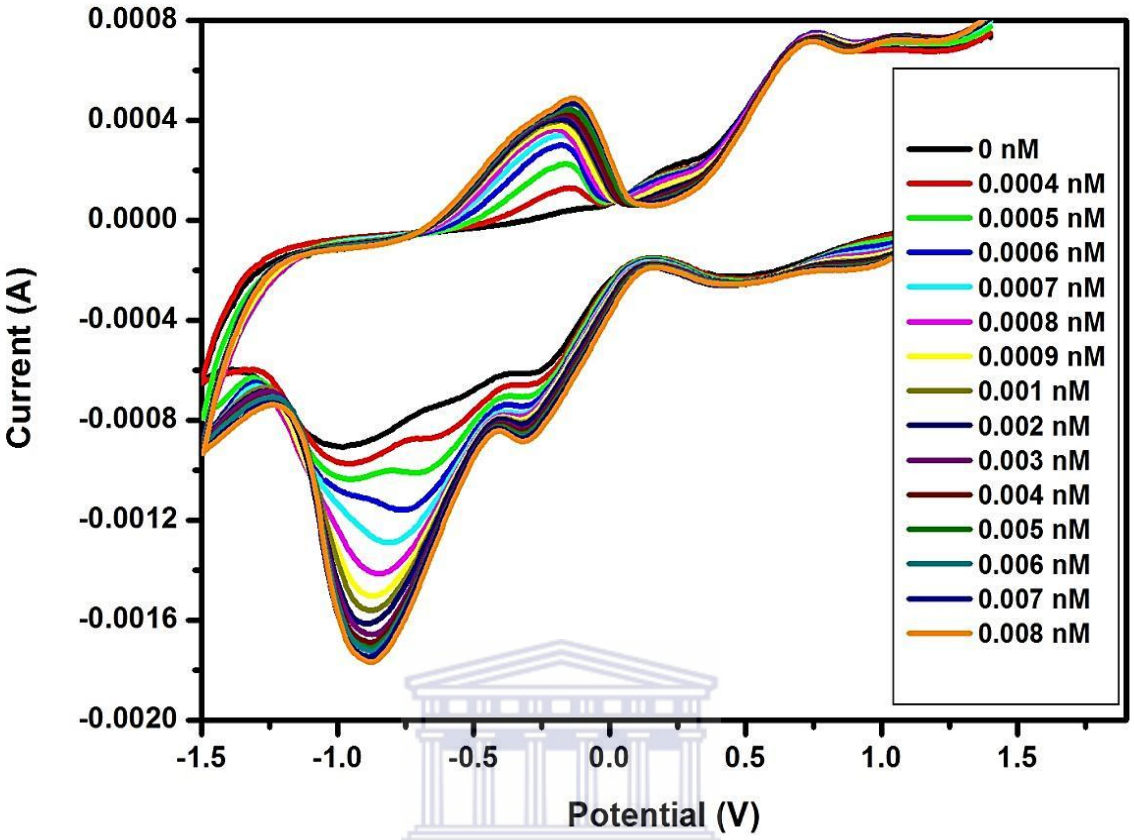

Figure 29: Cyclic voltammograms of CYP3A4/TGA-PdTeQDs/Cyst/Au biosensor responses to successive addition of IDV in phosphate buffer on pH 7.4 at 500 mV/s

The detection was done using lower concentration ranges from 0.0004-0.008 nM as shown in **Fig 29**. Three reduction peaks were observed at (E_{pc} = -0.25 V), (E_{pc} = -0.6 V) and (E_{pc} = -0.9 V), where the reduction peak at -0.25 V increased with increasing concentrations of analyte while the reduction peaks at -0.6 V and -0.9 V combined at high concentration and shifted to more negative potential. The observed overall reduction peak of the biosensor appeared at -0.8 V which overlapped the reduction peak of TGA-PdTe quantum dots peak indicating that quantum dots enhanced the catalytic behaviour of the biosensor. The sensitivity of biosensor

was 0.01259 mA/nM and K_M^{app} value was 0.59429 mM. The detection limit of biosensor was 4.3 ng/mL.

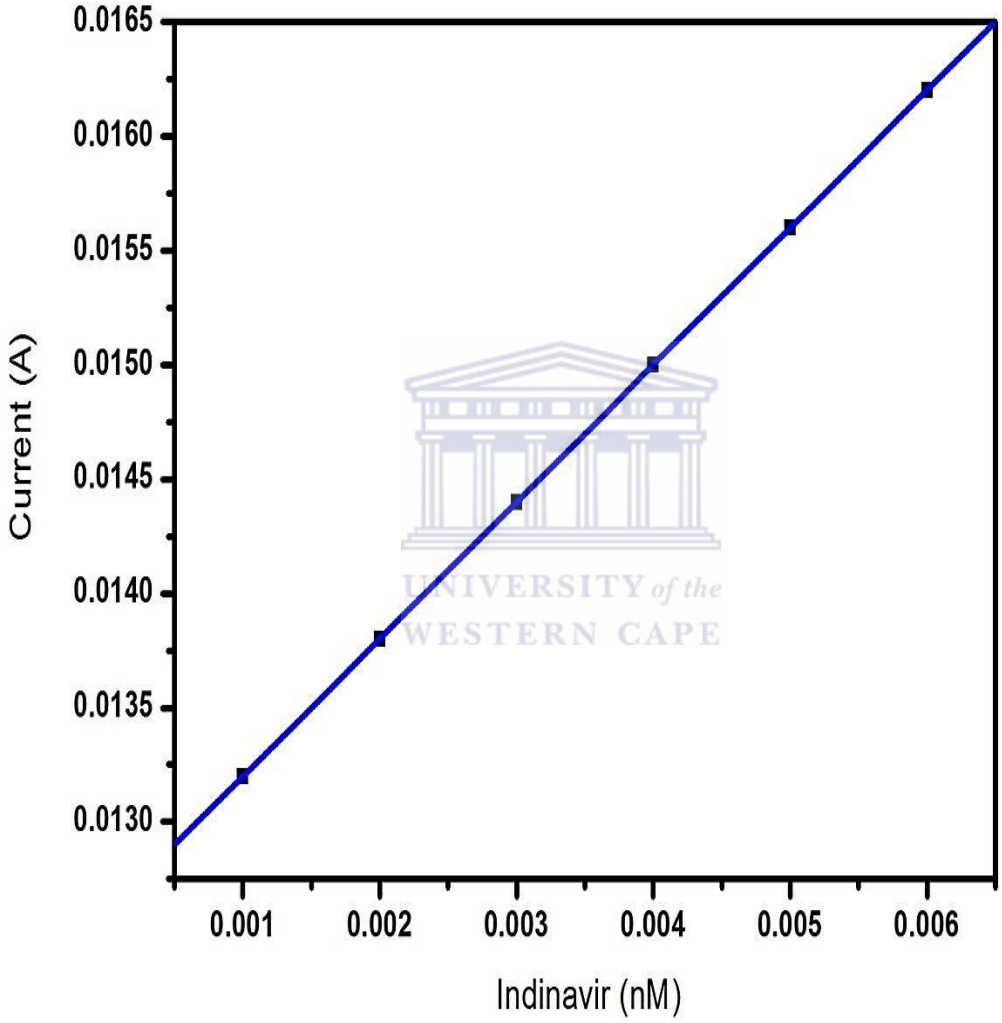

Figure 30: Calibration curve drawn from the linear region of the biosensor responses in Fig 29

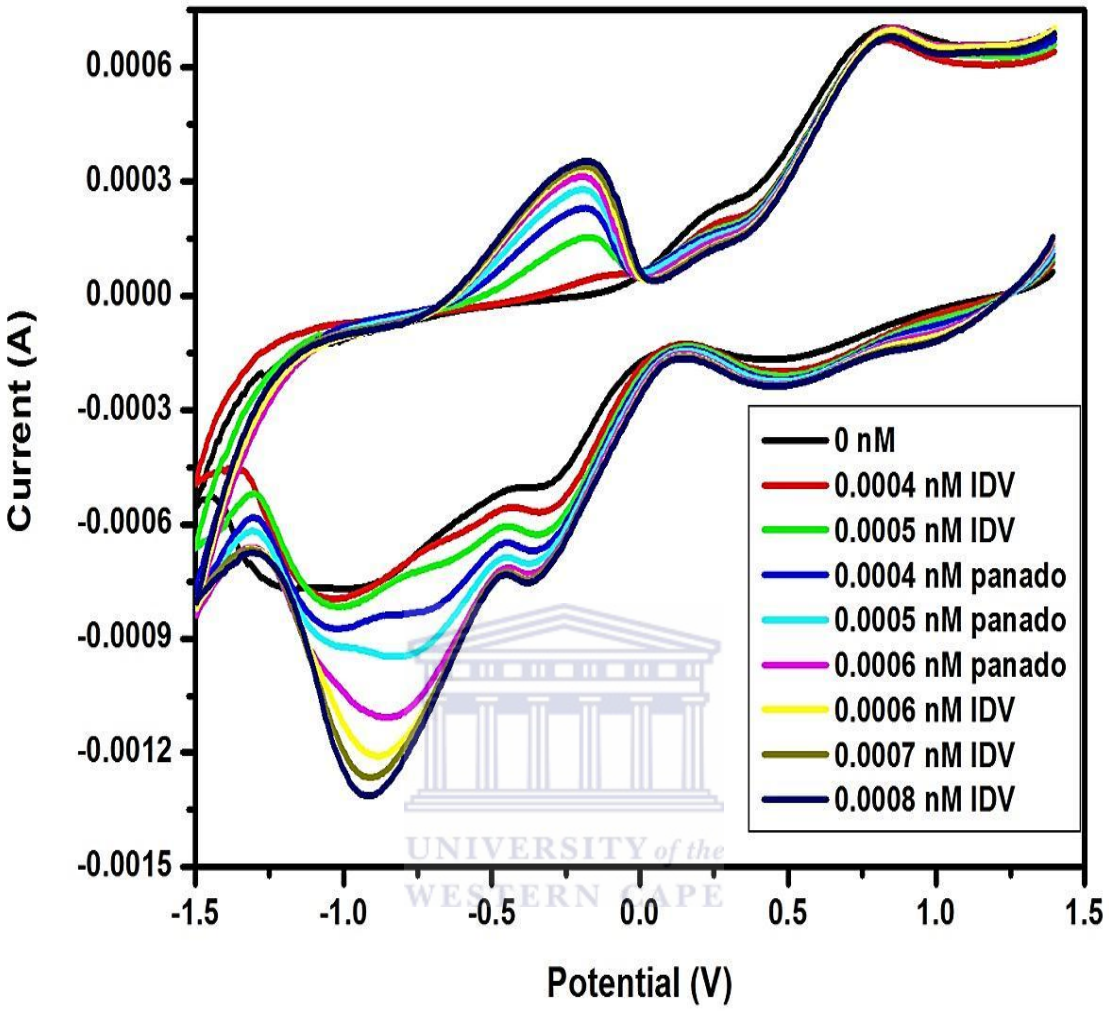

Figure 31: Cyclic voltammograms of CYP3A4/TGA-PdTeQDs/Cyst/Au biosensor with successive additions of IDV and acetaminophen

Acetaminophen is a medicine recommended for relief of mild to moderate pain and fever such as headaches, toothache and pain associated with colds and flu. It is metabolised extensively in the liver and excreted in the urine mainly as inactive glucuronide and sulphate conjugates. The risk of paracetamol toxicity may be increased in patients receiving other potentially hepatotoxic drugs or drugs that induce liver microsomal enzymes such as alcohol and anticonvulsant agents.

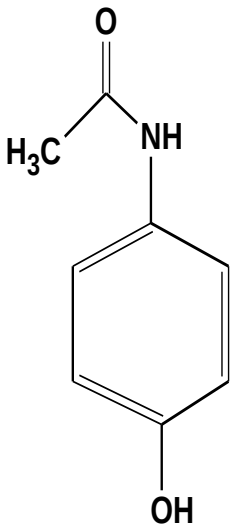

Figure 32: Schematic representation of acetaminophen

.

The interference studies of indinavir drug and acetaminophen was performed using small concentrations as shown in **Fig 32**. Acetominophen had an effect on indinavir due to the increased catalytic response when small concentrations were added since indinavir drug competes with other drugs for CYP3A4. This indicated that indinavir drug should not be administered concurrently with acetaminophen because the competition for CYP3A4 by HIV protease inhibitors creates serious life threatening events (Lin, 1999).

5.5.2 Stability of biosensor

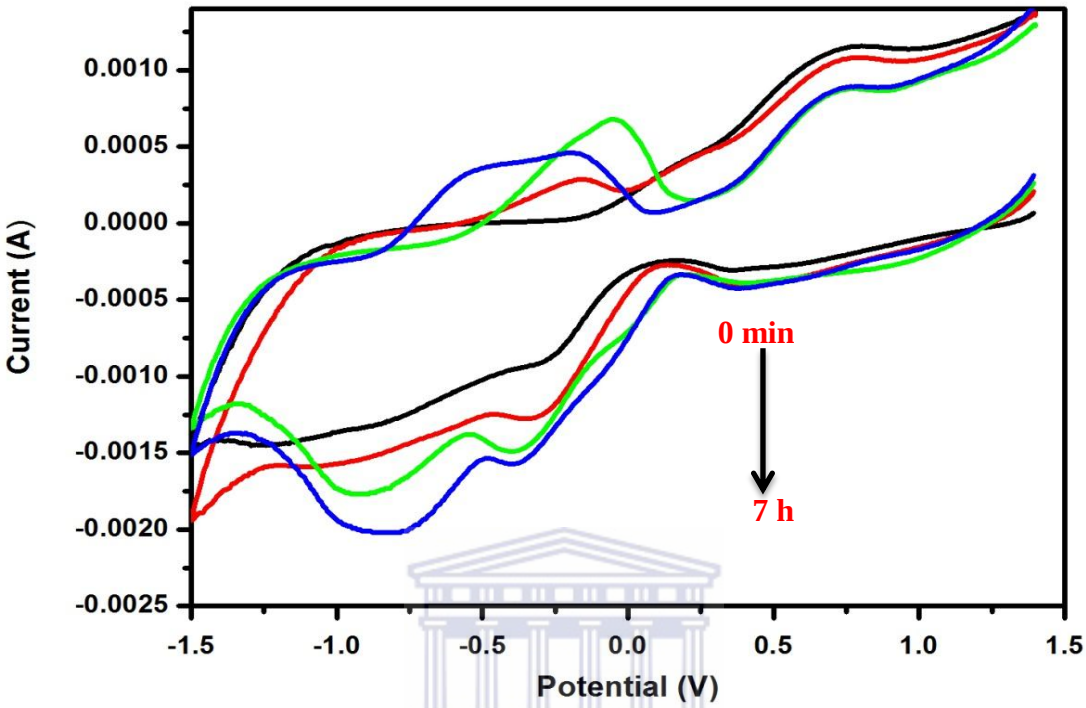

Figure 33: Cyclic voltammograms of CYP3A4/TGA-PdTeQDs/Cyst/RDE in 0.1 M PBS at 500 mV/s

The stability of a biosensor is influenced by variation of time, temperature and materials immobilised. In this study the stability was studied to measure the response of 0.0004 nM indinavir drug and results are presented in **Fig 33** with an indication of the short-term stability of the biosensor by monitoring the time which resulted in dramatic increase in the stability of the sensor from 0 min to 7 h. The biosensor lost its activity after a storage of 15 h, this loss was due to temperature changes undergone from storage temperature to room temperature (Shankaran *et al*., 2003) .When the sensor was rotated using rotating disk electrode as shown in **Fig 34**, the speed of rotation disturbed the stability reaction because the substrate might be surface bound onto electrode blocking the electron transfer and caused a

decrease in the peak current after 7 h. Further stability measurements were performed by UV-Vis spectroscopy as indicated in **Fig 35**(a) Herein indinavir drug is shown to exhibit a sharp absorption bands at 210 nm and 260 nm while **Fig 35**(b) (redline) showed absorption band of CYP3A4 in the absence of indinavir which shifted to shorter wavelength 205 nm as compared to indinavir band. An extended absorption band of the enzyme at 240 nm was observed with an associated energy band gap of 4.7 eV and 0.05 nM of indinavir was added into the CYP3A4 solution to check the binding and stability by monitoring the time. The spectra showed a decrease in absorption peaks and a slight shift from 0 min to 1 h indicating the binding of indinavir onto the active site of the enzyme.

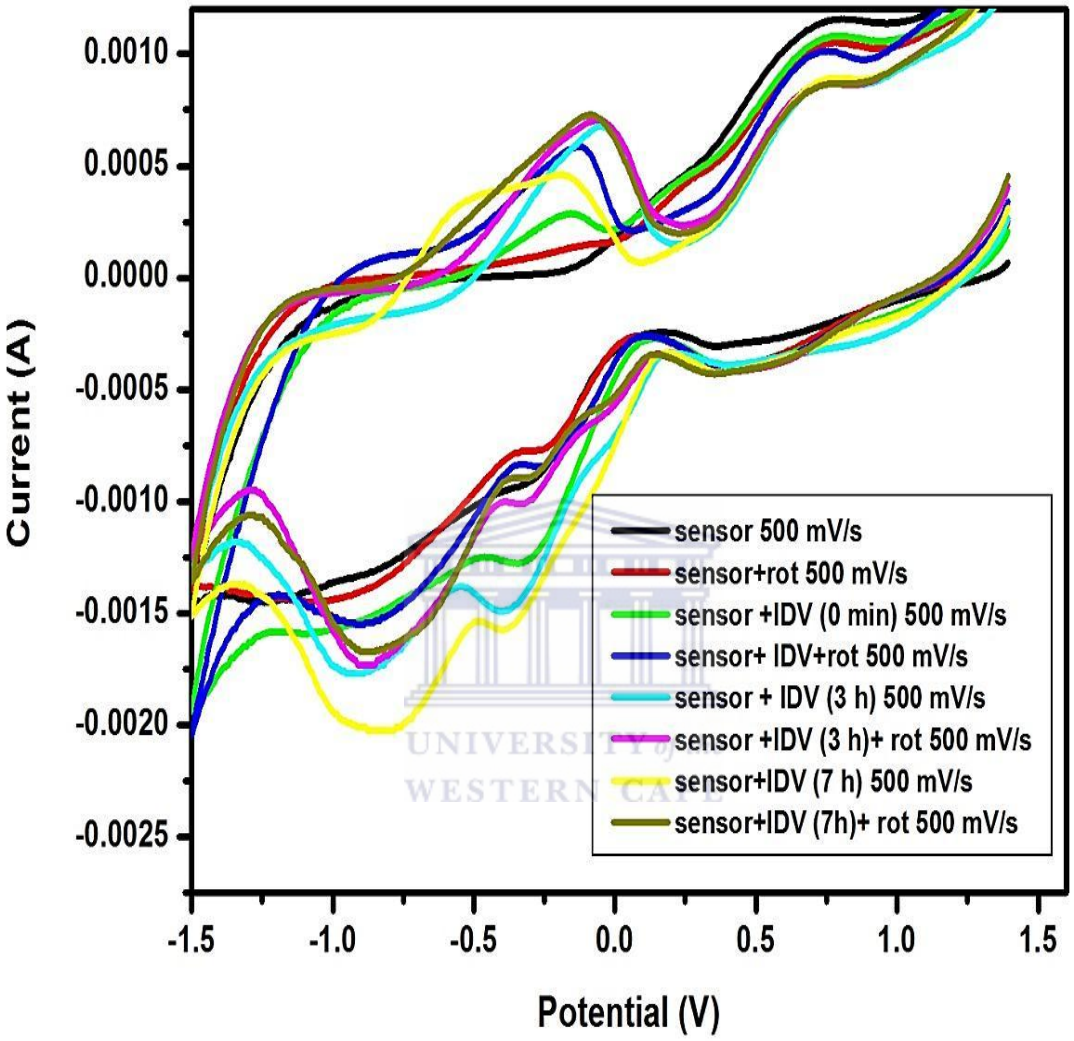

Figure 34: Cyclic voltammograms of CYP3A4/TGA-PdTeQDs/Cyst/RDE with and without rotating the electrode in 0.1 M PBS at 500 mV/s

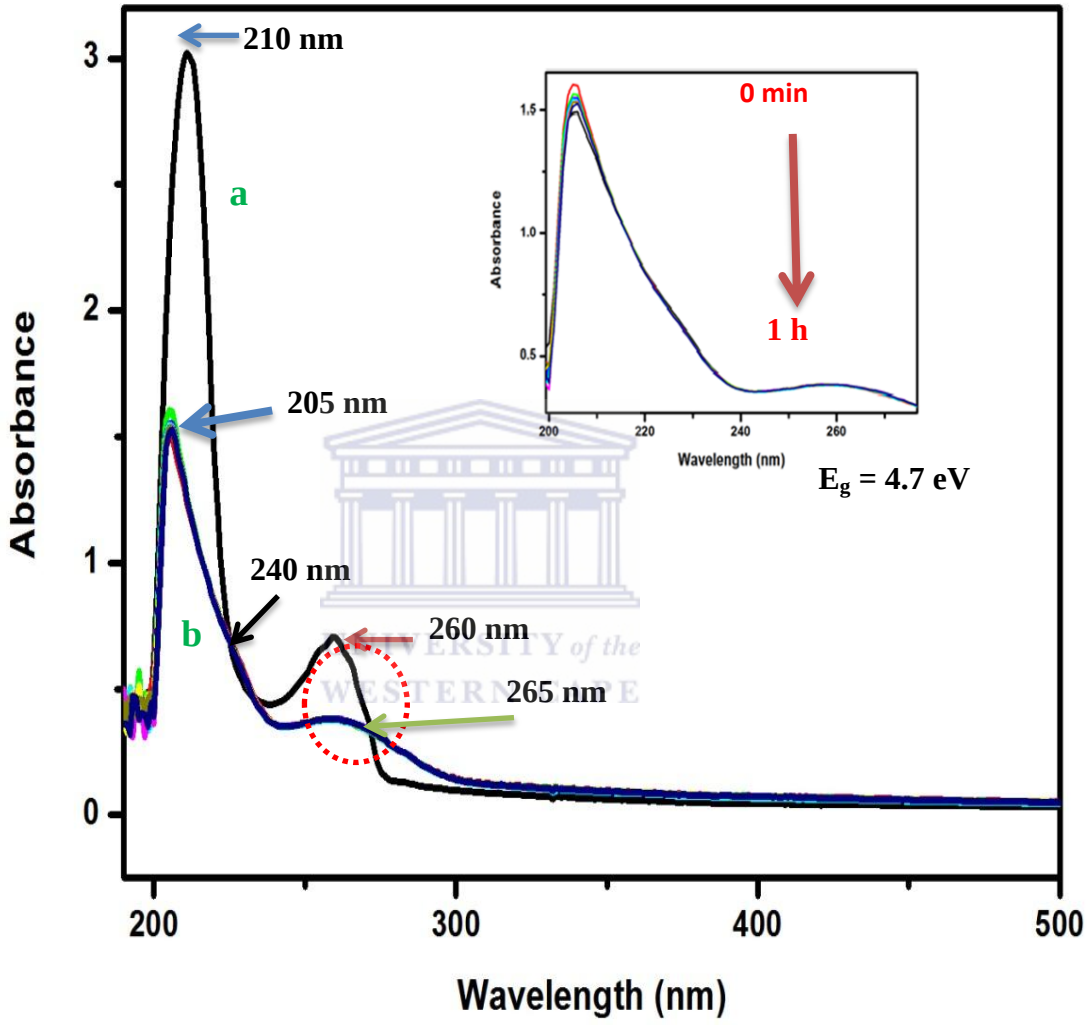

Figure 35: UV-Vis of (a) indinavir drug (b) CYP3A4/IDV at 0.05 nM

5.6 Microscopic studies of biosensor

5.6.1. High resolution scanning electron microscopy (HRSEM)

A **B**

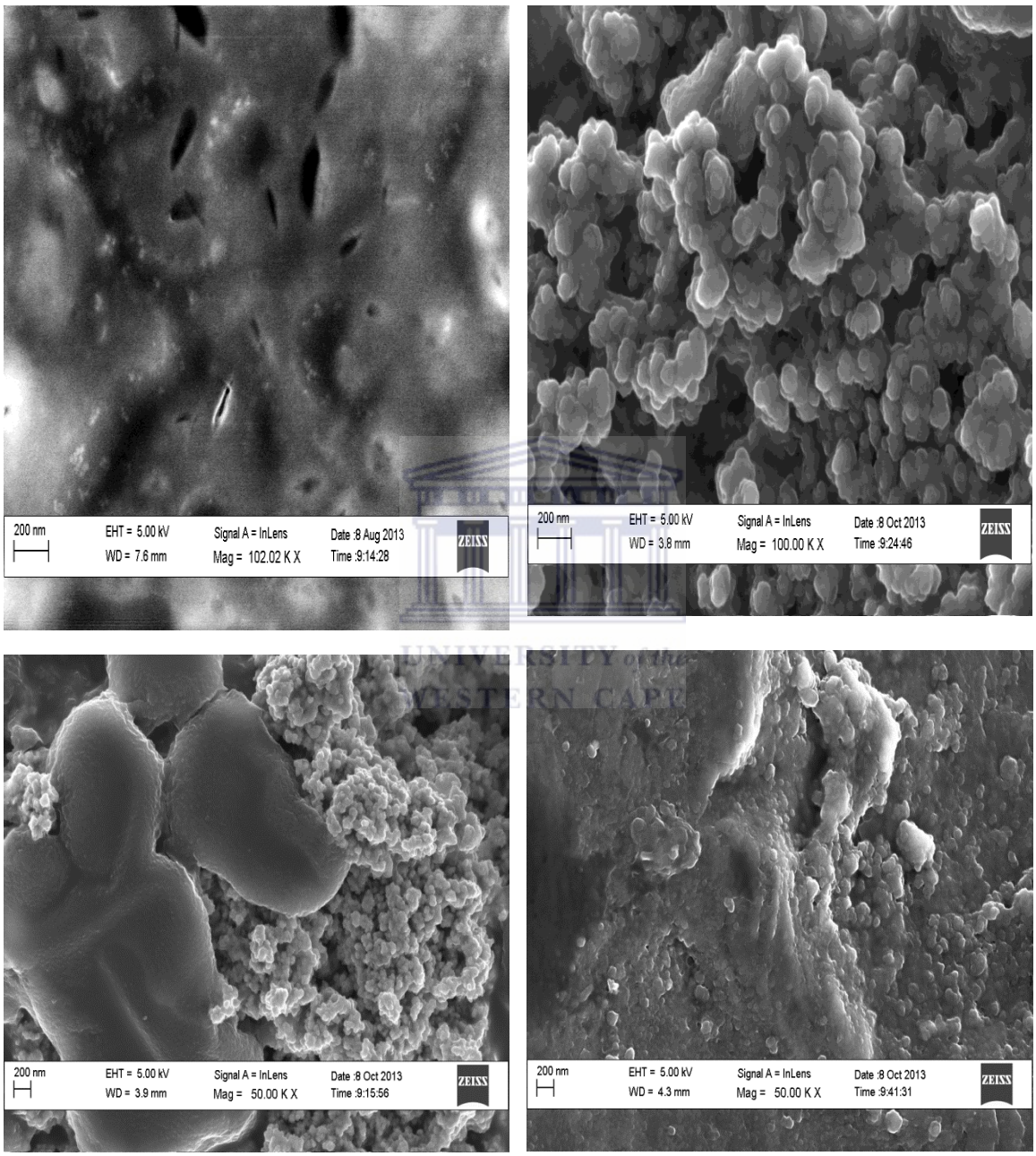

C **D**

Figure 36: (A)-(D) Represents the HRSEM of Cyst, TGA-PdTeQDs, Cyst/TGA-PdTeQDs and Cyst/TGA-PdTeQDs/CYP3A4 done on aluminum stub

Figure 36(A) shows some holes on the aluminum stub surface while **Fig 36**(B) shows agglomorated spherical bubbles of different sizes of PdTe quantum dots. **Fig 36**(C) indicates the association between the interaction of cysteamine amino group and carboxylic group of capping agent which showed big irregular shape and unreacted quantum dots while **Fig 36**(D) showed a smooth surface due to binding of activated carboxylic group from the quantum dots and amine group of CYP3A4 enzyme.

5.7 UV-Vis spectrophotometry of biosensor

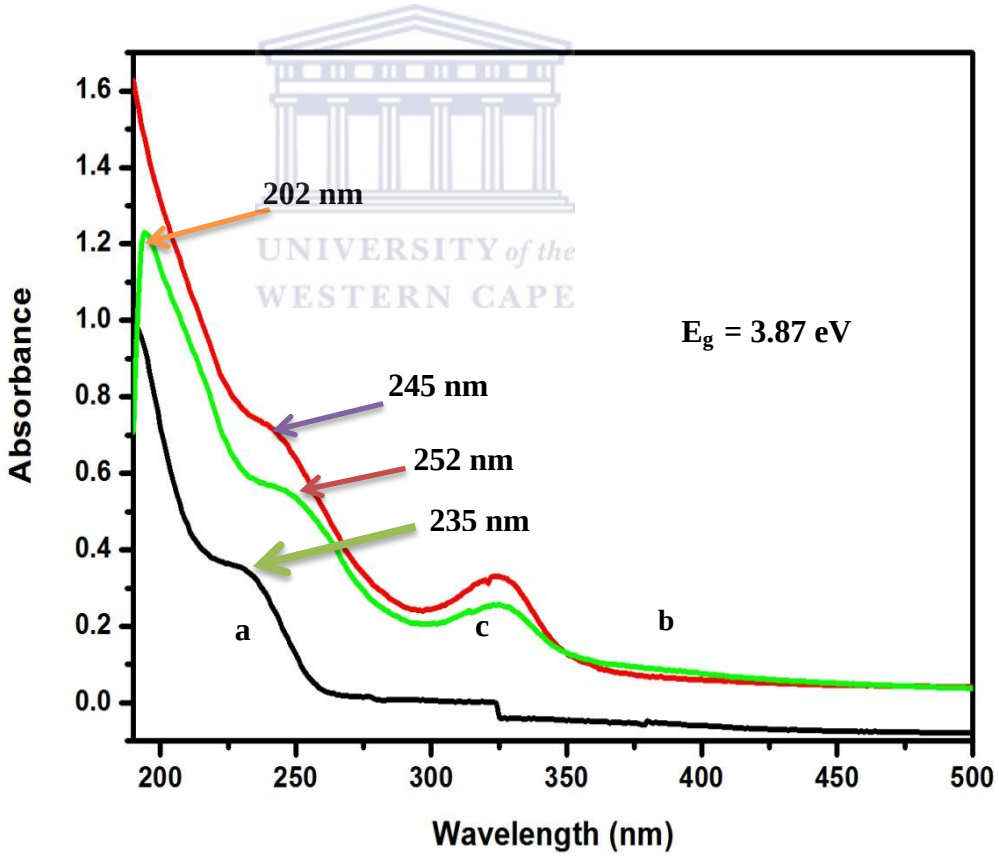

Figure 37: UV-Vis spectra of (a) Cyst, (b) Cyst/TGA-PdTeQDs and (c) Cyst/TGA-PdTeQDs/CYP3A4 biosensor in 0.1 PBS pH 7.4

Cysteamine exhibited a broad absorption peak at 235 nm which shifted to 245 nm (b) due to interaction of cysteamine and PdTe quantum dots in the presence of EDC/NHS cross linkers and PdTe quantum dots absorption band at 325 nm. In **Fig 35**(c), the absorption band at 202 nm was attributed to CYP3A4 and the shift observed from 245 nm to 252 nm was attributed to the binding of free activated carboxylic group from the quantum dots and amino group of the enzyme that has led to a decrease in absorption peak intensity. An absorption band at 325 nm also observed in biosensor with associated energy band gap of 3.87 eV, this indicates the biocompatibility of quantum dots.

Chapter six

6.1 Characterisation of 3-MPA-PdTeQDs

6.1.1 UV-Vis spectrophotometry of 3-MPA-PdTeQDs

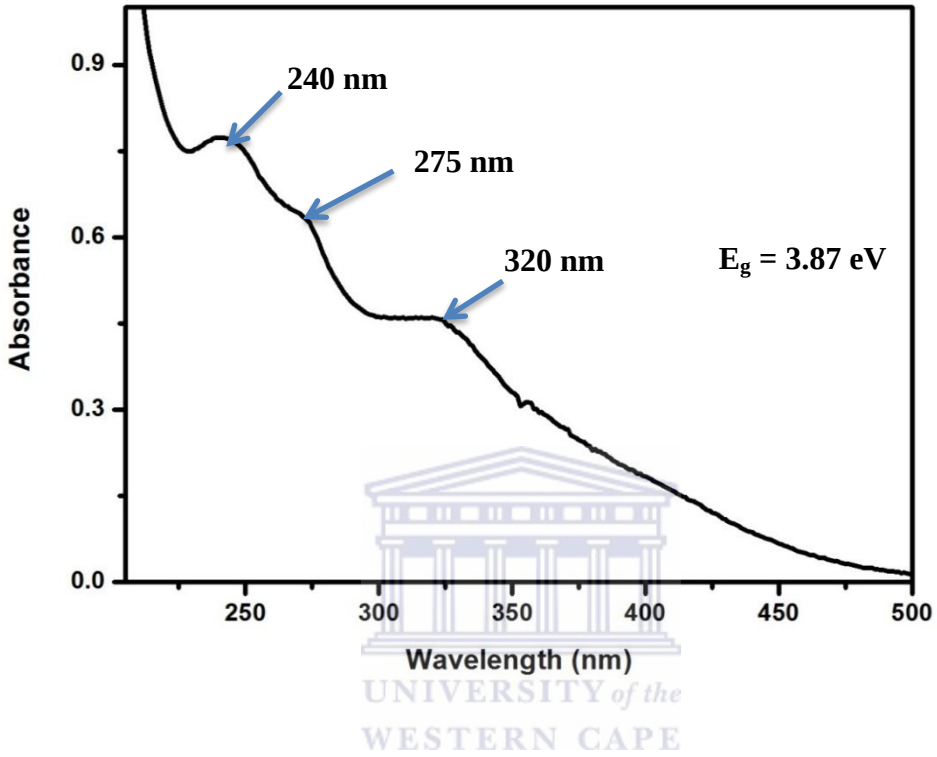

Figure 38: UV-Vis spectrum of 3-MPA-PdTeQDs

Figure 38 shows the absorbance band at 240 nm exhibited a shift to lower wavelength as compared to UV-Vis absorption band seen in chapter 5. The shift was attributed to ligand–to-metal charge transfer. A new additional absorbance band at 275 nm was attributed to tellurium and 3-MPA capping agent which did not appear in TGA-PdTeQDs in chapter 5.The absence of absorption peak at 420 nm confirmed the reduction of Pd^{2+} ions into Pd^{0} and further growth of the nanoparticles (Luo *et al*., 2004) while absorption band at 320 nm was attributed to PdTe quantum dots with an associated band gap of 3.87 eV. The reason for synthesising 3-MPA capped-PdTe quantum dots was to investigate the effect of the capping agent on the quantum dots size and colloidal stability. **Fig 39** shows the fluorescence spectra

of 3-MPA-PdTeQDs where a shift to lower wavelengths at different refluxing time was observed. This is indicative of smaller particle sizes between 510 nm and 420 nm with constant fluorescence intensity (Li *et al*., 2013) as compared to TGA-PdTeQDs indicated in Chapter 5. The enhancement of fluorescence intensity may be attributed to strong interaction between the thiol group of 3-MPA and Pd ion in PdTe particle. This interaction was further analysed by IR spectra of MPA and 3-MPA-PdTeQDs shown in **Fig 40,** a very sharp band was observed at 1700 cm^{-1} which also was observed in chapter 5. Similar results found in chapter 5 are due to same functional groups of capping agents.

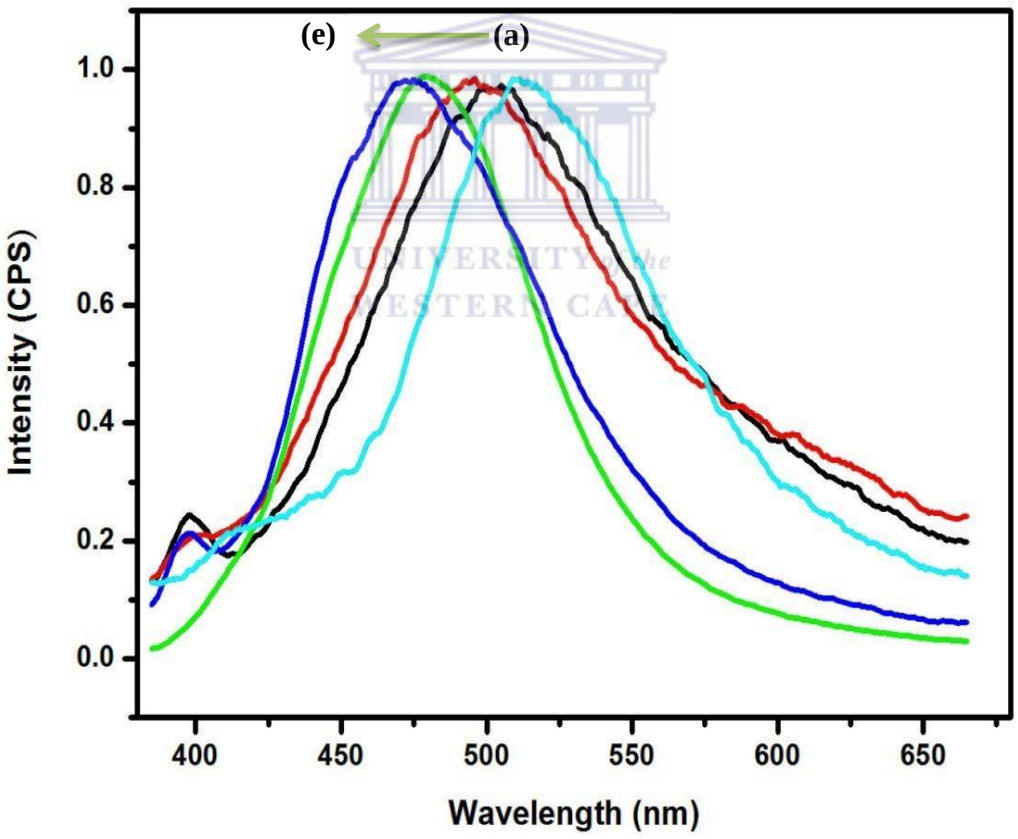

Figure 39: Fluorescence spectra of 3-MPA-PdTeQDs

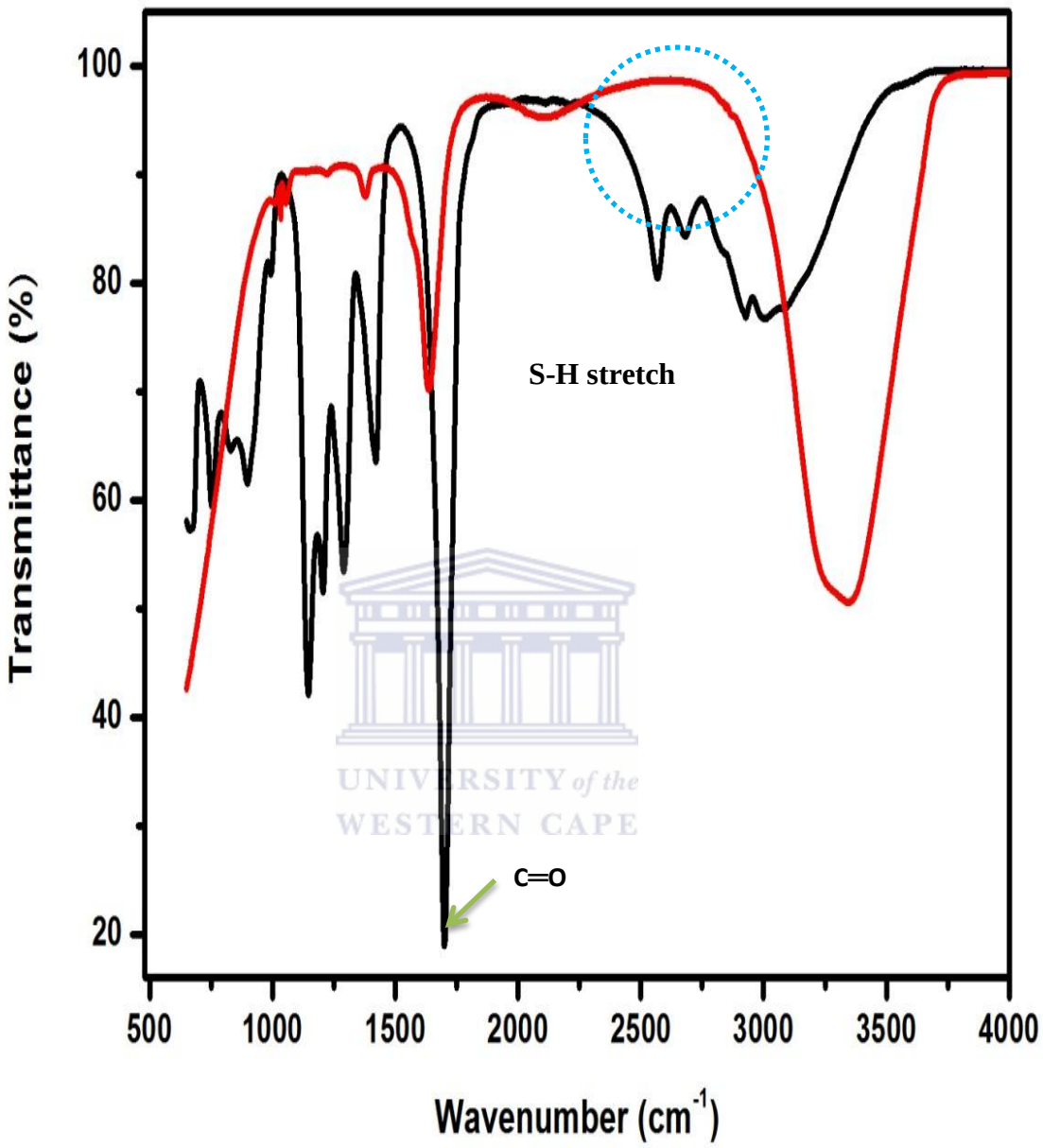

Figure 40: FT-IR spectra of 3-MPA-PdTeQDs

6.2 Electrochemical characterisation of 3-MPA-PdTeQDs

6.2.1 Electrochemistry of 3-MPA-PdTeQDs

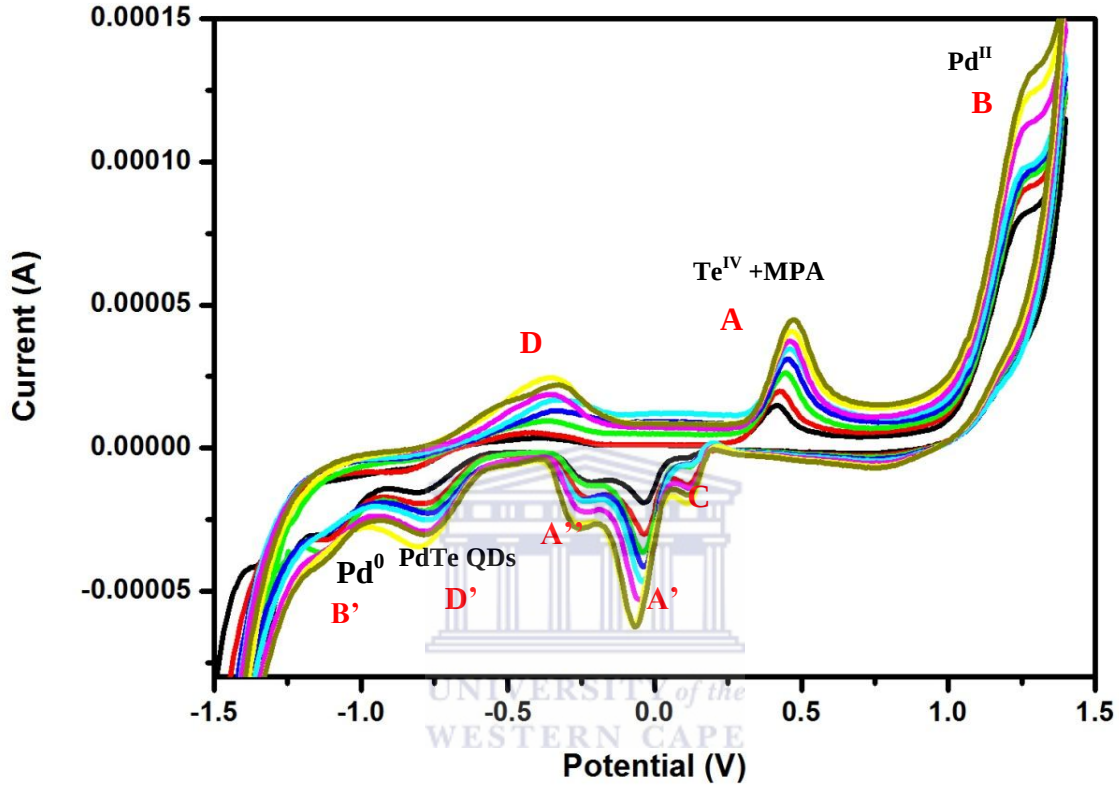

Figure 41: A multi-scan rate studies of 3-MPA-PdTeQDs using cyclic voltammetry in 0.1 M phosphate buffer solution

A multi-scan rate study of 3-MPA-PdTe quantum dots on gold electrode was performed as shown in **Fig 41**. This was carried out to investigate electrochemistry of quantum dots in the potential window between -1.5 V to 1.5 V, scan rates of 5 mV/s to 21 mV/s. Anodic peak positions of tellurium and capping agent are shifted to positive potentials from (0.43 -0.5 V) with increasing scan rates while the cathodic peaks shifted negative potentials from (0-0.15 V) indicating the slow electron transfer process between redox probe. Oxidation peak A at

(0.52 V) is attributed to overlapping of Te^{4+} and 3-MPA while peak B at (1.25 V) was associated with oxidation of Pd^{II} with a slight shift to more positive potential as compared to the CV for TGA-PdTe quantum dots. The reduction peak A′ at (-0.5 V) was associated with the reduction of Te^{IV} to Te^{0} and peak A′′ at (0.3 V) indicates further reduction Te^{0} to Te^{2-}. Reduction peak C at (0.15 V) is due to reduction of carboxylic acid of capping agent (3-MPA) and reduction peak of PdTe quantum dots at D (-0.75 V) appeared at the same position as seen in chapter 5 while the oxidation peak at (-0.4 V) was not present. The reduction of Pd^{II} to Pd^{0} peak B' was observed at (-1.1 V). The electron transfer of Au/Cyst/3-MPA-PdTe quantum dots was observed in **Fig 42** where by reduction peaks of PdTe quantum dots shifted to more positive potential and peaks crossing as the scan rates increased.

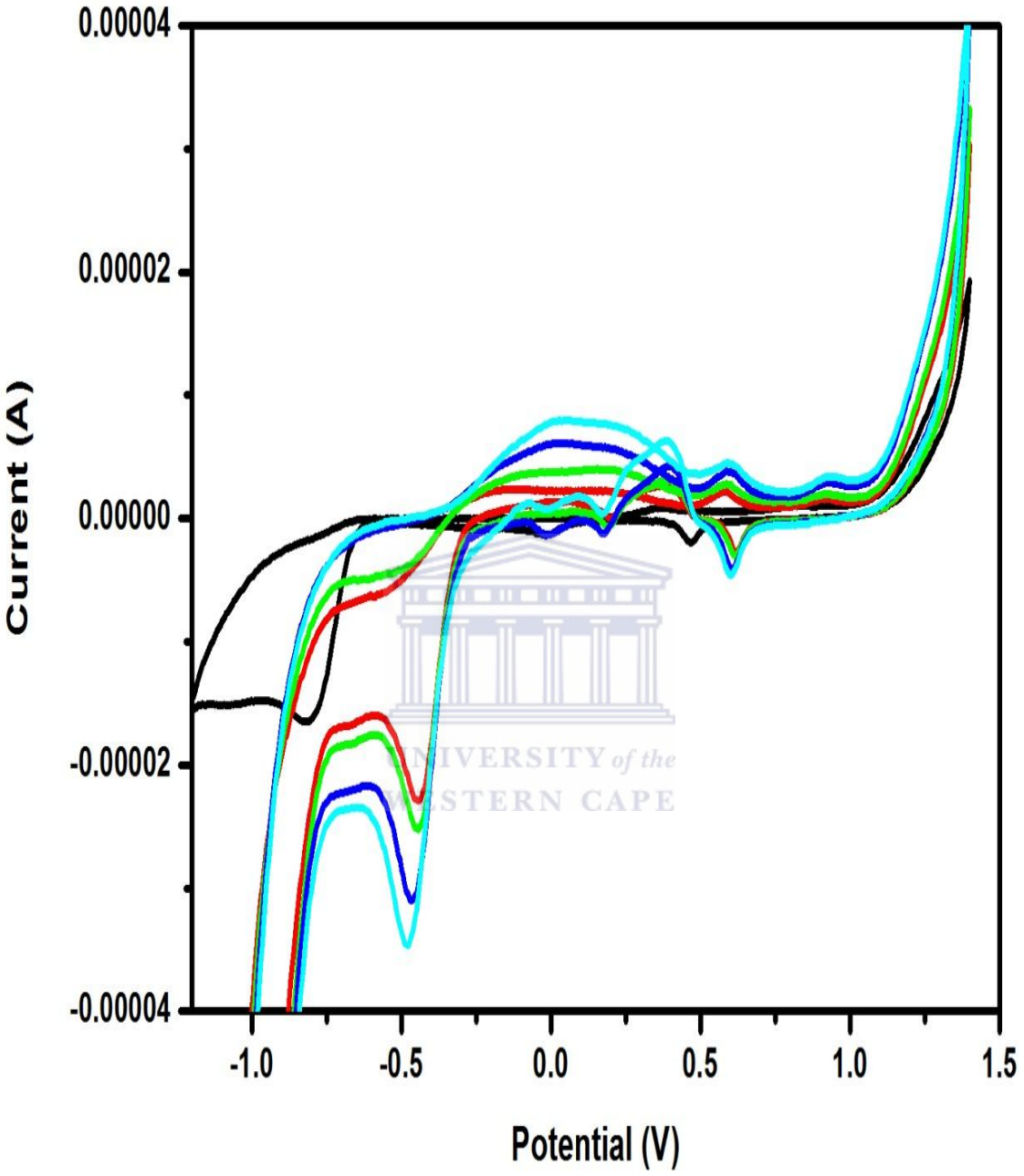

Figure 42: Cyclic voltammograms of Au/Cyst/3-MPA-PdTeQDs in 0.1 M phosphate buffer solution at different scan rates

6.3 Microscopic studies of 3-MPA-PdTeQDs

6.3.1 High resolution transmission electron microscopy (HRTEM)

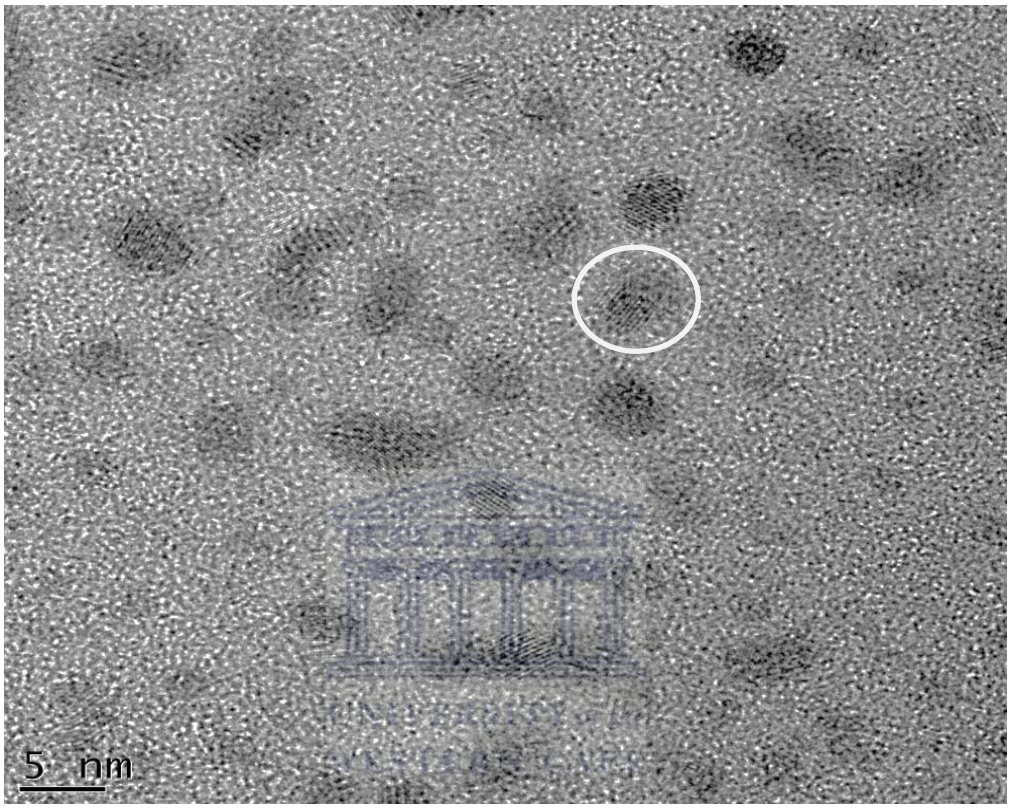

Figure 43: HRTEM of MPA-PdTeQDs

A diameter of about less than 5 nm was obtained for the quantum dots as observed in **Fig 43** with an existance of lattice fringes indicating that MPA-PdTe quantum dots exhibited a crystalline structure (Duan *et al*., 2009). As shown in this figure, there are some dark layers covering the nanoparticles due to excess capping agent on the surface of the quantum dots.

6.4 Biosensor measurements

6.4.1 Electrochemistry of biosensor

Biosensor measurements were carried using low small concentrations in the range (-1.5 to +1.5 V). In **Fig 44**, the observed biosensor reduction peaks showed an increased response with increasing concentrations of the analyte. Three reduction peaks appeared at (E_{pc} = -0.25 V), (E_{pc} = -0.52 V) and (E_{pc} = -0.75 V) with increasing concentration. The reduction peak at -0.25 V was more enhanced with a slight shift to negative potential (0.25 V), the calibration curve in **Fig.45** gave a sensitivity value of 0.01389 mA/nM with K_M^{app} value of 0.05671 mA. The detection limit of the biosensor was 6.2 ng/mL

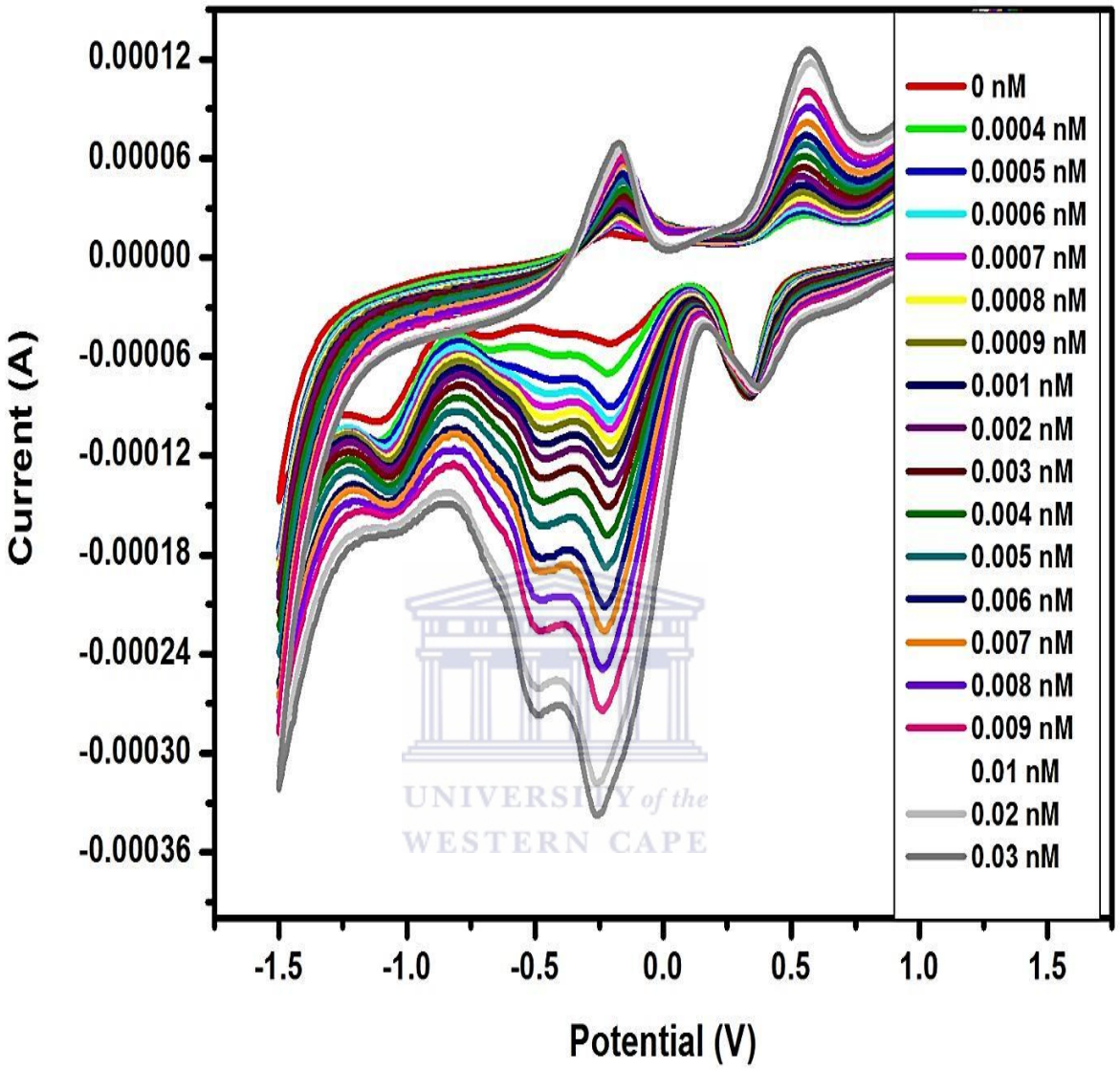

Figure 44: Cyclic voltammograms of CYP3A4/MPA-PdTeQDs/Cyst/Au in 0.1 M phosphate buffer solution at 500 mV/s

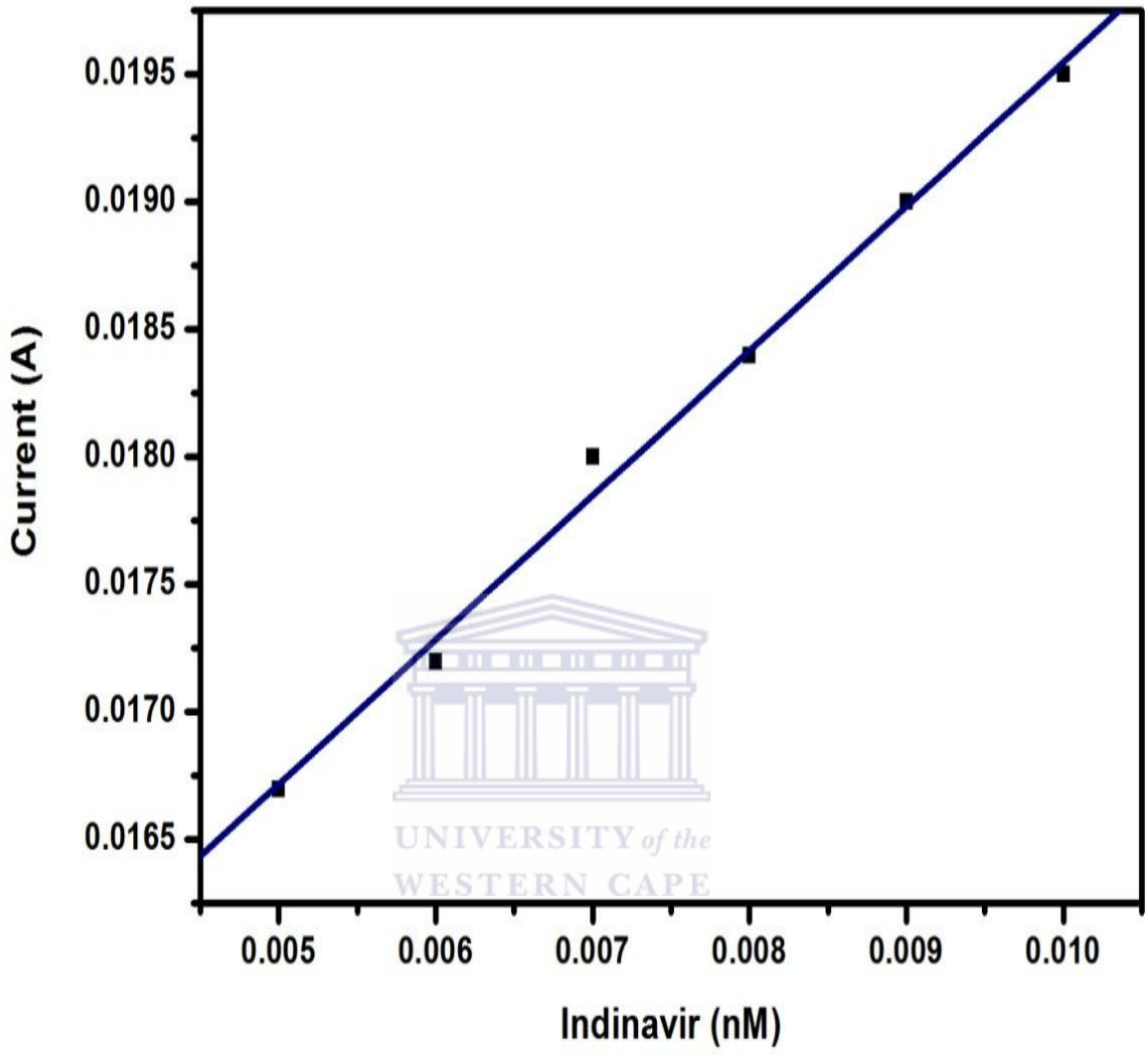

Figure 45: Calibration curve drawn from the linear region of the biosensor responses in Fig 44

6.4.2. Stability of biosensor

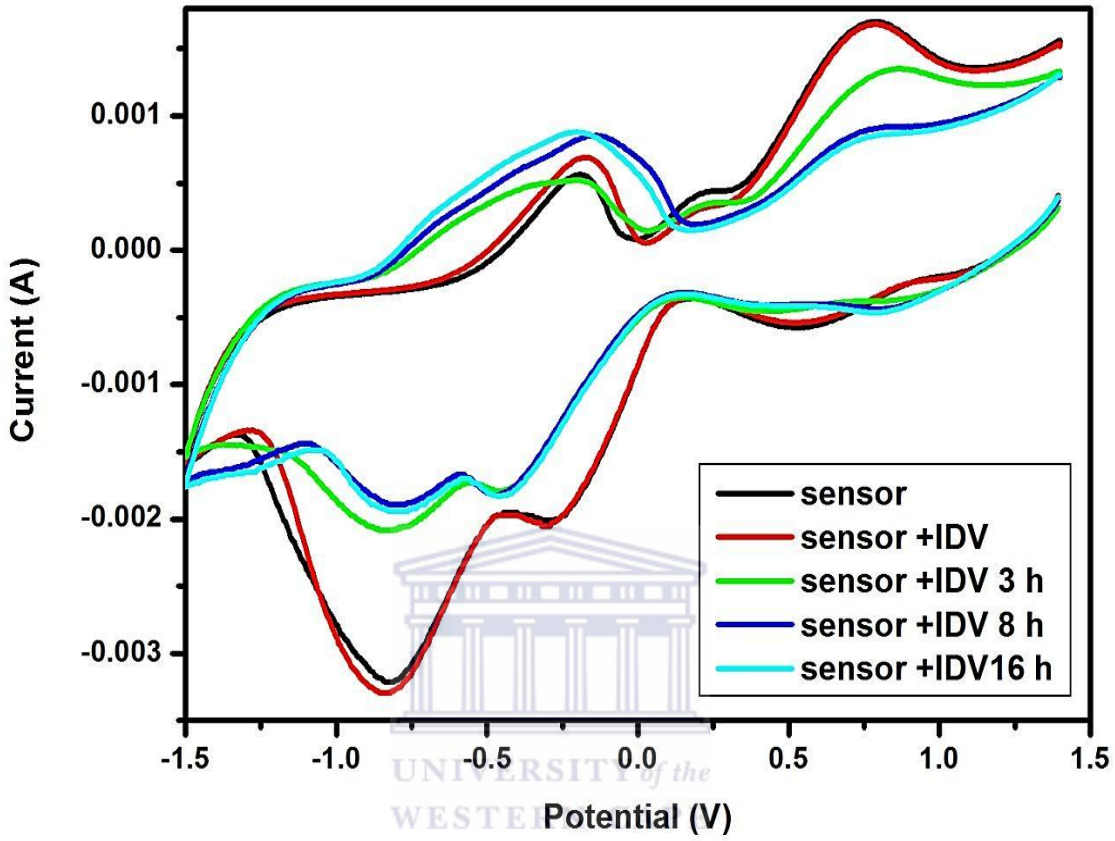

Figure 46: Cyclic voltammograms of CYP3A4/MPA-PdTeQDs/Cyst/RDE biosensor stability in 0.1 M PBS

In **Fig 46**, the measurements were carried out as a function of time for the evaluation stability of biosensor stability. The response was observed (redline) after the addition of 0.0004 nM indinavir concentration. A huge response decreased by 40 % from 3 h to 16 h indicating that the biosensor was not stable when kept for a long time. The decreased peak currents was due to the leakage of enzyme during electrochemical measurement which may be also be degrading with time (Lu *et al*., 2007). Measurements were taken when the biosensor was

rotated using rotating disc electrode as shown in **Fig 47**. The analyte was surface bound to the electrode and observed a shift and decrease in peak current.

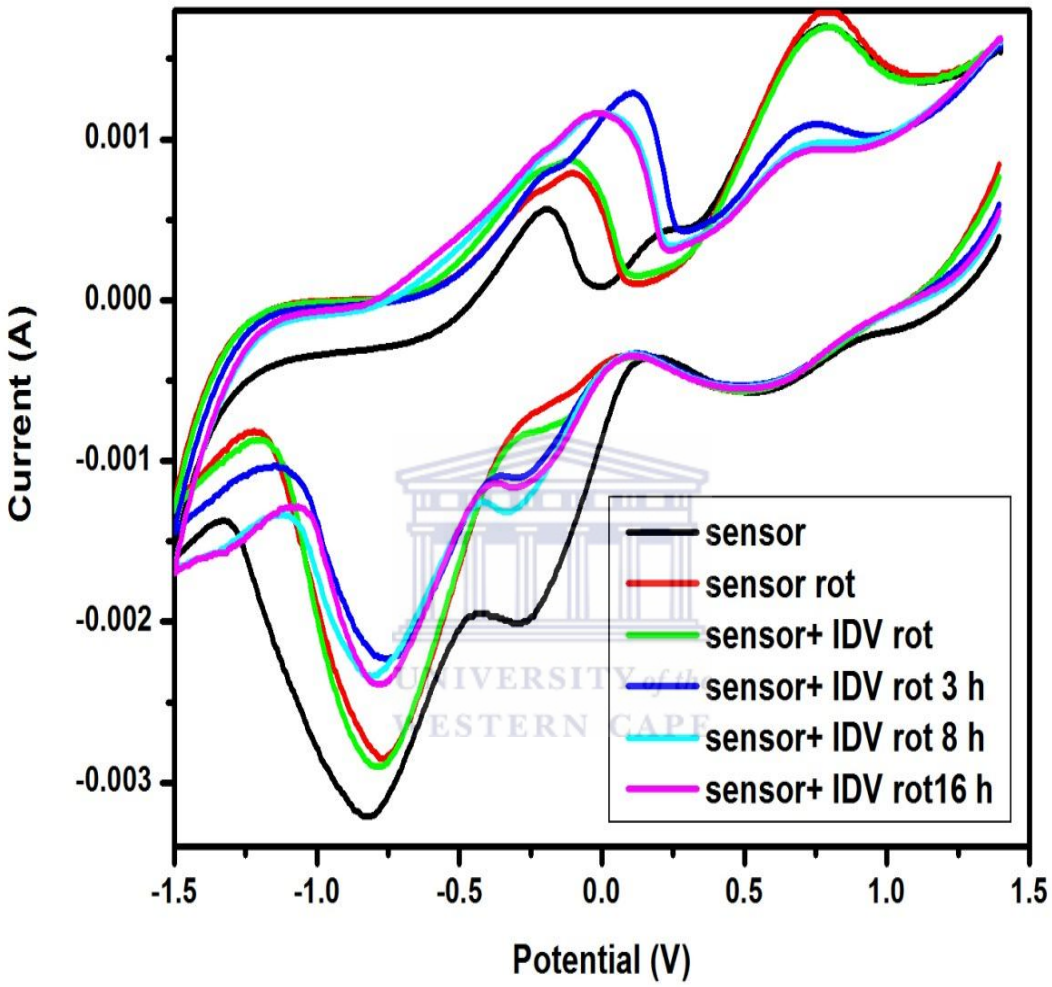

Figure 47: Cyclic voltammograms of CYP3A4/3-MPA-PdTe QDs/Cyst/RDE biosensor stability in 0.1 M PBS

6.5 Microscopic studies of biosensor

6.5.1 High resolution transmission electron microscopy

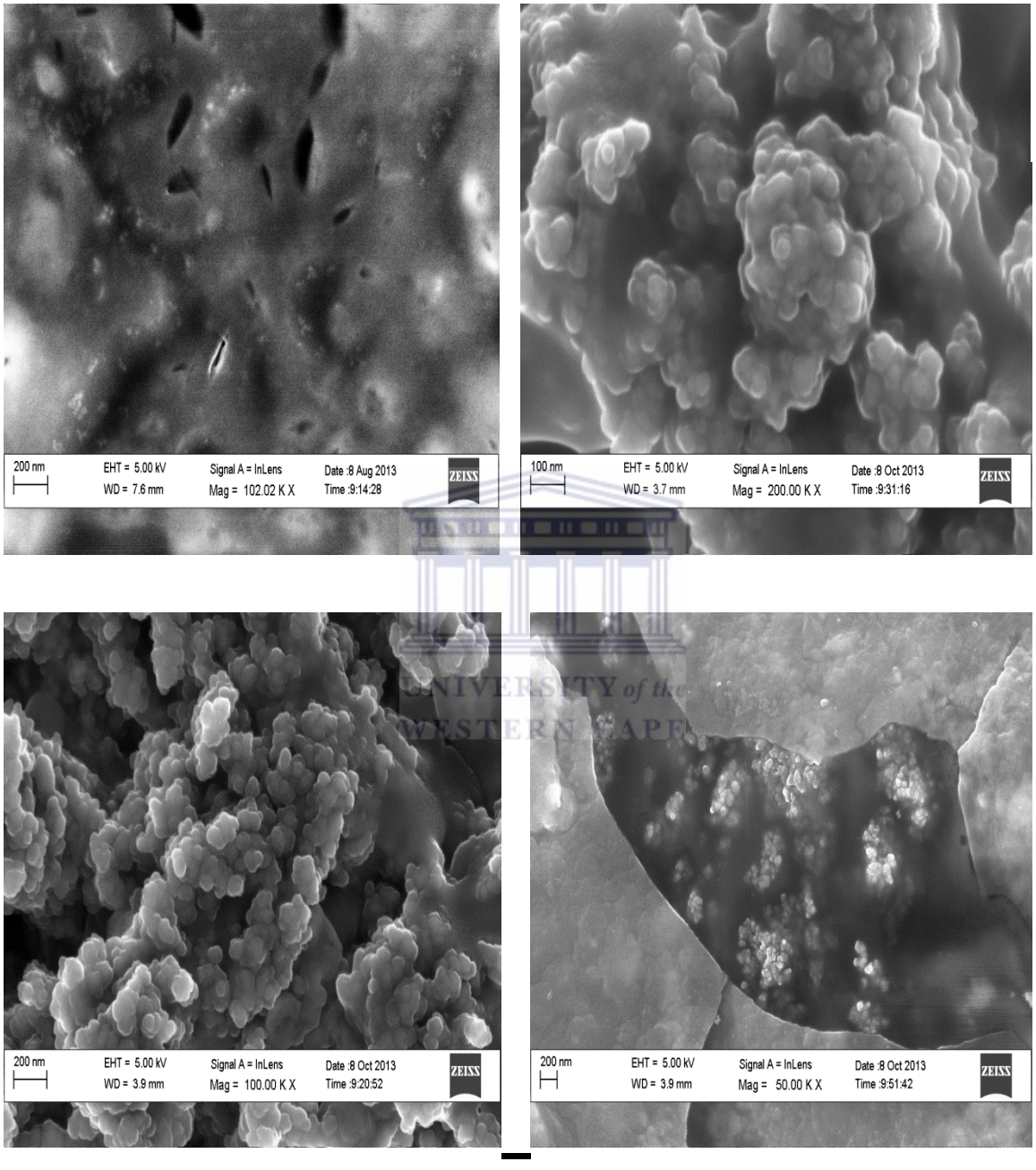

Figure 48: (A)-(D) Represents the HRSEM of Cyst, TGA-PdTeQDs, Cyst/TGA-PdTeQDs and Cyst/TGA-PdTeQDs/CYP3A4 performed on aluminium stub

.

Figure 48 (C) gave better morphology of uniform spherical bubbles attributed to binding of cysteamine onto quantum dots capped than **Fig 48**(B) associated with agglomorated spherical bubbles of different sizes and **Fig 48**(D) showed unbound Cyst/PdTeQDs onto CYP3A4 and a smooth layer on the surroundings

Chapter seven

7.0 Conclusion

The study describes approaches to the synthesis and chemical surface functionalization of quantum dots with capping agents including thioglycolic acid and 3-mercaptopropionic acid. Functionalization of quantum dots with capping agents are important in the field of sensors, and their influence on quantum dots surface was investigated by spectrophotometric and electrochemical analysis and the sensor parameters are collected in Table 1 below.

Table 1: Optical and electrochemical properties of quantum dots

Material	Size distribution (nm)	Shape	Absorption band (nm)	Bandgap (eV)	λ_{max} (nm)	E_{pc} (V)
3-MPA-SnSeQDs	3		350	3.5		0.38
TGA-PdTeQDs	5	Spherical	320	3	411	0.75 V
3-MPA-PdTeQDs	5	Spherical	320	3.87	410	0.75 V

The excellent electrochemical transduction characteristics of the three surface bound quantum dots were used as the principle for sensor development. When the quantum dots were immobilized on electrode together with CYP3A4, the resultant bioelectrode was shown to undergo monooxygenation which is a net reduction reaction. This procedure can be applied in heme-enzyme linked biosensor system for the determination of not only drug metabolism but also the detection of other analyte of clinical, environmental and nutritional importance. The differences in the sensitivities and detection limits (as shown in Table 2) of the biosensors constructed with different capping agents demonstrate one possible method of controlling the performance of this class of biosensor.

Table 2: Sensitivities and detection limits of biosensors

Biosensor	Sensitivity (mA/nM)	Detection limit (ng/mL)
CYP3A4/3-MPA-SnSeQDs/L-cyst/Au	0.221	3.22
CYP3A4/TGA-PdTeQDs/Cyst/Au	0.01259	4.3
CYP3A4/3-MPA-PdTeQDs/Cyst/Au	0.01389	6.2

The detection limits of the three biosensors (i.e. 3.22, 4.3 and 6.2 ng/mL) fall within the range found in vivo studies, where the maximum plasma concentration (C_{max}) 8 h after drug intake was ranged from 5 - 15 ng/mL (Goncalves, 2007).

References

1. Gerber, J.G. Using pharmacokinetics to optimize antiretroviral drug-drug interactions in the treatment of human immunodeficiency virus infection. *Clinical infection diseases* **2000**, *30* (2) S123-9.
2. Hoetelmas, R.M.W.; Meenhorst, P.L.; Mulder, J.W.; Burger, D.M.; Koks, C.H.W.; Beijnen, J.H. Clinical pharmacology of HIV protease inhibitors: focus on saquinavir, indinavir and ritonavir. *Pharmacy World and Science* **1997**, *19* (4), 159-175.
3. de Requena, D.G.; Gallego, O.; De Mendoza, C.; Corral, A.; Jiménez-nácher, I.; Soriano, V. Indinavir plasma concentrations and resistance mutations in patients experiencing early virological failure, *AIDS Research and Human Retroviruses* **2003**, *19* (6), 457-459.
4. Michaud, V.; Bar-Magen, T.; Turgeon, J.; Flockhart, D.; Desta, Z.; Wainberg, M.A. The dual role of pharmacogenetics in HIV treatment: mutations and polymorphisms regulating antiretroviral drug resistance and deposition. *Pharmacology Review* **2012**, *64*, 803-833.
5. Lewis II, J.S.; Terriff, C.M. Protease Inhibitors: a therapeutic breakthrough for the treatment of patients with human immunodeficiency virus. *Clinical Therapeutics* **1997**, *19* (2), 187-214.
6. Rich, D.H.; Sun, C.Q.; Vara Prasad, J.V.; Pathi-asseril, A.; Toth, M.V. Effect of hydroxyl group configuration in hydroxyetyhlamine dipeptide isosteres on HIV protease inhibition: evidence for binding modes. *Medical Chemistry* **1991**, *34*, 1222-12225.
7. Zhong, L.; Yeh, K.C. Determination of indinavir in human cerebrospinal fluid and plasma by solid-phase extraction and high-performance liquid chromatography with column switching. *Chromatography B* **1999**, *734*, 63-71.
8. Sarasa-Nacenta, M.; López-Púa, Y.; Mallolas, J.; Blanco, J.L.; Gatell, J.M.; Carné, X. Simultaneous determination of the HIV-protease inhibitors indinavir, amprenavir,

ritonavir, saquinavir and nelfinavir in human plasma by reversed-phase high-performance liquid chromatography. *Chromatography* **2001**, *757*, 325-332.

9. Moyle, R. Resistance to antiretroviral compounds: implication for clinical management of HIV infection. *Microbiology immunology and Infectious Disease* **1995**, *5*, 170-182.
10. Wlodawer, A.; Vondrasek, J. Inhibitors of HIV-1 protease: A major Success of Structure-Assisted Drug Design. *Annual Review of Biophysics and Biomolecular Structure* **1998**, *27*, 249-284.
11. Clavel, M.D.; Hance, M.D. HIV drug resistance. *The New England Journal of Medicine* **2004**, *350*, 1023-1035.
12. Kohl, N.E.; Emini, E.A.; Davis, L.J; Heimbach, J.C.; Dixon, R.A.; Scolnick, E.M.; Sigal, I.S. Active human immunodeficiency virus protease is required for viral infectivity. *Proceeding of National Academy of Sciences* **1988**, *85*, 4686-4690.
13. Wensing, A.M.J.; van Maarseveen, N.M.; Nijhuis, M. Fifteen years of HIV protease inhibitors: raising the barrier to resistance. *Antiviral Research* **2010**, *85*, 59-74.
14. Ignaszak, A.; Hendricks, N.; Waryo, T.; Songa, E.; Jahed, N.; Ngece, R.; Al-Ahmed, A.; Kgarebe, B.; Baker, P.; Iwuoha, E.I. Novel therapeutic biosensor for indinavir-A protease inhibitor antiretroviral drug. *Pharmaceutical and Biomedical Analysis* **2009**, *49*, 498-501.
15. Burger, D.M.; de Graaf, M.; Wuis, E.W.; Koopmans, P.P.; Hekster, Y.A. Determination of indinavir, an HIV-protease inhibitor, in human plasma by reversed-phase high-performance liquid chromatography. *Chromatography* B **1997**, *703*, 235-241.
16. Lin, J.H. Human immunodeficiency virus protease inhibitors from drug design to clinical studies. *Advanced Drug Delivery Reviewers* **1997**, *27*, 215-233.
17. van Heeswijk, R.P.G.; Veldkamp, A.L.; Mulder, J.W.; Meenhorst, P.L.; Lange, J.M.A.; Beij-nen, J.H.; Hoetelmans, R.M.W. Combination of protease inhibitors for the treatment

of HIV-1 infected patients: a review of pharmacokinetics and clinical experience. *Antiviral Therapy* **2002**, *6*, 201-229.

18. Chiba, M.; Hensleigh, M.; Nishime, J.A.; Balani, S.; Lin, J.H. Role of cytochrome P450 3A4 in human metabolism of MK-639, a potent human immunodeficiency virus protease inhibitor. *Drug Metabolism and Disposition* **1997,** *25*, 1219-1222.
19. Norris, P.J; Rosenberg, E.S. CD4+T helper cells and the role they play in viral control. *Molecular Medicine* **2002**, *80*, 397-405.
20. Dresser, G.P.; Spence, D.; Bailey, D.G. Pharmaceutics pharmacodynamics consequences and clinical relevance of cytochrome P450 3A4 inhibition. *Clinical Pharmacokinetics* **2000**, *38*, 41-57.
21. Ford, J.; Khoo, S.; Back, D.J. The intercellular pharmacology of antiretroviral protease inhibitors. *Antimicrobial Chemotherapy* **2004**, *54*, 982-990.
22. Cressy, T.R.; Lallemant, M. Pharmacogenetics of antiretroviral drugs for the treatment of HIV-infected patients: an update. Infection Genetics and Evolution **2007**, *7*, *333*-342.
23. Arts, E.J.; Hazuda, D.J. HIV-1 antiretroviral drug therapy. *Cold Spring Harbor Perspectives in Medicine* **2012**, *2*, a007161.
24. Porkona, J.; Machala, L.; Rezacova, P.; Konvalinka, J. Current and novel inhibitors of HIV protease. *Viruses* **2009,** *1*, 1209-1239.
25. Tomasselli, A.G.; Heinrikson, R.L. Targeting the HIV-protease in AIDS therapy: a current clinical perspective. *Biochemica et Biophysica A*cta **2000**, *1477*, 189-214.
26. Marzolini, C.; Troillet, N.; Talenti, A.; Baumann, P.; Decosterd, L.A.; Eap, C.B. Efavirenz decreases methadone blood concentrations. *AIDS* **2000** *14*(9), 1291-1292.
27. Foisy, M.L.; Sommadossi, Jean-Pierre. Rapid quantification of indinavir in human plasma by high-performance liquid chromatography with ultraviolet detection. *Chromatography B* **1999**, *721*, 239-247.

28. Frappier, S.; Breilh, D.; Diarte, E.; Ba, B.; Ducint, D.; Pellegrin, J.L.; Saux, M.C. Simultaneous determination of ritonavir and saquinavir, two human immunodeficiency virus protease inhibitors, in human serum by high-performance liquid chromatography. *Chromatography Biomedical Applications* **1998,** *714*, 383-339.
29. Weiss, R.A. Special anniversary review: twenty-five years of human immunodeficiency virus research: successes and challenges. *Clinical and Experimental Immunology* **2008**, *152,* 2001-210.
30. Zuber, R.; Anzenbacherova, E.; Anzenbacher, P. Cytochrome P450 and experimental models of drug metabolism. *Cell and Molecular Medicine* **2002**, *6* (2), 189-198.
31. Wirde, M.; Gelius, U. Self-assembled monolayers of cystamine and cysteamine on gold electrode studied by XPS and voltammetry. *Langmuir* **1999**, *15*, 6370-6378.
32. Vicent, J.L.; Snyder, A.Z.; Fox, M.D.; Shannon, B.J.; Andrewa, J.R.; Raichle, M.E.; Buckner, R.L. Coherent spontaneous activity identifies a hippocampal-parietal memory network. *Neurophysiology* **2006**, 96, 3517-3531.
33. Bawendi, M.G.; Steigerwald, M.L.; Brus, L.E. The quantum mechanics of larger semiconductor clusters. *Annual Review of Physical Chemistry* **1990**, *41*, 477-496.
34. Steigbigel, R.T.; Frost, R.A.; Fuhrer, J. Wasting in the acquired immunodeficiency syndrome is associated with multiple defects in the serum insulin-like growth factor system. *Clinical Endocrinology* **1996**, *44*, 501-514.
35. Zhang, H.; Zhou, Z.; Yang, B. The Influence of Carboxyl Groups on the Photoluminescence of mercaptocarboxylic acid-stabilized CdTe Nanoparticles. *Physical Chemistry B* **2003**, *107,* 8-13.
36. Chan, W.C.W.; Nie, S. Quantum dots bioconjugates for ultrasensitive nonisotopic detection. *Science* **1998**, *281,* 2016-2018.

37. Sam, S.; Touahir, L.; Andresa, J.S.; Allongoe, P.; Chazalviel, J.-N.; Gouget-Laemmel, A.C.; de Villeneuve, C.H.; Moraillon, A.; Ozanam, F.; Gabouze, N.; Djebbar, S. Semiquantitative study of the EDC/NHS activation of acid terminal groups at modified porous silicon surfaces. *Langmuir* **2009**, *26* (2), 809-814.
38. Sethi, R.S. Transducer aspects of biosensors. *Biosensors and Bioelectronics* **1994**, *9*, 243-264.
39. Khatei, J.; Koteswara Rao, K.S.R. Hydrothermal synthesis of CdTe QDs: their luminescence quenching in the presence of bio-molecules and observation of bistable memory effect of CdTeQDs/PEDOT: PSS heterostructure. *Materials Chemistry and Physics* **2011,** *144977*, 1-6.
40. Murray, C.B.; Norris, D.J.; Bawendi, M.G. Synthesis and characterisation of nearly monodisperse CdE (E = sulphur, selenium, tellurium) semiconductor nanocrystallites. *Journal of American Chemical Society* **1993**, *115*, 8706-8715.
41. Dey, S.; Vimal, K.J. Platinum Group Metal Chalcogenides. Their synthesis and applications in catalysis and metal science. *Platinum Metals Reviews* **2004,** *48*(1), 16-29.
42. Thevenot, D.R., Toth, K., Durst, R.A. Wilson, G.S. Electrochemical biosensors: recommended definitions and classification. *Biosensor and Bioelectronics* **2001**, *16*, 121-131.
43. Ngoepe, M.; Choonara, Y.E.; Tyagi.C.; Tomar, L.K.; du Toit, L.C.; Kumar, P.; Ndesendo, V.L.; Pillay, V. Integration of biosensors and drug delivery technologies for early detection and chronic of illness. *Sensors* **2013,** *13*, 7680-7713.
44. Trojanowicz, M.; Krwaczyfiskivel, T. Electrochemical Biosensors Based on Enzymes Immobilized in Electropolymerized Films. *Mikrochimica Acta*. **1995**, *121*, 167-181.

45. Poznyak, S.K.; Osipovich, N.P.; Shavel, A.; Talapin, D.Dao, M., Eychimuller, A.; Gaponik, N. Size-dependent electrochemical behaviour of thiol-capped CdTe nanocrystals in aqueous solution. *Physical Chemistry B* **2005,** *109*, 1094-1100.
46. Guratna, C. Drug metabolism and pharmacokinetics in drug discovery: A prime for bioanalytical chemists, part I. *Bioanalytical Systems* **2000**, *19*(1), 17-23.
47. Khene, S.; Moeno, S.; Nyokong, T. Voltammetry and electrochemical impedance spectroscopy of gold electrodes modified with CdTe quantum dots and their conjugates with nickel tetraamino phthalocynine. *Polydron* **2001**, *30*, 2162-2170.
48. Ndangili, P.M.; Jijana, A.N.; Baker, P.G.L.; Iwuoha, E.I. 3-mercaptopropionic acid capped ZnSe quantum dot-cytochrome P450 3A4 enzyme biotransducer for 17ß-estradiol.*Electroanalytical Chemistry* **2011**, *653*, 67-74.
49. Bruckensten, S.; Shay, M. An in situ weighing study of the mechanism for the formation of the adsorbed oxygen monolayer at a gold electrode. *Electroanalytical Chemistry* 1985, *188*, 131-136.
50. Colvin, V.L.; Schlamp, M.C.; Allivisatos, A.P. Light-emitting diodes made from cadmium selenide nanocrystals and a semiconducting polymer. *Nature* **1994**, *370*, 354-357.
51. Gaponik, N.; Talapin, D.V.; Rogach, A.L.; Hoppe, K.; Shvchenko, E.V.; Kornowski, A.; Eychmuller, A.; Weller, H. Thiol-capping of CdTe nanocrystals: An alternative to organometallic synthetic routes. *Physical Chemistry B* **2002**, *106*, 7177-7185.
52. Chen, C.-C.; Yet, C.P.; Wang, H.-N.; Chao, C.-Y. Self-assembly of monolayers of cadmium selenide nanocrystals with dual color emission. *Langmuir* **1999**, *15*, 6845-6850.
53. Priyam, A.; Chatterjee, A.; Das, S.K.; Saha, A. Synthesis and spectral studies of cysteine-capped CdS nanoparticles. *Research on Medical Intermediates* **2005**, *31*(8), 691-702.

54. Nxusani, E.; Ndangili, P.M.; Olowu, R.A.; Jijana, A.N.; Waryo, T.; Jahed, N.; Ajayi, R.F.; Baker, P.; Iwuoha, E.I. 3-Mercaptopropionic acid capped Ga_2Se_3 nanocrystal-CYP3A4 biosensor for the determination of 17-alpha-ethyl estradiol in water. *Nano Hybrids* **2012**, *1*, 1-22.
55. Hager, G.; Brolo, A.G. Adsorption/desorption behaviour of cysteine and cysteine in neutral and basic media: electrochemical evidence for differing thiol and disulphide adsorption to a Au (111) single crystal electrode. *Electroanalytical Chemistry* **2003**, *551*, 291-301.
56. Weirse, D.G.; Lohrengel, M.M.; Schultze, J.W. Electrochemical properties of sulphur adsorbed on gold electrodes. *Electroanalytical Chemistry* **1978**, *92*, 121-131.
57. Nemade, K.R.; Waghuley, S.A. UV-Vis spectroscopic study of one pot synthesized strontium oxide quantum dots. *Results in Physics*. **2013**, *3*, 52-54.
58. Frasco, M.F.; Chaniotakis, N. Semiconductor quantum dots in chemical sensors and biosensors. *Sensors* **2009**, *9*, 7266-7286.
59. Shervedani, R.K.; Bagherzadeh, M.; Mozaffari, S.A. Determination of dopamine in the presence of high concentration of ascorbic acid by using gold cysteine self-assembled monolayers as a nanosensor. *Sensors and Actuators* B **2006**, *115*, 614-621.
60. Mozaffari, S.A.; Shervedani, R.K. Preparation and electrochemical characterisation of a new nanosensor based on self-assembled monolayer of cysteamine functionalized with phosphate groups. *Surface and Coatings Technology* **2005**, *198*, 123-128.
61. Weng, S.; Du, D. Studies on electrochemical behaviour of hydroquinone at L-cysteine self-assembled monolayers modified gold electrode. *Sensors* **2002**, *2*, 41-49.
62. Brett, C.M.A.; Kresak, S.; Hianik, T.; Brett, A.M.O. Studies on self-assembled alkanethiol monolayers formed at applied potential on polycrystalline gold electrode. *Electroanalysis* **2003**, *15* (6), 557-565.

63. Campuzano, S.; Pedrero, M.; Montemayor, C.; Fatás, E.; Pingarrón, J.M. Characterization of alkanethiol-self-assembled monolayers-modified gold electrodes by electrochemical impedance spectroscopy. *Electroanalytical Chemistry* **2006**, *586*, 112-121.

64. Duan, J.; Song, L.; Zhan. J. One-pot synthesis of highly luminescent CdTe quantum dots by microwave irradiation reduction and their Hg^{2+}-sensitive properties. *Nano Research* **2009**, *2*, 61-68.

65. Shumyantseva, V.V.; Bulko, T.V.; Rudakov, Y.O.; Kuznetsova, G.P.; Samenkova, N.F.; Lisitsa, A.V.; Karuzina, I.I.; Archakov, A.I. Electrochemical properties of cytochrome P450 using nanostructured electrodes: Direct electron transfer and electrocatalysis. *Inorganic Biochemistry.* **2007**, *101*, 859-865.

66. Peng, H.; Zhang, L.; Soeller, C.; Travas-Sejdic, J. Preparation of water-soluble CdTe/CdS core/shell quantum dots with enhanced photostability. *Luminescence* **2007**, *127*, 721-726.

67. Bistolas, N.; Wollenberger, U.; Jung, C.; Scheller, F.W. Cytochrome P450 biosensors-a review. *Biosensors and Bioelectronics* **2005**, *20*, 2408-2423.

68. Shankaran, D.R.; Uehara, N.; Kato, T. A metal dispersed sol–gel biocomposite amperometric glucose biosensor. *Biosensor and Bioelectronics* **2003**, *18*, 721–728.

69. Luo, X.L.; Xu, J.J.; Du, Y.; Chen, H.Y. A glucose biosensor based on chitosan-glucose oxidase-gold nanoparticles biocomposite formed by one-step electrodeposition. *Analytical Biochemistry* **2004,** *34(*2*)*, 284-289.

70. Hamizi, N.A.; Ying, C.S.; Johan, M.R. Synthesis with different Se concentration and optical studies of CdSe quantum dots via inverse micelle technique. *International Journal of Electrochemical Science* **2012**, *7*, 4727-4734.

71. Iwuoha, E.I.; Joseph, S.; Zhang, Z.; Smyth, M.R.; Fuhr, U.; Ortiz de Montellano, P.R. Drug metabolism biosensors: electrochemical reactivities of cytochrome P450cam

immobilised in synthetic vesicular systems. Pharmaceutical and Biomedical Analysis **1998**, *17*, 1101-111.

72. Sadik, O.A; Mwilu, S.K.; Aluoch, A. Smart electrochemical biosensors: from advanced materials to ultrasensitive devices. *Electrochemical Acta* **2010**, *55*, 4287-4295.
73. Clark, L.C.; Lyons, C. Electrode systems for continuous monitoring in cardiovascular surgery. Annals of the New York Academy of Sciences **1962**, *102*, 29-45.
74. McCann, P.J. IV-VI semiconductors for mid-infrared optoelectronic devices. *Springer Series in Optical Sciences* **2006**, 118, 237-264.
75. Pearson, G.L.; llegems, M. Phase studies in III-IV, II-IV, IV-VI compound semiconductor alloy systems. *Material Science* **1975**, *5*, 345-371.
76. Michalet, X.; Kapanidis, A.N.; Laurence, T.; Pinaud, F.; Doose,S.; Pflughoefft, M.; Weiss. S. The power and prospects of fluorescence microscopies and spectroscopies. *Annual Review of Biophysics and Biomolecular structure* **2003**, *32*, 161-82.
77. Hambrock, J.; Birkner, A.; Fischer, R.A. Synthesis of CdSe nanoparticles using various organometallics cadmium precursors. *Material Chemistry* **2001**, *11*, 3197-3201.
78. Xing, Y.; Rao, J. Quantum dot bioconjugates for in vitro diagnostics and in vivo imaging. *Cancer Biomarkers* **2008**, *4*, 307-319.
79. Brus, L.E. Quantum Size Effects in the Electronic Properties of Small Semiconductor Crystallites. *Proceedings of the 17th Jerusalem Symposium on Quantum Chemistry*: *Molecule-Surface Interactions* **1984**, *17*,431-435**.**
80. Yanezwa, T.; Kunitake, T. Practical preparation of anionic mercapto ligand-stabilized gold nanoparticles and their immobilization. *Colloids and Surfaces A* **1999**, *149*,193-199.
81. Sherverdani, R.K.; Mozaffari, S.A. Copper (II) nanosensor based on a gold cysteamine self-assembled monolayer functionalized with salicylaldehyde. *Analytical Chemistry* **2006**, *78*, 4957-4963.

82. Bard, A.J.; Faulkner, L.R. In Electrochemical Methods: Fundamentals and applications, 2nd ed. John Wiley & Sons: New York, **2001, p290**.

83. Zhang, Y.; Tan, Y.-W.; Stormer, H.L.; Kim, P. Experimental observation of the quantum Hall effect and berry phase in grapheme. *Nature* **2005**, *438*, 201-204.

84. Song, R.; Liu, Y.; He, L. Synthesis and characterisation of mercaptoacetic acid-modified ZnO nanoparticles. *Solid State Science* **2008**, *10*, 1563-1567.

85. Liu, Y.-S.; Sun, Y.; Vernier, P.T.; Liang, S.Y.C.; Gundersen, M.A. pH-sensitive photoluminescence of CdSe/ZnSe/ZnS quantum dots in human ovarian cancer cells .*Physical Chemistry C* **2007**, *111*, 2872-2878.

86. Zhao, D.; Jimei, Z.; Quanxi, D.; Ning, D.; Shichao, X.; Bo, S.; Yuehua, B. Adaption of Au nanoparticles and CdTe quantum dots in DNA detection. *Chinese Journal of Chemical Engineering* **2007**, *15* (6), 791-794.

87. Liu, Y.-F.; Yu, J.-S. In situ synthesis of highly luminescent glutathione-capped CdTe/ZnS quantum dots with biocompatibility. *Colloid and Interface Science* **2010**, *351*, 1-9.

88. Chen, Y.F.; Rosenzweig, Z. Luminescent CdS quantum dots as selective ion probes. *Analytical Chemistry* **2002**, *74*, 5132-5138.

89. Mashazi, P.W.; P.Westbroek, P.; Ozoemena, K.I.; Nyokong, T. Surface Chemistry and electrochemicalytic behaviour of tetra-carboxylic substituted ion, cobalt and manganese pathalocyanine monolayer on gold electrode. *Electrochemical Acta* **2007**, *53*, 1858-1869.

90. Goncalves, M.T.; Pires, B.X.F.; Bedoc, D.C.G.; de Souza, V.C.; de Abreu, L.R.P.; de Santana, D.P. Determination of Indinavir in human plasma and its use in pharmacokinetic study. *Revista Braseleira de- Ciencias Farmaceuticals*. **2007,** *43*(4), 640-647.

91. Schneider, E.; Clark, D.S. Cytochrome P450 (CYP) enzymes and the development of CYP biosensors. *Biosensors and Bioelectronics* **2013**, *39*, 1-13.

92. Mena, M.L.; Yánez-Sedeño, P.; Pingarrón, J.M. A comparison of different strategies for the construction of amperometric enzyme biosensors using gold nanoparticles-modified electrodes. *Analytical Biochemistry* **2005**, *36*, 20-27.

93. Hendricks, N.R.; Waryo, T.T.; Arotiba, O.; Jahed, N.; Baker, P.G.L.; Iwuoha, E.I. Microsomal cytochrome P450-3A4 (CYP3A4) nanobiosensor for the determination of 2,4-dichlorophenol-An endocrine disruptor compound. *Electrochimica Acta* **2009**, *54*, 1925-1931.